To the Graduate Council:

I am submitting herewith a dissertation written by Hong Guan entitled "The Study of the Characteristics of Packing Material for Preparative Liquid Chromatography." I have examined the final copy of this dissertation for form and content and recommend that it be accepted in partial fulfillment of the requirements for the degree of Doctor of Philosophy, with a major in Chemistry.

Georges Guiochon, Major Professor

We have read this dissertation
and recommend its acceptance:

Accepted for the Council:

Associate Vice Chancellor and
Dean of The Graduate School

THE STUDY OF THE CHARACTERISTICS OF PACKING MATERIAL FOR PREPARATIVE LIQUID CHROMATOGRAPHY

A Dissertation

Presented for the

Doctor of Philosophy

Degree

The University of Tennessee, Knoxville

Hong GUAN-SAJONZ

May, 1996

ACKNOWLEDGEMENTS

I would like to extend a special thanks to Professor Georges Guiochon for his patience and guidance throughout my graduate career. Also, I want to thank the members of our research group, especially Dr. Fred Charton, Dr. Moustapha Diack, Mr. Tivadar Farkas, Dr. Attila Felinger, Dr. Stephen Jacobson, Dr. Matial Sarker, Dr. Brett Stanley, Mr. Tong Yun, Dr. Guoming Zhong, and my husband and colleague Mr. Peter Sajonz for their support and contributions to this dissertation. Special thanks also go to Dr. Helen Greenblatt and Mr. Klaus Lohse (BTR, Wilmington, DE), Mr. Per Jageland (EKA-NOBEL, Stratford, CT), Mr. Pat Hall and Ms. Lisa Spangler (PHARMACIA, Pitscataway, NJ), Mr. Lou Bellafiore (TECHNIKROM), Dr. Jon Fisher and Mr. Peter Stormer (TOSOHAAS, Montgomeryville, PA), Dr. Yan-Bo Yang (VYDAC, Hesperia, CA), Mr. Robert Cooley (YMC, Wilmington, NC) for insightful discussions, and Dr. Dorothy Coffey (Oak Ridge National Laboratory, Oak Ridge, TN) for the Scanning Electron Microscopy pictures.

The gifts of the ODS packing materials by EKA-NOBEL, VYDAC, YMC and BTR, the RESOURCE-Q anion exchange columns by PHARMACIA, and the DEAE-5PW anion exchange column by TOSOHAAS for a 30-day free trial are gratefully appreciated.

I would also like to acknowledge the support from the University of Tennessee Computing Center (UTCC), especially Ms. Sue Smith of UTCC.

ABSTRACT

The study of the characteristics of packing material for preparative liquid chromatography was carried out on two types of commonly used stationary phases: the octadecyl-bonded silica adsorbents (ODS) for Reversed Phase Liquid Chromatography (RPLC) and the ion exchange resins for Ion Exchange Liquid Chromatography (IXLC).

For RPLC, an overall look at the column performance reproducibility was made first by packing a series of five columns with the same stationary phase and under the same conditions. Four 10 μm spherical C_{18} stationary phases were used: KROMASIL, VYDAC, YMC and ZORBAX. The retention factors, column efficiencies, and equilibrium isotherms were determined for a series of compounds and the results were compared. It was found that these columns have significantly different performance. The source for this irreproducibility was investigated from the packing density view point, which in part was done by applying Inverse Size Exclusion Chromatography (ISEC) to determine the column external porosity. As a result, the column external porosity varies from column to column. This study was followed by packing more columns with the same stationary phase but under various packing pressures. It was found that the column external porosity decreases and packing weight increases as the packing pressure increases. Isotherm parameters obtained on one column, after being modified by the respective packing volumes or weights, can be applied to another to predict band profiles with satisfactory accuracy.

For IXLC, the emphasis was put on the mass transfer kinetics between proteins and the ion exchanger stationary phase. One Tosohaas DEAE-5PW TSK-Gel and two Pharmacia RESOURCE-Q anion exchange columns were used. Breakthrough curves were acquired for the

determination of the equilibrium isotherm on each column. An average rate coefficient of the mass transfer kinetics was determined for each breakthrough curve by applying a lumped kinetic model coupled with the ideal model of the mass balance equation in liquid chromatography. This rate coefficient was found to increase linearly as the average sample concentration increases. The column performance reproducibility study in IXLC was made on the two identical RESOURCE-Q columns (same code number but different lot number). Their thermodynamic properties were found to be significantly different from each other, indicating the difficulties one might encounter in the future if preparative liquid chromatography is to become a major technique of separation in the pharmaceutical industry.

TABLE OF CONTENTS

CHAPTER **PAGE**

CHAPTER 1. INTRODUCTION 1

General Background 1

Mass Balance Equation 2

Relation Between the Concentrations in the Stationary and the Mobile Phase 3

Linear and Nonlinear Chromatography 4

Band Profile Calculation 5

Overview 7

CHAPTER 2. REPRODUCIBILITY, ACCURACY, AND CORRECTION OF ISOTHERM DATA MEASURED BY CHROMATOGRAPHY 13

Introduction 13

Theory 14

Experimental 16

Equipment 16

Columns 17

Chemicals 17

Procedures 18

Detector Calibration 19

Results and Discussion 19

Linear Chromatography Data (k' and N_o) 19

Chromatograms 20

Equilibrium Isotherms 20

Isotherms Normalized by the Ratios of k's 22

Alternate Determination of the Coefficient a 23

Isotherms Normalized by the Ratios of ϵ_e's 24

Conclusion 25

CHAPTER 3. STUDY OF PHYSICO-CHEMICAL PROPERTIES OF SOME PACKING MATERIALS. I - MEASUREMENTS OF THE EXTERNAL POROSITY OF PACKED COLUMNS BY INVERSE SIZE EXCLUSION CHROMATOGRAPHY 27

Introduction 27

Theory 30

Experimental 33

Equipment 33

Columns 34

Chemicals 34

Procedures 35

Results and Discussion 37

Column Internal and External Porosities 37

The Pore Size Distributions of a Chromatographic Column 41

Conclusion 42

CHAPTER 4. STUDY OF THE PHYSICO-CHEMICAL PROPERTIES OF SOME PACKING MATERIALS. II - GENERAL PROPERTIES OF THE PARTICLES 44

Introduction 44

Theory 46

Experimental 49

Equipment 49

Columns 50

Chemicals 50

Measurement of the Apparent Density of the Packing Materials 51

Scanning Electron Micrography (SEM) of the Packing Materials 51

Results and Discussion 52

Visual Examination of the Particles 52

Unaccessible Volume Fraction 53

Solid Volume Fractions 54

Closed Pores Porosity 55

Column Total Porosity 56

Conclusion 57

CHAPTER 5. EFFECT OF THE PACKING PRESSURE ON THE PERFORMANCE OF C_{18} REVERSED PHASE LIQUID CHROMATOGRAPHIC

COLUMNS 59
Introduction 59
Theory 61
Thermodynamics of Phase Equilibrium 61
Inverse Size Exclusion Chromatography (ISEC) 64
Determination of the Different Volume Fractions 64
Experimental 66
Equipment 66
Columns 66
Chemicals 67
Procedures 68
Detector Calibration 69
Results and Discussion 70
Linear Chromatography Data 70
Chromatograms 71
Equilibrium Isotherms 71
Column Volume Fractions 72
Packing Material Density 73
Isotherm Correction by Packing Weight 74
Conclusion 75

CHAPTER 6. STUDY OF THE MASS TRANSFER KINETICS OF BSA ON TSK-GEL DEAE-5PW ANION EXCHANGER IN A WIDE

CONCENTRATION RANGE 76
Introduction 76
Theory 78
Experimental 80
Column 80
Materials 80
Equipments 81
Sample Preparation 81
Procedures 82
Detector Calibration 82
Column Regeneration 83
Results and Discussion 83
Adsorption Isotherms 83
Mass Transfer Kinetics Data 85
Conclusion 88

CHAPTER 7. STUDY OF THE REPRODUCIBILITY AND MASS TRANSFER KINETICS OF BSA ON TWO IDENTICAL RESOURCE-Q COLUMNS 89
Introduction 89
Theory 90
Experimental 92
Columns 92

Materials 92
Equipments 92
Sample Preparation 93
Procedures 93
Detector Calibration 94
Results and Discussion 94
Column Phase Ratio 94
Adsorption Isotherms 95
Mass Transfer Kinetics - Rate Coefficient Independent of the Concentration 96
Mass Transfer Kinetics - Rate Coefficient Concentration Dependence . . . 96
Conclusion 97

CHAPTER 8. CONCLUSIONS 98

LIST OF REFERENCES 100

APPENDIX 111

VITA 202

LIST OF TABLES

TABLE **PAGE**

2.1 Column Packing Conditions (10 μm particles); Column Dimension 10 cm x 0.46 cm i.d 112

2.2 Column Characteristics 113

2.3 KROMASIL: k' and N_0 Measurements 114

2.4 VYDAC: k' and N_0 Measurements 115

2.5 YMC: k' and N_0 Measurements 116

2.6 ZORBAX: k' and N_0 Measurements 117

2.7 Isotherm Studies on KROMASIL Columns 118

2.8 Isotherm Studies on VYDAC Columns 119

2.9 Isotherm Studies on YMC Columns 120

2.10 Isotherm Studies on ZORBAX Columns 121

3.1 KROMASIL Porosities 122

3.2 VYDAC Porosities 123

3.3 YMC Porosities 124

3.4 ZORBAX Porosities 125

3.5 Incremental Pore Distribution on KROMASIL Columns (% of Total Pore Volume) 126

3.6 Incremental Pore Distribution on VYDAC Columns (% of Total Pore Volume) . 127

3.7 Incremental Pore Distribution on YMC Columns (% of Total Pore Volume) . . . 128

3.8 Incremental Pore Distribution on ZORBAX Columns (% of Total Pore Volume) 129

4.1 Density of the Packing Materials 130

4.2 Unaccessible and Total Porosities of the Columns Studied 131

4.3 Volume Fractions Occupied by Silica, the Bonded Chains and the Closed Pores 132

5.1 Calculated Equilibrium Isotherm Coefficients on KROMASIL® Columns 133

5.2 Calculated Equilibrium Isotherm Coefficients on ZORBAX® Columns 134

5.3 Porosities of KROMASIL® Columns 135

5.4 Porosities of ZORBAX® Columns 136

5.5 Packing Density Data for KROMASIL® and ZORBAX® Columns 137

6.1 Parameters of the bi-Langmuir and Langmuir Adsorption Isotherms of Bovine Serum Albumin (BSA) on TSK-Gel DEAE-5PW Column (b_2=0.0) 138

6.2 Mass Transfer Rate Coefficient Concentration Dependence 139

7.1 RESOURCE-Q Columns Characteristics 140

7.2 Adsorption Isotherm Coefficients for the two RESOURCE-Q Columns (pH = 6.0, flow rate = 1.0 mL/min) 141

7.3 Mass Transfer Rate Coefficient. Parameters of the Concentration Dependence (pH=6.0, flow rate = 1.0 mL/min) 142

LIST OF FIGURES

FIGURE		PAGE
2.1	Band profiles used for the determination of the isotherm by ECP. KROMASIL columns	143
2.2	Band profiles used for the determination of the isotherm by ECP. VYDAC columns	144
2.3	Band profiles used for the determination of the isotherm by ECP. YMC columns	145
2.4	Band profiles used for the determination of the isotherm by ECP. ZORBAX columns	146
2.5	FA isotherms of 3-phenyl-1-propanol on KROMASIL	147
2.6	FA isotherms of 3-phenyl-1-propanol on VYDAC	148
2.7	FA isotherms of 3-phenyl-1-propanol on YMC	149
2.8	FA isotherms of 3-phenyl-1-propanol on ZORBAX	150
2.9	Comparison between experimental (symbols) and calculated (lines) band profiles for column YMC #2. Profiles calculated with the isotherm measured on the same column (solid line), with the isotherm measured on column #5 (dotted line), with the isotherm obtained by taking the average values of a ($a = k'/F$, Table 2.9, last row) (dashed line), and with the isotherm obtained by taking the average values of a and b after being corrected by the porosity (Table 2.9, row ϵ_e-ECP) (chain	

dot line) 151

3.1 Plot of the logarithm of molecular masses of the polystyrene standards injected versus their elution volumes @ 1.000 mL/min flow rate of methylene chloride. KROMASIL columns. □ column #1; ▵ column #2; + column #3; ▿ column #4; ○ column #5 152

3.2 Plot of the logarithm of molecular masses of the polystyrene standards injected versus their elution volumes @ 1.000 mL/min flow rate of methylene chloride. VYDAC columns. Symbols, see Figure 3.1 153

3.3 Plot of the logarithm of molecular masses of the polystyrene standards injected versus their elution volumes @ 1.000 mL/min flow rate of methylene chloride. YMC columns. Symbols, see Figure 3.1 154

3.4 Plot of the logarithm of molecular masses of the polystyrene standards injected versus their elution volumes @ 1.000 mL/min flow rate of methylene chloride. ZORBAX columns. Symbols, see Figure 3.1 155

3.5 Plot of the logarithm of molecular masses of the polystyrene standards injected versus their elution volumes @ 0.050, 0.200, 1.000, and 5.000 mL/min flow rates. ZORBAX column #2 156

3.6 Average pore size distribution of KROMASIL columns 157

3.7 Average pore size distribution of VYDAC columns 158

3.8 Average pore size distribution of YMC columns 159

3.9 Average pore size distribution of ZORBAX columns 160

4.1 SEM microphotography of KROMASIL particles.

a: x5000 161

b: x1000 162

4.2 SEM microphotography of VYDAC particles.

a: x5000 163

b: x1000 164

4.3 SEM microphotography of YMC particles.

a: x5000 165

b: x1000 166

4.4 SEM microphotography of ZORBAX particles.

a: x5000 167

b: x1000 168

5.1 Dependence of the retention factor on the packing pressure (psi). The percentage numbers in the figure legend represent the rsd of the results obtained on all ten columns. ACE: acetone; BAC: benzyl acetate; BAL: benzyl alcohol; CRE: m-cresol; DPH: 2,6-dimethyl phenol; MBE: methyl benzoate; PPR: 3-phenyl-1-propanol.

a: KROMASIL 169

b: ZORBAX 170

5.2 Dependence of the column efficiency on the packing pressure (psi). The percentage numbers in the figure legend represent the rsd of the results obtained on all ten columns. ACE, BAC, BAL, CRE, DPH, MBE, PPR: same as in Figure 5.1.

a: KROMASIL 171

b: ZORBAX 172

5.3 Chromatograms obtained for 4.2 mg of 3-phenyl-1-propanol on eight of the ten columns. Mobile phase, 45/55 (v/v) methanol/water, 1 mL/min. Stationary phase, KROMASIL.

a: Plots of C (mg/mL) versus time (min) 173

b: Plots of C (mg/mL) versus the retention factor 174

c: Plots of C (mg/mL) versus the ratio of the retention factor and the phase ratio 175

5.4 Same as Figure 5.3, but stationary phase ZORBAX.

a: Plots of C (mg/mL) versus time (min) 176

b: Plots of C (mg/mL) versus the retention factor 177

c: Plots of C (mg/mL) versus the ratio of the retention factor and the phase ratio 178

5.5 Comparison between the experimental chromatogram (symbols) and the band profile calculated on column #10. Solid line: calculation made with the isotherm coefficients obtained on the same column and with its stationary phase volume V_p. Long chain line: calculation made with the isotherm coefficients obtained on the same column and with its geometrical volume V_t. Short chain line: calculation made with the isotherm coefficients obtained on the #1 column, without modification. Dotted line: calculation made with the isotherm coefficients obtained on the #1 column, modified by the weight ratio of packing material.

a: KROMASIL. 179

b: ZORBAX 180

5.6 Plot of the column total porosity ϵ_T ($\diamond$), external porosity ϵ_e (+), and internal

porosity ϵ_i (□), versus the packing pressure P (psi).

a: KROMASIL. Solid line: $\epsilon_T = -2.7\text{x}10^{-6}*P + 0.6$; Long chain line: $\epsilon_e = -3.4\text{x}10^{-6}*P + 0.4$; Short chain line: $\epsilon_i = -6.2\text{x}10^{-7}*P + 0.3$ 181

b: ZORBAX. Solid line: $\epsilon_T = -2.0\text{x}10^{-6}*P + 0.6$; Long chain line: $\epsilon_e = -3.9\text{x}10^{-6}*P + 0.4$; Short chain line: $\epsilon_i = -1.1\text{x}10^{-6}*P + 0.3$ 182

6.1 Calculated isotherm data points (symbols) and the bi-Langmuir model fitting (lines) plotted as q versus C. Inset shows the Langmuir model fitting (lines). Experimental conditions: pH=7.5 and 1 mL/min flow rate, diamonds and solid lines; pH=6.0 and 1 mL/min, triangles and dotted lines; 2 mL/min, stars and dashed lines; and 3 mL/min flow rate, crosses 183

6.2 Scatchard plots of the isotherm data (symbols and lines correspond to conditions as described in Figure 6.1), q/C versus q 184

6.3 Comparison between the experimental breakthrough curves (symbols) and the simulated ones (lines) when the rate coefficient k_f is assumed to be independent of the sample concentration. Buffer pH = 7.5; Flow rate = 1.0 mL/min; k_f = 0.00133 s^{-1} 185

6.4 Same as Figure 6.3, but with Buffer pH = 6.0; Flow rate = 1.0 mL/min; k_f = 0.00167 s^{-1} 186

6.5 Same as Figure 6.3, but with Buffer pH = 6.0; Flow rate = 2.0 mL/min; k_f = 0.00167 s^{-1} 187

6.6 Comparison between the experimental breakthrough curves (symbols) and the simulated ones (lines) when the average rate coefficient k_f changes with the concentration. Simulated breakthrough curves are for the model with a constant

best average rate coefficient which, however, depends on the height of the concentration step (solid lines) and for a model with a rate coefficient depending on the concentration (dashed lines). Buffer pH = 7.5; Flow rate = 1.0 mL/min. The inset illustrates the sensitivity of the curve fitting on the value of a constant rate coefficient for the lowest step concentration. Symbols - experimental results; solid line - calculation with the best rate coefficient; dashed line - calculation with a 10% larger rate coefficient; dotted line - calculation with a 10% lower rate coefficient. 6 minutes are subtracted from the time of the experimental data . . . 188

6.7 Same as Figure 6.6, but with Buffer pH = 6.0; Flow rate = 1.0 mL/min 189

6.8 Same as Figure 6.6, but with Buffer pH = 6.0; Flow rate = 2.0 mL/min 190

6.9 Rate coefficient concentration dependence. Plot of the average rate coefficient k_f versus the average sample concentration C_{ave} (symbols and lines as described in Figure 6.1). Correlation obtained:

At pH = 7.5, 1.0 mL/min, $k_f = (9.3*C+1.9)/1000$;

At pH = 6.0, 1.0 mL/min, $k_f = (9.6*C+0.6)/1000$;

At pH = 6.0, 2.0 mL/min, $k_f = (18.8*C+0.4)/1000$ 191

7.1 Calculated isotherm data points (symbols) and the bi-Langmuir model fitting (lines) plotted as q versus C. Resource-Q column No.1: ◇ and solid line; Resource-Q column No.2: + and dashed line 192

7.2 Comparison between the experimental breakthrough curves (symbols) and the simulated ones (lines) when the rate coefficient k_f is assumed to be independent of the sample concentration. Resource-Q column No.1.

a: For low sample concentrations 193

b: For high sample concentrations 194

7.3 Same as Figure 7.2, but for Resource-Q column No.2.

a: For low sample concentrations 195

b: For high sample concentrations 196

7.4 Comparison between the experimental breakthrough curves (symbols) and the simulated ones (lines) when the rate coefficient k_f changes with the concentration. Resource-Q column No.1.

a: For low sample concentrations 197

b: For high sample concentrations 198

7.5 Same as Figure 7.4, but for RESOURCE-Q column No.2.

a: For low sample concentrations 199

b: For high sample concentrations 200

7.6 Rate constant concentration dependence for both Resource-Q columns No. 1 and 2. Plot of the average rate coefficient k_f versus the average sample concentration C_{ave} 201

LIST OF SYMBOLS

a	first coefficient of the Langmuir isotherm
a_C	Courant number
a_1	a numerical coefficient of the bi-Langmuir isotherm
a_2	a numerical coefficient of the bi-Langmuir isotherm
b	second coefficient of the Langmuir isotherm
b_{Vt}	second coefficient of the Langmuir isotherm calculated by column geometrical volume
b_{Vp}	second coefficient of the Langmuir isotherm calculated by packing volume
b_w	second coefficient of the Langmuir isotherm calculated by packing weight
b_1	a numerical coefficient of the bi-Langmuir isotherm
b_2	a numerical coefficient of the bi-Langmuir isotherm
C	mobile phase concentration
C_i	mobile phase concentration at the *i*th concentration step
d	column inner diameter
d_p	packing material actual density
D_a	apparent axial dispersion coefficient
D_L	axial dispersion coefficient
F	phase ratio
H	height equivalent to a theoretical plate
k'	retention factor
k_f	lumped mass transfer coefficient in the solid film linear driving force model

l	column length
Mr_n	average molecular weight of the polymer standards
N_0	column efficiency under linear conditions
P	pressure
Q	actual stationary phase concentration
q	concentration in the stationary phase in equilibrium with the mobile phase
q_i	stationary phase concentration in equilibrium with the ith concentration step which has the mobile phase concentration C_i
q_s	column saturation capacity
$q_{s,Vt}$	column saturation capacity calculated by column geometrical volume
$q_{s,Vp}$	column saturation capacity calculated by packing volume
$q_{s,w}$	column saturation capacity calculated by packing weight
r	column radius
St	Stanton number
t	time
t_p	injection time
t_R	retention time of the band maximum
t_0	column hold-up time
u	mobile phase linear flow-velocity or average interstitial velocity
V	retention volume of the point of the diffuse boundary at concentration C
V_a	volume of the layer of C_{18} bonded chains
V_c	closed pore volume
V_e	inter-particle, interstitial, or external pore volume

$V_{F,i}$ retention volume of the ith concentration step

$V_{F,i+1}$ retention volume of the $i+1$th concentration step

V_i internal pore volume

V_k column geometrical volume

V_n volume of the pores having a size equal to or larger than ϕ_n

V_p packing volume

V_s stationary phase solid volume

V_T total accessible pore volume inside the column

$V_{T,u}$ column total accessible volume by uracil

$V_{T,b}$ column total accessible volume by benzene

V_U unaccessible volume

V_0 column hold-up volume

W empty column weight

W^* empty column and packing weight

W_p packing weight

z abscissa or distance along the column length

Δt_w band width at half height

ϵ_a volume fraction of the layer of C_{18} bonded chains

ϵ_c volume fraction of the closed pores

ϵ_e column external porosity

ϵ_i column internal porosity by chemical engineering definition

ϵ_i' column internal porosity by chemistry definition

ϵ_s volume fraction of the skeleton of solid silica

ϵ_T column total porosity

$\epsilon_{T,b}$ column total porosity from benzene

$\epsilon_{T,u}$ column total porosity from uracil

ϵ_U unaccessible volume fraction

ρ_a density of alkyl chains

ρ_s density of solid silica

ϕ_n average diameter of the pores from which the polymer standards are excluded

Abbreviations:

ACE acetone

Ave. average

BAC benzyl acetate

BAL benzyl alcohol

DPH 2,6-dimethyl phenol

ECP elution by characteristic points

FA frontal analysis

ISEC inverse size exclusion chromatography

IXLC ion exchange liquid chromatography

MBE methyl benzoate

MCR m-cresol

PPR 3-phenyl-1-propanol

psd pore size distribution

RPLC reverse phase liquid chromatography

rsd	relative standard deviation
SEC	size exclusion chromatography
SFL	solid film linear driving force model
Std.	standard deviation
URA	uracil

CHAPTER 1.

INTRODUCTION

General Background

An early study divided the general goals of separation into two broad categories: preparative and analytical [Rogers, 1968]. For a given separation system in preparative work, the total value of product increases approximately as the amount of isolated material increases. "Therefore, preparative separations tend to be continuous in operation and large in scale. Some of them are plant scale - enormous industrial processes such as distillation, extraction, and smelting, typically producing many tons of separated products per day" [Giddings, 1991]. Analytical goals, on the other hand, focus on the information generated in the separation process. "In a strict analytical sense, separation methods are simply tools to multiply the quantity of detailed information available about complex mixtures and to enhance the quality of that information" [Giddings, 1991].

Despite of the various separation techniques that have been developed, chromatography remains to play an important role in analysis [Willard *et al*, 1988; Skoog *et al*, 1988; Strobel *et al*, 1989]. It was first discovered in the early 20th century by a Russian botanist Tswett [Tswett, 1905; Sakodynskii, 1970; Sakodynskii, 1972; Verzele *et al*, 1986]. However, it was not until mid-1930s that the importance of chromatography became recognized by chemists and biochemists. The development of chromatographic technique was followed by the discoveries of paper chromatography [Martin *et al*, 1941], size exclusion chromatography [Lathe *et al*, 1956], and affinity chromatography [Cuatrecasas *et al*, 1971], *etc*, which made it become a powerful tool

used for the separation and purification of various components over a wide range of production rates (from a few mg in one run to several hundreds tons per year) [Spedding *et al*, 1947; Mair *et al*, 1956; Chang *et al*, 1976; Roz *et al*, 1976; Kato *et al*, 1982a,b; Bonmati *et al*, 1984; Verzele *et al*, 1986; Regnier, 1987; Guiochon *et al*, 1987; Huang *et al*, 1989; Fulton *et al*, 1991; King *et al*, 1992; Liapis, 1993; Nicoud *et al*, 1993; Horvath *et al*, 1994].

Mass Balance Equation

The fundamental equation used in liquid chromatography, both analytical and preparative, is the mass balance equation. For a single component system it can be expressed as[1] [Wicke, 1939; Wilson, 1940; DeVault, 1943]

$$\frac{\partial C}{\partial t} + F\frac{\partial Q}{\partial t} + u\frac{\partial C}{\partial z} = D_L\frac{\partial^2 C}{\partial z^2} \tag{1.1}$$

where C and Q are the concentrations of the solute in the mobile and stationary phases, respectively, F the phase ratio, and D_L the axial dispersion coefficient. For a multi-component system, this mass balance equation is written for each single component.

In order to apply the mass balance equation to a liquid chromatography system, there requires some basic conditions. First, the column has to be radially homogeneous and the axial dispersion remains the same at all times. These conditions become critical for preparative chromatographic columns as they tend to be longer in length and/or bigger in diameter, *i.e*, when comparing with analytical chromatographic columns. Second, the mobile phase used should be incompressible and should not be adsorbed on to the stationary phase. Third, the sample component should have equal partial molar volume in both the mobile and the stationary phases.

---

[1]See List of Symbols.

Finally, there should be no thermal effects involved or additional thermodynamic relations will be needed [Guiochon *et al*, 1994].

The initial state (at time $t=0$) of a chromatographic column can be described by the initial condition. If the initial sample concentration in the column is zero, we then have $C_i(z,0) = 0$. If the initial sample concentration is known as C_a^0, we then have $C_i(z,0) = C_a^0$. The boundary condition(s), on the other hand, restrict that the amount of the sample, once injected, remains constant at all times during the experiment. In order to solve the differential mass balance equation (Eq. 1.1), a relation that links the sample stationary phase concentration Q and the mobile phase concentration C - the equilibrium or adsorption isotherm - is needed.

Relation Between the Concentrations in the Stationary and the Mobile Phase

In a chromatographic system, the continuous stream of the mobile phase pushes the sample components along the column, and the mobile phase drift thwarts the drive toward equilibrium resulting from the difference in the chemical potentials of each component in the two phases. Both the mass transfer kinetics between the bulk mobile phase stream and the inner surface of the pores of the packing particles and axial dispersion proceed at a finite rate. The relationship between the local concentrations of a compound in both phases should be given by a kinetic equation or by a set of several kinetic equations. These equations are little known and even their functional structure can only be approximated. However, it is known that chromatography is carried out under conditions where equilibrium is reached rapidly. Therefore, it can be assumed that the two phases are either always at equilibrium or near equilibrium. In the first case, the small residual difference between the local stationary phase concentration of a compound in the mobile phase and the equilibrium composition is accounted for as an apparent dispersion contribution. In the second

case, the difference between the actual composition of one phase (stationary or mobile phase) and its composition at equilibrium with the other phase can be considered as a perturbation, and the mass transfer kinetics between phases is assumed to be linear. In order to use the mass balance equation (Eq. 1.1) to calculate the band profile, the equilibrium isotherm must be determined in advance. Furthermore, it is also the key to scale up from analytical chromatography to preparative chromatography.

Linear and Nonlinear Chromatography

In linear chromatography, the equilibrium concentrations of a component in the stationary and the mobile phase are directly proportional to each other, *i.e.*, the equilibrium isotherm is a straight line beginning at the origin. The individual band shapes and the retention times are independent of the sample composition and amount. The peak height is proportional to the amount of each component in the injected sample. Linear chromatography accounts well for most of the phenomena observed in the analytical applications of chromatography, as long as the injected amounts of the sample components are kept sufficiently low.

In nonlinear chromatography, the equilibrium concentration of a component in the stationary phase is no longer proportional to that in the mobile phase, *i.e.*, the equilibrium isotherm is not linear any more. Furthermore, this isotherm also depends on the concentration of all the other components in the mixture. Therefore, the band shape, peak maximum, and retention time are all dependent on the sample composition and amount. This is the situation found in practically all preparative applications. The problems of nonlinear chromatography are extremely complex due to the interdependence of the individual band profiles caused by the dependence of the amount of any component adsorbed on the concentrations of all the species in solution.

Band Profile Calculation

Once the equilibrium isotherm has been determined and the initial and boundary conditions have been set, one can calculate or simulate the band profile by solving the differential mass balance (Eq. 1.1). Various models have been suggested to achieve this goal [Phillips *et al*, 1988; Howard *et al*, 1988; Golshan-Shirazi *et al*, 1989; Yu *et al*, 1989], as summarized below.

When the mass transfer kinetics inside the liquid chromatographic system is infinitely fast and axial diffusion negligible, the column efficiency is infinite. Then there is no axial dispersion, *i.e.*, $D_L = 0$, and there is always a constant equilibrium between the mobile and stationary phase. This is the ideal model of nonlinear chromatography [Wicke, 1939; Wilson, 1940; DeVault, 1943]. In this case, Eq. 1.1 becomes

$$\frac{\delta C}{\delta t} + F\frac{\delta q}{\delta t} + u\frac{\delta C}{\delta z} = 0 \tag{1.2}$$

Equation 1.2 can be solved in a closed form for one component system with many equilibrium isotherm models used [Golshan-Shirazi *et al*, 1988; Golshan-Shirazi *et al*, 1990].

In practice, however, the mass transfer kinetics can never be infinitely fast. If the agreement between the overloaded sample experimental chromatogram and the simulated band profile which is calculated by use of the ideal model is poor, this indicates the column used has a finite efficiency. In this case, the more complicated equilibrium-dispersive model should be used [Van Deemter *et al*, 1956; Giddings, 1965; Haarhoff *et al*, 1966]. Then Eq. 1.1 is replaced by

$$\frac{\delta C}{\delta t} + F\frac{\delta q}{\delta t} + u\frac{\delta C}{\delta z} = D_a\frac{\delta^2 C}{\delta z^2} \tag{1.3}$$

Here the axial dispersion coefficient D_L in Eq. 1.1 has been replaced by the constant apparent axial dispersion coefficient D_a, which lumps together all the contributions due to the nonequilibrium.

It can be calculated by

$$D_a = \frac{Hl}{2t_0} = \frac{Hu}{2} \tag{1.4}$$

where H is the height equivalent to a theoretical plate.

In nonlinear chromatography, there are no closed form solutions to the equilibrium-dispersive model based mass balance equation (Eq. 1.4). Numerical solutions, however, can be obtained by computational methods [Craig, 1944; Rouchon *et al*, 1987; Guiochon *et al*, 1988; Czok *et al*, 1990; Ma *et al*, 1991]. During this study, the Rouchon algorithm is used [Rouchon *et al*, 1987; Guiochon *et al*, 1988].

In Rouchon algorithm, part of the cell content is assumed to be frozen in time. Although this has no physical meaning, it leads to a fast and reasonably accurate computation method. The partial differential equation (Eq. 1.3) can then be replaced by

$$\frac{C_{z,t} - C_{z,t-1}}{\Delta t} + F\frac{q_{z,t} - q_{z,t-1}}{\Delta t} + u\frac{C_{z,t-1} - C_{z-1,t-1}}{\Delta z} = 0 \tag{1.5}$$

Because of truncations, numerical error is introduced and accumulated during the calculation when using this algorithm. It has been shown [Lin *et al*, 1989] that this error is equivalent to an apparent dispersion term that is given by

$$D_a = \frac{\Delta z u}{2}(a_C - 1) \tag{1.6}$$

where a_C is the Courant number [Courant *et al*, 1928] given by

$$a_C = \frac{u\Delta t}{(1 + k')\Delta z} \tag{1.7}$$

In order to apply the Rouchon algorithm, the Courant number a_C must be bigger than unity in

order to assure the convergence of the calculation. A Courant number of 2 was chosen during this study.

Overview

Much fundamental work has been done on the comparison of the properties of analytical columns packed with various packing materials [Colin *et al*, 1978a, b; Greyson *et al, 1982*], of columns packed with the same material but prepared with different reagents [Roumeliotis *et al*, 1978], and of columns packed with the same type of material but produced by different manufacturers [Smillie *et al*, 1978; Ogan *et al*, 1979; Ogan *et al*, 1980]. However, almost all these studies were undertaken using methods of linear chromatography, with the single aim to facilitate its analytical applications. Accordingly, they are mainly focused on the separation factors of the columns being compared, on the dependence of the retention factor on various experimental parameters, and on the column efficiency. While this last parameter depends mostly on the packing method used and on the skill of the operator and, with proper care, can be improved to a certain extent, the other two have been found to depend essentially on the origin of the material used, to be most difficult to adjust, and not easy to reproduce. Considerable attention has been paid to the column to column, batch to batch, and manufacturer to manufacturer reproducibilities of analytical performance [Wise *et al*, 1983; Sander *et al*, 1984; Olsson *et al*, 1989]. The first has generally been found to be excellent, the second acceptable, the third poor, as if the stationary materials produced using different processes were almost entirely different products.

Except for a recent report discussing the performance of overloaded chromatographic columns [Miller, 1991], little attention has been awarded to the column characteristics which are important in preparative chromatography. These are the kinetics of mass transfer and of

adsorption-desorption in the column and the equilibrium isotherms of the components of interest between the stationary and the mobile phase. The column efficiency is a measure of the rate of the mass transfer kinetics in the column. The initial slope of the isotherm is proportional to the retention factor, so many of the conclusions of analytical studies are applicable to this isotherm parameter. The nature of the isotherm, its initial curvature, and its saturation capacity are other parameters of importance for preparative chromatography. There is at present little comparative information on these parameters.

The goal of this work is to investigate the feasibility of a comparison of the performance of stationary phases for preparative liquid chromatography. A number of issues must be clarified, such as (I) what is the reproducibility of column parameters when several similar columns are prepared at the same time with the same packing; (ii) how close are the parameters of these columns; (iii) what is the origin of the column irreproducibility; (iv) how can the classical mass transfer kinetics data be used in preparative chromatography. The amount of data required for a thorough comparison could be considerable. The scope of the work has to be limited to the essential if the approach is to be useful for the selection of the best stationary phase for practical applications.

Two types of packing materials were studied, *i.e.*, octadecyl-bonded silica adsorbents (ODS) and anion exchanger resins. The corresponding chromatographic modes used are therefore: Reversed Phase Liquid Chromatography (RPLC), which uses polar mobile phase and nonpolar stationary phase, and Ion Exchange Liquid Chromatography (IXLC), which is based on the reversible binding between the electrically charged group of the compounds carried by the mobile phase and the oppositely charged ligand of the packing material. When applying RPLC, attention was focused on the column performance reproducibility. The source for the

irreproducibility was investigated from the packing density view point, which in part was done by applying Inverse Size Exclusion Chromatography (ISEC) to determine the column external porosity and packing density. For IXLC, emphasis was put on the mass transfer kinetics between proteins and the ion exchanger stationary phase.

The organization of this dissertation is the following:

Chapter 2 discusses the reproducibility, accuracy, and correction of isotherm data measured by chromatography on four commercially available 10 μm C_{18} packing materials: KROMASIL, VYDAC, YMC and ZORBAX. Each stationary phase was packed into five 10 x 0.46 cm columns. The mixture of 45/55 (v/v) methanol/water was used as the mobile phase and solvent. The column efficiencies and retention factors were determined for a series of compounds: acetone, benzyl acetate, benzyl alcohol, m-cresol, 2,6-dimethyl phenol, methyl benzoate, 3-phenyl-1-propanol, and uracil, all eluted under infinite dilution conditions. Chromatograms were obtained by overloading the columns with 35 mg/mL 3-phenyl-1-propanol solutions into each column and the equilibrium isotherms were determined. The results obtained were compared on a column-to-column basis. It was found that different columns packed with materials from the same lot have significantly different thermodynamic properties. Attempts made to correct the deviations among the isotherms by retention factors and phase ratios were unsuccessful. An early study exploring the source of the deviation was made by measuring the column external porosity data. As a result, the equilibrium isotherms obtained from different columns, after being corrected by the individual column external porosity, become less scattered, indicating a substantial relation between the packing density of the column and its performance.

In Chapter 3, the use of Inverse Size Exclusion Chromatography (ISEC) method to determine the external porosity of liquid chromatographic columns is proposed and described in

detail, in order to improve the understanding of the column packing density and of the bed consolidation that has been frequently encountered in preparative chromatography. A series of polystyrene standards with molecular masses ranging from 456 to 20,600,000 Dalton was injected into each of the columns used in Chapter 2. The internal and external pore volumes, hence porosities, of the columns were determined accurately from the plots of the logarithm of the molecular mass of the probes versus their retention volume. This procedure offers a simple, fast, and convenient method of determining the external porosity of the columns. This porosity correlates with the retention data and equilibrium isotherms, as illustrated in Chapter 2.

In Chapter 4, some general properties of the packing particles are investigated. First, Scanning Electron Microscopy (SEM) revealed the shape and illustrates the particle size distribution of the four different brands of spherical silica particles used in the packed columns in Chapter 2, showing that the packing materials are too irregular to allow their packing as a regular hexagonal assembly of the particles. Results given by Helium Pycnometry provided a direct estimate of the unaccessible volume fraction in a column. The retention volumes of benzene in methylene chloride and of uracil in methanol provided two independent estimates of the total column porosity which are in excellent agreement. Within 2 to 3 %, the sum of these two fractional volumes is equal to unity, as expected. Furthermore, estimates of the volume fractions of the column occupied by the bonded layer and the silica skeleton for two of the packing materials suggest that the closed pore porosity is 1 to 2 % at most therefore negligible.

In Chapter 5, the significance of the packing pressure on the performance of reversed phase liquid chromatographic columns is discussed. Two groups of ten analytical (10 x 0.46 cm) columns, packed with KROMASIL and ZORBAX 10 μm spherical C_{18} respectively, were used for this study. The packing pressure used for column # *j* in each group was 1,000 x *j* psi. The

weight of packing material inside each column increased with increasing packing pressure. The column external porosity, determined by Inverse Size Exclusion Chromatography (ISEC) method, decreased as the packing pressure increases, while the internal porosity remained constant. Linear chromatography data and equilibrium isotherms were determined by the same way as in Chapter 2. It was found that both the retention factor and the column efficiency of each compound increase linearly with increasing packing pressure. The isotherm data were normalized by the column geometrical volume, the stationary phase volume, and by the weight of packing material. The parameters obtained from the isotherm normalized by the first method cannot predict the band profile accurately. Better results were obtained from the second method. Close agreement was obtained between the parameters obtained by the third method. This allowed a reasonable prediction of the band profiles recorded on one column using isotherm data measured on another column. Considering the difficulties encountered in volume determinations, normalization of isotherm data by the packing weight seems to be the most practical solution.

Chapter 6 discusses the study on another type of commonly used stationary phase in preparative chromatography - ion exchange resin. The stationary phase used in this case is the TOSOHAAS TSK-Gel DEAE-5PW anion exchanger. The adsorption isotherms of Bovine Serum Albumin (BSA) on this column are determined in a pH = 7.5 buffer for a 1.0 mL/min flow rate and at pH = 6.0 for 1.0, 2.0 and 3.0 mL/min flow rates. The isotherm data were derived from the breakthrough curves obtained by step series Frontal Analysis (FA) method. The sample concentrations ranged from ca. 0 to 3 mg/mL. From the Scatchard plots, it was found that the bi-Langmuir isotherm model fits the adsorption isotherm data better than the single Langmuir isotherm model at both pH = 7.5 and 6.0, for flow rates up to 2.0 mL/min. The rate of the mass transfer kinetics was determined for each breakthrough curve by using a lumped kinetic model.

It was found that the average rate coefficient depends linearly on the average sample concentration.

In Chapter 7, the performance of two identical Pharmacia RESOURCE-Q anion exchange columns (same catalog number but different lot numbers) was studied for their reproducibility and mass transfer kinetics. The phase ratios of the two columns, derived from uracil retention volumes, were quite different. Series of breakthrough curves of Bovine Serum Albumin (BSA) in a pH = 6.0 buffer, at 1.0 mL/min flow rate were obtained for each column in the concentration range of 0 to 4 mg/mL. They were used to determine the adsorption isotherms. The experimental data obtained for both columns fit best to a bi-Langmuir isotherm model with a linear second term. The isotherm coefficients were significantly different for the two columns. This confirms the previous finding that columns packed with the same stationary phase could have quite different characteristics. An average rate coefficient of mass transfer kinetics was determined by fitting each breakthrough curve to the profiles calculated with a lumped kinetic model and identifying the parameter. This rate coefficient was found to depend linearly on the average sample concentration. This result is qualitatively the same as the one found earlier with TOSOHAAS DEAE-5PW TSK-Gel anion exchanger. However, the magnitude was very different for the two RESOURCE-Q columns used during this study and for the TOSOHAAS DEAE-5PW TSK-Gel anion exchanger of the previous study.

Each of these chapters was submitted separately to a scientific journal for publication. Most have been accepted and a few published already. Therefore each has its own introduction, theory, experimental, results and discussion, and conclusion sections. They have been modified slightly in order to fit into this dissertation.

Finally, in Chapter 8, the conclusions drawn during this study are summarized.

CHAPTER 2.

REPRODUCIBILITY, ACCURACY, AND CORRECTION OF ISOTHERM DATA MEASURED BY CHROMATOGRAPHY

Introduction

In spite of specific problems related to the relatively poor solubility of organic compounds in the aqueous mobile phases which have to be used in this mode, reversed phase chromatography is widely used in preparative applications for the same convenience reasons which have caused it to become the most important mode of analytical liquid chromatography for over twenty years [Poole *et al*, 1993]. The most popular adsorbent used in this method is octadecyl-bonded silica (ODS). Much work has been done on the acquisition, compilation, comparison, correlation, and prediction of retention data on ODS [Knox *et al*, 1969; Majors, 1972; Locke, 1973; Grushka, 1974; Martin *et al*, 1975; Unger *et al*, 1978; Colin *et al*, 1978a, b, c; Roumeliotis *et al*, 1978; Smillie *et al*, 1978; Ogan *et al*, 1979; Ogan *et al*, 1980; Greyson *et al*, 1982; Miller, 1991]. Comparisons have been made of the properties of ODS-packed columns with those of columns made of other packing materials [Colin *et al*, 1978a, b; Greyson *et al*, 1982], of columns packed with ODS prepared with different reagents [Roumeliotis *et al*, 1978], and of columns packed with ODS produced by different manufacturers [Smillie *et al*, 1978; Ogan *et al*, 1979; Ogan *et al*, 1980]. However, all these studies are mainly concerned with analytical applications.

In preparative chromatography, characteristics of the column or the packing material which are secondary in analytical applications acquire a great importance. The equilibrium

isotherms of the feed components of interest between the stationary and the mobile phase and the parameters of the mass transfer kinetics become dominant factors that directly affect column performance. Of special concern is the possibility to scale-up design and operating conditions acquired on small columns or to predict such conditions on the basis of theoretical considerations and characteristics of the packings measured on analytical scale columns [Guiochon *et al*, 1994]. Because of the complexity of this issue whose importance has been recognized only recently, there is comparatively little information available in this area.

Previous studies [Guan *et al*, 1994b, c] have shown a limited column-to-column reproducibility of the equilibrium isotherms, whether the columns had the same dimensions or not. This difference could be corrected for to a large extent by normalizing the equilibrium isotherm using the ratio of the retention factors. This correction allowed the use of the isotherm measured on one column for the prediction of the band profiles obtained with another one [Guan *et al*, 1994b]. It is completely empirical, however, and provides no clues regarding the origin of the problem. Further investigations during which the actual packing density of the columns could be directly or indirectly determined appeared necessary.

The goal of this chapter is a further investigation of the cause of the lack of reproducibility of isotherm data and an attempt at relating it to the lack of reproducibility of the apparent density of the column packing.

Theory

Under linear conditions, the sample concentrations in the stationary and the mobile phase at equilibrium are proportional and two parameters suffice to characterize the elution profile of a component, the retention factor k'

$$k' = \frac{t_R - t_0}{t_0} \tag{2.1}$$

where t_R is the retention time of the infinite diluted sample and t_0 is the column hold-up time, and the column efficiency for a zero sample size, N_0,

$$N_0 = 5.54 \left(\frac{t_R}{\Delta t_w}\right)^2 \tag{2.2}$$

where Δt_w is the band width at half height.

When the column is overloaded, the equilibrium concentrations in the stationary and mobile phase are no longer directly proportional. The retention factor does not suffice to characterize equilibrium but the whole equilibrium isotherm is needed. It can be determined by Elution by Characteristic Points (ECP) or Frontal Analysis (FA). The relative advantages and inconveniences of these methods are discussed elsewhere [Huber *et al*, 1971; Gerritse *et al*, 1972; Guiochon *et al*, 1994; Guan *et al*, 1994a, b].

The ECP method relates the equilibrium isotherm and the profile of the diffuse boundary of a large concentration band by

$$q = \frac{1}{V_p} \sum_{0}^{C} (V - V_0)\, \delta_i C \tag{2.3}$$

where V_p is the stationary phase volume in the column, V_0 is the column hold-up volume, V is the retention volume of the point of the diffuse boundary at concentration C, and $\delta_i C$ is the increment ($\sum \delta_i C = C$). Since the ECP method assumes infinite column efficiency [Guiochon *et al*, 1994]

and all columns have a finite efficiency, the isotherm data contains a model error [Huber *et al*, 1971; Gerritse *et al*, 1972; Guan *et al*, 1994a] which is minimized by using columns having a minimum of 2,000 theoretical plates [Guan *et al*, 1994a].

The FA method is independent of column efficiency [James *et al*, 1954; Schay *et al*, 1954; Huber *et al*, 1971; Gerritse *et al*, 1972; Eltekov *et al*, 1985; Eltekov *et al*, 1986; Guan *et al*, 1994c]. It measures the retention times of successive, abrupt concentration steps. The isotherm can then be determined by

$$q_{i+1} = q_i + \frac{(C_{i+1} - C_i)\,(V_{F,i+1} - V_0)}{V_p} \tag{2.4}$$

where q_i and q_{i+1} are the stationary phase concentrations in equilibrium with the ith and $i+1$th concentration steps, which have the mobile phase concentrations C_i and C_{i+1}, respectively.

The isotherm model used in this work is the Langmuir isotherm

$$q = \frac{a\,C}{1 + bC} \tag{2.5}$$

where q is the stationary phase concentration, C is the mobile phase concentration, a and b are numerical coefficients.

Experimental

Equipment

All experiments were made on a Hewlett-Packard (Palo Alto, CA) HP1090M liquid chromatograph with a diode-array UV detector and a computerized data acquisition system. All measurements were done with a flow rate of 1.000 mL/min and a detector wavelength of 250 nm,

except FA which was run at 270 nm.

Columns

The empty stainless steel columns were purchased from Alltech (Deerfield, IL). All columns are 10 cm long and 0.46 cm I.D. Samples of four 10 μm spherical C_{18} ODS packing materials were obtained: KROMASIL (Eka-Nobel, Stratford, CT), VYDAC (Hesperia, CA), YMC (Wilmington, NC), and ZORBAX (BTR, Wilmington, DE). Each material was slurry packed into five columns on the same day, starting with column #1 and ending with column #5. The lot numbers of each material and the column packing conditions are listed in Table 2.1[2]. The methods used for packing the columns were those recommended by the respective manufacturers.

Chemicals

Uracil (Cat. No. 13078-8), m-Cresol (Cat. No. C8572-7, 99%), Benzyl alcohol (Cat. No. B1620-8, >99%), Methyl benzoate (Cat. No. M2990-8, 99%) and 2,6-dimethyl phenol (Cat. No. D17500-5, 99%) were purchased from Aldrich (Milwaukee, WI); Acetone (Cat. No. AX0120-8, >99.5%) was purchased from EM Science (Gibbstown, NJ); Benzyl acetate (Cat. No. 45850, >99%), 2-isopropyl phenol (Cat. No. 59720, >98%) and 3-phenyl-1-propanol (Cat. No. 79000, >98%) were purchased from Fluka (Buchs, Switzerland).

Both the mobile phase and the solvent used to dissolve samples were 45/55 (v/v) methanol/water mixture. Methanol (Cat. No. 9093-33) was purchased from J. T. Baker (Phillipsburg, NJ). Water was freshly bidistilled/deionized in the laboratory, using a Thermolyne (Barnstead, Dubuque, IA) water-deionizing system consisting of two cartridges, one HN high-

[2] See Appendix for all Tables.

capacity DI cartridge (Cat. No. D8901) and one HG organic-removal cartridge (Cat. No. D8904). All samples and solvents were filtered on 0.45 μm pore size filters before use.

Procedures

Samples used for the measurements of k' and N_0 were 75.7 μg acetone and 25.0 μg each of m-cresol, benzyl alcohol, methyl benzoate, benzyl acetate, 2-isopropyl phenol, 2,6-dimethyl phenol and 3-phenyl-1-propanol. A 0.66 μg uracil sample was injected into each column for the determination of the system hold-up time and the average total porosity of the column, data which were later used for the equilibrium isotherm determinations by ECP and FA. The phase ratios were determined from the column porosities derived from inverse size-exclusion chromatography [see Chapter 3]. Before using them for the calculation of k', ECP or FA data, retention volumes are corrected for the hold-up volume of the apparatus. The later is determined by replacing the column with a small connecting union, 2 mm long and 0.78 mm i.d. (volume ca 1 μL). The results are summarized in Table 2.2. Each k' and N_0 measurement was made twice and the data listed in the Table is their average.

The ECP measurements were made by injecting 0.120 mL of 5.00 mg/mL, 20.00 mg/mL and 34.78 mg/mL 3-phenyl-1-propanol solutions into each column. The chromatograms obtained with the largest sample were used to calculate the ECP isotherm coefficients for each column [Guan *et al*, 1994a]. Each measurement was made twice and the final result was taken as the average.

FA measurements were made by designing a program that has 16 successive concentration step changes. Two pumps, one for the 45/55 (v/v) methanol/water mobile phase and the other one for a 34.00 mg/mL solution of 3-phenyl-1-propanol in the same solvent, were used for this

purpose. The detector response was saturated at concentrations above ~ 22 mg/mL, preventing the acquisition of data at higher concentrations.

Detector Calibration

ECP requires detector calibration in order to translate the detector signal (mAu) into solute concentration (mg/mL). Calibration was performed by pumping solutions of known concentration directly into the detector cell until a stable signal was obtained. A third-order polynomial gave an excellent fit to the experimental data. The best coefficients of the fit were obtained by applying the polynomial regression in SigmaPlot (Jandel, San Rafael, CA) to the experimental data points.

Results and Discussion

Linear Chromatography Data (k' and N_0)

The values obtained for k' and N_0 are listed in Tables 2.3 (KROMASIL), 2.4 (VYDAC), 2.5 (YMC), and 2.6 (ZORBAX). Although the columns were packed successively, with materials of the same lot, and had the same dimensions, there are usually minor column-to-column fluctuations of k' but very large such fluctuations of N_0. For the retention factor, the relative standard deviation (rsd) is always less than 2%; it is less than 1% with VYDAC (except with acetone). For the column efficiency, the rsd is 15 to 20% for KROMASIL, slightly less for VYDAC, and of the order of 5% for YMC and ZORBAX. This may be explained in part by the tough conditions of packing the KROMASIL columns. For KROMASIL and VYDAC, the efficiency of the first column packed was markedly poorer than the efficiency of the other four columns. The efficiency varies significantly from one compound to another, with the highest efficiency being recorded for benzyl acetate (only two minor exceptions).

As previously reported [Smillie *et al*, 1978; Ogan *et al*, 1979; Ogan *et al*, 1980], columns packed with different stationary phases give different values of k' and N_0 for the same compounds, although these packing materials differ only in the particle pore size distribution. Retention tends to be highest on KROMASIL and lowest on ZORBAX. Although the packing pressure used for the YMC and ZORBAX columns differ by 50% (Table 2.1), their efficiencies are close.

Acetone appears to be slightly retained on all the columns. This compound was used by some to measure the column hold-up volume in reversed-phase liquid chromatography. This is not a safe practice [Kirkland *et al*, 1984].

Chromatograms

The chromatograms obtained for the largest sample injected on each column are shown in Figures 2.1 to 2.4[3]. They differ from column to column, the main differences being in the retention time of the band front. The differences are much more important between band profiles on columns packed with different materials, indicating markedly different equilibrium isotherms.

Equilibrium Isotherms

The equilibrium isotherms were determined using both the ECP and FA methods. The FA isotherms are illustrated in Figures 2.5 to 2.8. As in previous work [Guan *et al*, 1994b], the differences between equilibrium isotherms obtained for columns packed with the same ODS phase are significant. By contrast, isotherms obtained at several week intervals on the same column would not be distinguished from each other on the figures. The isotherm coefficients were derived

[3] See Appendix for all Figures.

by applying the SAS non-linear regression routine available at the University of Tennessee Computer Center (UTCC) to the isotherms obtained by both ECP and FA methods. The results are listed in Tables 2.7 (KROMASIL), 2.8 (VYDAC), 2.9 (YMC), and 2.10 (ZORBAX). As we can see, the overall agreement between the isotherm coefficients derived by ECP and FA is quite good. Note also that the rsd of the isotherm coefficients are generally between 1 and 2%, which can be considered as quite satisfactory.

In general, ECP tends to give a better estimate of coefficient *a* since it gives many data points in the low concentration range where the isotherm data is mainly controlled by the initial slope of the isotherm. Frontal analysis, on the other hand, gives a better estimate of the coefficient *b* since it is possible to reach much higher concentrations in FA than in ECP. An excellent fit of the experimental data and an accurate isotherm can be obtained by combining in the nonlinear regression the FA and ECP data and giving the same total weight to each set of data points.

Based upon these isotherm coefficients, it is possible to calculate the band profiles and compare them with the experimental chromatograms. The agreement between the two sets of profiles was excellent for all the columns examined when the calculation is performed with the isotherm measured on the column on which the profiles are recorded. Data are shown only for the YMC phase (Figure 2.9, solid line and symbols). A comparison of the experimental band profiles (symbols) and the profiles calculated using the isotherm determined on a different column is also shown in Figure 2.9 (dotted line). The agreement is poor and illustrates the difficulties which may be encountered when trying to optimize the experimental conditions of a preparative separations using data measured with an analytical column.

Isotherms Normalized by the Ratios of k's

The most probable source of the differences observed between the equilibrium isotherms measured on columns packed with the same ODS phase is a difference in packing density [Guiochon *et al*, 1995]. In this case, it is possible to correct for these differences by using the ratio of the retention factors on two columns. This correction is justified by the relationship

$$k' = F a = \frac{1-\epsilon_T}{\epsilon_T} a \qquad (2.6)$$

where F is the phase ratio and ϵ_T the total column porosity [Guiochon *et al*, 1994]. If the packing densities of two columns are different, their phase ratios must be different, while the coefficients of the isotherm should remain unaffected. This correction is practical because k' is easy to measure on a preparative column. This procedure could be used to adjust the isotherm data measured on an analytical column for its use in calculating the band profiles on a new preparative column. The choice of the base k' to be used for the normalization is arbitrary. I used here the average value of the retention factors k'_{ave} obtained for each set of 5 columns (Tables 2.3 to 2.6, far right column, line PPR).

For each column, a new isotherm was obtained by multiplying the experimental values of q obtained originally by the ECP and FA methods by the ratio of the retention factor of the corresponding column k'_i to k'_{ave}. By applying the SAS nonlinear regression routine to this newly obtained set of isotherms I can calculate the new isotherm coefficients. The results in the case of the ECP isotherms are given in Tables 2.7 to 2.10 (lines k'_i/k'_{ave} and k'-ECP). The same trend was observed for the FA isotherms. After normalization by the ratios of the retention factors, the rsd of the new set of values of the coefficient a for the KROMASIL, YMC, and ZORBAX

columns is larger than before, meaning that the correction is not successful (for the VYDAC columns, the rsd is unchanged). If I eliminate the data for the worst of the five columns in the case, there is some improvement. On the other hand, no changes are observed for the coefficient *b*.

These results confirm a previous finding, that the isotherm coefficient *b* is much less affected by changes in the experimental parameters than the coefficient *a* [Guan *et al*, 1994a]. Equation 2.5 can be rewritten

$$q = \frac{b q_s C}{1 + b C} \tag{2.7}$$

where q_s is the column saturation capacity. Obviously, q_s is a function of the packing density while *b* is not. However, the previous result, that the normalization of the isotherms obtained from columns packed with a given ODS phase by the ratios of the retention factors could decrease moderately the extent of the deviations between these isotherms [Guiochon *et al*, 1994] is not confirmed.

The failure of a correction by the retention factor does not invalidate the assumption that column-to-column fluctuations of the packing density explain the lack of reproducibility of the isotherm data. This failure results probably from the serious difficulties presented by the precise determination of thermodynamic data, retention factors under linear conditions or isotherm data.

Alternate Determination of the Coefficient a

In principle, the retention factor is related to the first coefficient of the equilibrium isotherm by Eq. 2.6. Rather than determining *a* from the ECP of FA measurements, it is possible to derive it from retention data measured under linear conditions and the phase ratio. The

corresponding values of a for all columns are also listed in Tables 2.7 to 2.10 (last row). It is observed that the relative standard deviation of these values is smaller than the rsd of the values of a derived from either ECP or FA, two to three times smaller in the cases of KROMASIL and VYDAC. However, the average value obtained by this method is significantly lower than the ECP value, by 2.7, 10, 6.3, and 6.4% for KROMASIL, VYDAC, YMC, and ZORBAX, respectively. This systematic deviation is much larger than the correction which would be required for the ECP model error, a reduction by approximately 1.5% for a 3000 plate column [Guan *et al*, 1994a]. It is too large to be acceptable.

A comparison of the experimental band profiles (symbols) to those calculated using the average values of a (from k'/F) and b and the values of the phase ratio and efficiency of the column considered (dashed line) is shown in Figure 2.9. The agreement between the two sets of profiles is too poor to be acceptable and this invalidates the procedure.

Isotherms Normalized by the Ratios of ϵ_e's

The column external porosity ϵ_e can be determined directly by inverse size exclusion chromatography [see Chapter 3]. The results of these measurements are listed in Table 2.2. Using the same method as in the previous section (normalization by k'), but using the ϵ_e ratios instead, I obtained a new set of isotherm coefficients, listed in Tables 2.7 to 2.10 under lines $\epsilon_{e,i}/\epsilon_{e,ave}$ ratio and ϵ_e -ECP. As seen in these Tables, the rsd of the new set of values of the coefficient a for the five KROMASIL, VYDAC, YMC columns is significantly reduced compared to the rsd of the experimental data. For the five ZORBAX columns it increases only slightly. The same trend is observed for the FA isotherms (results not listed in the Tables). No changes were observed for the coefficient b.

Using the average value of the new set of coefficients a the band profile on the YMC column # 2 was calculated as before. The result is shown in Figure 2.9 (chain dot line). The calculated band profile is now very close to the experimental chromatogram. This suggests that the correction procedure used here is successful.

Conclusion

Neither directly nor indirectly can the use of the retention factor acquired under linear chromatography conditions permit the derivation of a suitable correction of isotherm data allowing the calculation of band profiles on a column using isotherm data measured on another column, packed with the same stationary phase.

Other than the model error introduced by ECP, I have no satisfactory explanation for a value of a lower when derived from k' than from ECP measurements. A small density of high energy adsorption sites on the surface of the stationary phase, nothing rare with silica-based stationary phases, might cause a difference between the retention factor at infinite dilution (determined by the Henry constant on these high energy sites) and the limit slope of the isotherm (determined by the bulk properties of the surface) but the deviation would be in the opposite direction. More probably, the estimates of the column hold-up volumes and of the phase ratio are inaccurate. The errors made propagate differently to the values of the retention factors and of the isotherm coefficients derived from experimental data.

Another approach available for a correction of isotherm data is the direct determination of the external porosity of the columns by inverse size exclusion chromatography [see Chapter 3; Halász *et al*, 1978]. The procedure used for these determinations are discussed separately [see Chapter 3]. The correction provides satisfactory results and could be applied in actual practice

without serious difficulties.

CHAPTER 3.

STUDY OF PHYSICO-CHEMICAL PROPERTIES OF SOME PACKING MATERIALS.

I - MEASUREMENTS OF THE EXTERNAL POROSITY OF PACKED COLUMNS BY INVERSE SIZE EXCLUSION CHROMATOGRAPHY

Introduction

The practical importance of the pores located inside solid materials has long been recognized [Stanek *et al*, 1972; Brace *et al*, 1972; Hashimoti *et al*, 1973; Deen *et al*, 1981; Sing, 1982; Delage *et al*, 1983; Kaizuma, 1984; Do, 1984; Su *et al*, 1985; Tiller *et al*, 1985; Herino *et al*, 1987; Kathawalla *et al*, 1988; Wang *et al*, 1989; Zheng *et al*, 1989; Talu *et al*, 1989; Zhao *et al*, 1992; Zhang *et al*, 1993; Rice, 1994; Hudak, 1994]. Porosity plays an active role in the performance of packed beds [Stanek *et al*, 1972], construction materials [Brace *et al*, 1972; Delage *et al*, 1983], chemical reactors [Hashimoto *et al*, 1973; Do, 1984], membranes [Deen *et al*, 1981; Kathawalla *et al*, 1988], gas chromatographic columns [Haizuma, 1984], filtration systems [Tiller *et al*, 1985], or in the choice of machining direction [Rice, 1994], *etc*. Various studies have been carried out on porous materials, both theoretically [Whitaker, 1967; Haring *et al*, 1970; Kocirik *et al*, 1974; Novak *et al*, 1975; Smith, 1986] and experimentally [Herino *et al*, 1987; Pakula *et al*, 1971; Komiyama *et al*, 1974; Meyer *et al*, 1985; Bhattacharja

et al, 1989; Kerch *et al*, 1990]. Much effort has been devoted to the control of the pore size distribution of solid substrates [Ruckenstein *et al*, 1981; Ternan *et al*, 1982; Northrop *et al*, 1991; Murakata *et al*, 1992; Wang *et al*, 1992]. It is only recently that the importance of pore size distribution on the performance of stationary phases for gas or liquid chromatography has been recognized as being profound. One good example is the development of "perfusion" chromatography [Afeyan *et al*, 1990; Afeyan *et al*, 1991; Liapis *et al*, 1992; McCoy *et al*, 1993] and the attention given to the related issue of pore connectivity [Liapis, 1993]. The detailed investigation of the influence of the pore size distribution on column performance requires a convenient, accurate and rapid method for its determination.

Various methods have been used or proposed to determine the pore volume or the pore size distribution [Brunauer *et al*, 1938; Ritter *et al*, 1945; Bambrick *et al*, 1969; Felch *et al*, 1971; Ternan *et al*, 1973; Donnet *et al*, 1974; Semonian *et al*, 1977; Ouchlyama *et al*, 1984; Glinka *et al*, 1985; Gethner, 1986; Adkins *et al*, 1986; Mishra *et al*, 1988; Davies *et al*, 1990; Roos *et al*, 1990; Krueger *et al*, 1991; Li *et al*, 1994; Merrill, 1994]. The most common and traditional methods of porosity determination are nitrogen BET [Brunauer *et al*, 1938], mercury porosimetry [Ritter *et al*, 1945], the *K* method [Donnet *et al*, 1974], and the flow method [Semonian *et al*, 1977]. These methods have a limited accuracy [Ternan *et al*, 1973; Wotzak, 1974] or may damage the sample [Feldman, 1984]. In recent years, new methods such as neutron scattering [Glinka *et al*, 1985; Gethner, 1986], capillary condensation hysteresis [Adkins *et al*, 1986], nuclear magnetic resonance [Davies *et al*, 1990], coulometric measurement [Roos *et al*, 1990], X-ray [Krueger *et al*, 1991], and MRI [Merrill *et al*, 1994] have been proposed. However, these methods are still at the development stage.

Among the numerous methods used for the porosity determination which are listed above,

none uses a liquid chromatographic technique. This is a serious inconvenience for the determination of the internal or external porosity of chromatographic columns. An additional instrument is required if any of the above methods is to be used. The result may not be accurate because the pore size distribution measured from bulk packing material may be quite different from that of a packed liquid chromatographic column [Guiochon *et al*, 1995]. This is especially true for the external pore size distribution.

In 1975 Halász [Halász, 1975; Halász *et al*, 1978; Nikilov *et al*, 1980; Werner *et al*, 1980; Groh *et al*, 1981; Crispin *et al*, 1982] introduced the idea of using inverse size exclusion chromatography (ISEC) to determine the porosity inside a liquid chromatographic column. In size exclusion chromatography (SEC) [Pedersen, 1962; Yau *et al*, 1979; Yau *et al*, 1989], sample mixtures that are dissolved in the mobile phase/solvent can be separated according to their different molecular sizes. Large molecules can only enter large pores, therefore they have a shorter elution time than small molecules, which are able to enter small pores. Classical SEC uses the known pore structure of a selected adsorbent to determine the molecular mass distribution of a polymer mixture. Conversely, if the molecular mass of a series of polymer standards is known, we can determine the pore size distribution of an unknown stationary phase from the distribution of their retention times. For current purpose, the advantage of this method is that it operates simply on the very column investigated. The same instrument is used as for conventional HPLC studies. Compared with the traditional porosimetry methods, this procedure is less time-consuming and gives more accurate and dependable results.

Knox and co-workers [Knox *et al*, 1984; Knox *et al*, 1987] showed that it is possible to convert the calibration graphs to pore size distributions following a complex procedure. For current purpose, however, the semi-empirical method of Halász and Martin [Halász *et al*, 1978]

was chosen. As it constitutes a mere linear transformation of the calibration graph, the resulting distributions are too broad and the mean pore size determined may not agree well with the one determined by other methods. However, the procedure is simple, practical, and convenient to compare columns which differ by their degree of consolidation.

In their study, Halász and Martin [Halász *et al*, 1978] applied inverse SEC to the determination of the internal porosity of the column packing. In the current work, however, I am more interested in the column external porosity. In Chapter 2, I have shown that the deviation between the equilibrium isotherms measured on columns packed with the same ODS phase can be corrected by the ratio of the respective column external porosities. This means that we can derive the equilibrium isotherm for a preparative scale liquid chromatographic column by normalizing the equilibrium isotherm obtained on an analytical column packed with the same stationary phase by the ratios of their external porosities. The significance of this work is important for applications in preparative chromatography.

Theory

The principle of the method of determination of the external porosity of a column is an extension of the procedure described by Halász and Martin [Halász *et al*, 1978] for the determination of the internal porosity of packing materials. Conventional size exclusion chromatography (SEC) consists of separating the components of a polymer sample by their molecular mass on a column packed with an adsorbent whose volume pore size distribution is known to encompass the molecular volumes of the sample components [Yau *et al*, 1979; Yau *et al*, 1989]. Provided standard samples of known molecular masses derived from a known monomer are available for calibration, experiments show that there is a correlation between the average

molecular mass (or the degree of polymerization) of these polymers, Mr_n, and the average diameter of the pores from which they are excluded, ϕ_n, assuming that all the polymeric chains remain in the same conformation of a random coil [Yau *et al*, 1979]. For polystyrene dissolved in methylene chloride, we have [Halász *et al*, 1978]

$$Mr_n = 2.25\ \phi_n^{1.7} \tag{3.1}$$

where ϕ_n is given in angstroms (Å). This correlation is based on the fact that the access of molecular coils into pores is limited by steric hindrance caused by the wall [Giddings, 1991]. The retention volume of macromolecules of increasing size decreases in the proportion to the column porosity which corresponds to the volume of the layer against the pore wall having a thickness equal to the molecular radius. For each packing material, there are two thresholds, a low and a high one. Molecules larger than the high threshold have no access to any significant fraction of the internal pores; they are totally excluded from it. Molecules smaller than the low threshold have access to the entire pore volume; they are not excluded. Molecules of intermediate size have access to part of the pores, as indicated by Eq. 3.1. The validity of this correlation relies on the assumption that the polymer samples used, although having different molecular masses, have the same structure and that the same solvent is used.

Conversely, in inverse SEC, solutions of known polymeric samples are injected into a column packed with an unknown adsorbent. The retention behavior of these solutes can be correlated with the pore size distribution of the packing material. For polystyrene samples eluted by methylene chloride through a bed of chemically bonded C_{18} silica, the correlation is obtained by solving Eq. 3.1 for ϕ_n. It becomes [Halász *et al*, 1978]

$$\phi_n \sim 0.621\ (Mr_n)^{0.588} \tag{3.2}$$

Thus, inverse SEC will provide the pore size distribution of the sample of adsorbent studied. If we assume that all the pores that have a size equal to or larger than ϕ_n have a volume V_n and that all the pores that have a size equal to or larger than ϕ_{n+1} have a volume V_{n+1} ($\phi_{n+1} > \phi_n$), the volume of the pores that have a size larger than ϕ_n and smaller than ϕ_{n+1} is given by

$$\Delta V_{n+1,n} = V_{n+1} - V_n \tag{3.3}$$

$\Delta V_{n+1,n}$ can be derived from the inverse SEC data. We have to note, however, that axial dispersion and mass transfer resistance are omnipresent in chromatography and blur the data derived from ISEC. Furthermore, the derivation of a pore size distribution (psd) from the retention volume behavior of a series of polymeric samples of different molecular weights is a convolution problem which does not have a unique solution. The use of a large number of polymeric samples would improve significantly the probability of achieving a reasonably close approximation of the psd, as indicated by Eq. 3.3.

The total volume of a liquid chromatographic column, V_k, can be written as the sum of three contributions

$$V_k = V_e + V_i + V_U \tag{3.4}$$

where V_e is the inter-particle, interstitial, or external pore volume; V_i is the internal pore volume; and V_U is the unaccessible volume. This last volume can be split into three different contributions, V_s, the stationary phase solid volume; V_c, the closed pore volume; and V_a, the volume of the layer of C_{18} bonded chains. These three volumes, which are being discussed separately [see Chapter 4], can be lumped together into the unaccessible volume, V_U, for all practical purposes of this study except for the calculation of the apparent density of the packing.

In order to use inverse SEC to determine the porosity of chromatographic columns, the following conditions must be met [Halász *et al*, 1978]:

(1) There is no adsorption, whether irreversible or reversible, of the polymeric samples used on the stationary phase studied;

(2) The standard polymer molecules remain discrete and do not agglomerate in the solvent used as mobile phase;

(3) There is instantaneous, quasi-reversible equilibrium between the two phases during the whole experiment;

(4) The elution peak profile is close to Gaussian, with an asymmetry factor smaller than 2;

(5) The stationary phase studied is rigid;

(6) The mobile phase flow rate is constant ($\pm 1\%$);

To satisfy the first two requirements, good solvents of polystyrene, such as methylene chloride or tetrahydrofuran, should be used. Polystyrene samples do not aggregate in the dilute methylene chloride solutions used in this work [Yau *et al*, 1979]. To satisfy the third requirement, the columns studied should have a minimum efficiency. Although the value of this threshold is arguable, the columns used in the present work having an efficiency in excess of 2500 theoretical plates [see Chapter 2] do meet this condition. The peaks obtained in this work were close to symmetrical. Finally, the silica particles used are rigid and the equipment used in this work delivers flow rates stable within better than 0.1% [El Fallah *et al*, 1991].

Experimental

Equipment

All measurements were carried out with a Hewlett-Packard (Palo Alto, CA) HP1090M

liquid chromatograph equipped with a diode-array UV detector, an automatic sampling system, and a computerized data acquisition system. One of the features of this apparatus, which is critically important in the present study, is the high stability and accuracy of the solvent delivery system [El Fallah *et al*, 1991]. Accordingly, the reproducibility of the measurements of the retention volumes was better than 0.1% and their accuracy is between 0.1 and 0.2%.

Columns

The empty stainless steel columns (10 cm long, 0.46 cm i.d.) were purchased from Alltech (Deerfield, IL). Samples of four 10 μm spherical C_{18} ODS packing materials were obtained, KROMASIL from Eka-Nobel (Stratford, CT), VYDAC from The Separation Group (Hesperia, CA), YMC from YMC (Wilmington, NC), and ZORBAX from BTR (Wilmington, DE). Each material was packed into five columns by conventional slurry packing [Bristow, 1978], under the pressure recommended by the packing manufacturer. All the columns containing the same phase were packed on the same day, starting with column #1 and ending with column # 5. The lot numbers of each material and the column packing conditions are listed in Table 2.1.

Chemicals

Polystyrene standards with molecular masses ranging from 2,000 to 1,860,000 were obtained from SUPELCO (Bellefonte, PA). Polystyrene standards with molecular masses of 456, 1,050, 3,840,000, 5,840,000, and 20,600,000 were obtained from TOSOH (Tokyo, JAPAN). Polystyrene standards with molecular masses of 8,420,000 and 10,200,000 were obtained from American Polymer Standards (Mentor, OH). Benzene (Mr_n = 78.11) was purchased from EM Science (Gibbstown, NJ).

Methylene chloride (J.T. Baker, Phillipsburg, NJ) was used both as the mobile phase and the sample solvent. Unless specified otherwise, all measurements were carried out with UV detection at 254 nm, at a mobile phase flow rate of 1.000 mL/min.

Procedures

A total of 19 polystyrene standards with molecular masses ranging from 456 to 20,060,000 Dalton were injected into each column. Benzene was used for calibration and for the determination of the total accessible porosity of the column. Each injection was repeated at least three times. The results listed are the average of these three retention volumes. Plots of the logarithm of the probe molecular mass versus its retention volume showed that for each packing material there is a bimodal pore size distribution (See next section and Figures 3.1 to 3.5). These two distributions correspond to the internal porosity (between ca 10 and 150 Å) and the external porosity (above a few hundreds Å), respectively. In all cases, the borderline between the two porosities is around Mr_n = 23,000 Dalton, corresponding to an average pore size, ϕ_n, of 228 Å (Eq. 3.2).

The total pore volume was taken as the retention volume of benzene. It was practically equal to that of uracil under reverse phase chromatography conditions (see later). The external pore volume was derived from the intermediate point between the two pore size distributions (see later). The porosities were calculated using the total column volume, V_k, itself derived from the geometrical dimensions of the column tubing

$$V_k = \pi r^2 l \qquad (3.5)$$

where r is the column radius (here, r = 0.23 cm) and l the column length (l = 10.0 cm).

Before packing, the mass, W, of each empty column was obtained on an analytical balance. After the end of the whole series of experiments, each column was dried under a stream of ultra-pure nitrogen (inlet pressure, ca. 30 psi), at a temperature of ca. 50 °C, for at least 8 hours, after what its mass was measured as W^*. The mass of solid material inside the column is $W_p = W^* - W$. This mass and the relative weight concentrations of silica and alkyl bonded chains are used to calculate the volume of support and of stationary phase inside the column, V_s and V_a [see Chapter 4].

The volume fraction of the external pores, or external porosity ϵ_e, corresponding to a retention volume V_e, hence to the exclusion pore size, ϕ_e, and the total pore volume fraction or total porosity, ϵ_T, are defined by

$$\epsilon_e = \frac{V_e}{V_k} \qquad \epsilon_T = \frac{V_T}{V_k} \tag{3.6}$$

Two values are used for V_T, the retention volume of benzene in methylene chloride and the retention volume of uracil in methanol. The values of the column total porosity corresponding to these retention volumes are respectively $\epsilon_{T,b}$ and $\epsilon_{T,u}$. They are very close to each other.

The internal porosity, ϵ_i, is better defined by referring it to the actual volume of the particles, excluding the external porosity. In this way, the influence of variations of the external porosity due to a different extent of consolidation of the packing [Guiochon *et al*, 1995] is eliminated. It becomes

$$\epsilon_i = \frac{V_i}{V_k (1 - \epsilon_e)} \tag{3.7}$$

Total, external, and internal porosities are related by

$$\epsilon_T = \epsilon_i (1 - \epsilon_e) + \epsilon_e \qquad (3.8)$$

This closure relationship can be used to derive ϵ_i from independent determinations of ϵ_T and ϵ_e, as done in this work. It will be used in a forthcoming paper to ascertain the consistency of the results obtained when these three porosities are obtained from different, independent measurements [Guan *et al*, in preparation].

Results and Discussion

The results of the determinations of the values of the different porosities of concern here are reported in Tables 3.1 to 3.4. They include the total, internal, and external porosities. The total porosity is derived from the retention volume of either benzene in methylene chloride or uracil in methanol. Both methods give results which are in close agreement, albeit slightly different, as discussed separately [see Chapter 4].

Column Internal and External Porosities

Plots of the logarithm of the molecular mass of the polystyrene probes versus their elution volume are given for the four stationary phases studied, KROMASIL (Fig. 3.1), VYDAC (Fig. 3.2), YMC (Fig. 3.3), and ZORBAX (Fig. 3.4). The numbers on each figure indicates the corresponding column. The degree of column-to-column reproducibility of the experimental data is generally excellent. Only the data for the first columns packed with KROMASIL (Fig. 3.1) and, to a lesser degree, VYDAC (Fig. 3.2) deviate significantly from the data obtained with the other four columns.

In each case, the plot obtained consists of two curves, each one approximately linear. These two curves correspond to the retention contributions of the two different types of pores in the column packing, the pores located inside the packing particles (internal pores) and the pores which are between the packing particles (external pores), respectively. If I disregard the five points corresponding to benzene, the polymer with Mr_n = 23,000, and the three largest polystyrene samples (see rational below), I observe that the remaining 15 points are located on two different straight lines whose slopes and intercepts are easily obtained by proper linear regressions. The coordinates of the intercepts (the exclusion pore size, ϕ_e, and the elution volume, V_e) of the two lines are listed in Tables 3.1 (KROMASIL), 3.2 (VYDAC), 3.3 (YMC), and 3.4 (ZORBAX). They are in lines 1 and 2, respectively.

I assume that all the pores inside the column having a size equal to or larger than ϕ_e belong to the inter-particle or external porosity, while the pores smaller than ϕ_e belong to the intra-particle or internal porosity. The corresponding elution volume, V_e, is the external pore volume of the column, from which the external porosity is derived (Eq. 3.6).

The reasons to eliminate benzene and the compound at Mr_n = 23,000 from the linear regression are as follows. Benzene is a small molecule which is outside the range of selectivity of the packing materials used (see Figures 3.1 to 3.4). Its usefulness is in giving the column total porosity. The probe at Mr_n = 23,000 (ϕ_n = 228 Å, Eq. 3.2) is intermediate. It seems to be already slightly excluded from the external porosity, without being completely excluded from the internal porosity. So, it does not belong to either correlation. This is related to the ambiguity found in defining these two porosities and their boundary. Some large pores, *e.g.*, cavities located at the surface of the particles, cannot be simply assigned to one or the other type of pores. The three heaviest probes have retention volumes which tend to be slightly larger than those of the

lighter polystyrene standards and than those predicted by extrapolation of the second straight line. These volumes are a function of the flow velocity and sample size (see later), although data acquired at very low sample size and flow velocities seem to be consistent with the other data pertaining to the external porosity. This abnormal behavior is observed for all four phases and is especially obvious in Figures 3.1 and 3.2. It can be explained by the influence of the mobile phase flow velocity on the retention of large random coil polymers as classically observed in size exclusion chromatography [Yau *et al*, 1979; Yau *et al*, 1989] or in hydrodynamic chromatography [Stegeman *et al*, 1991; Stegeman *et al*, 1993].

To verify this assumption, I randomly chose the ZORBAX column #2 (Figure 3.5). I had previously injected all the polystyrene standards into this column at a flow rate of 1.000 mL/min. The results were used for the determination of the column porosity (see Figure 3.4 and Table 3.4). The experiment was repeated at a flow rate of 5.000 mL/min. Afterward, the column was dried for weighing (see Experimental section) and stored after closing both ends by plastic stoppers. A week later the column was retrieved and the injection of the whole series of polystyrene standards was repeated, at flow rates of 0.050, 0.200, and 1.000 (for reproducibility check) mL/min. The results are shown in Figure 3.5.

There are no differences between the two series of experimental results obtained at a flow rate of 1.000 mL/min, demonstrating the excellent consistency of the solvent delivery system and the stability of the structure of the column packing. However, the elution volumes of all the polystyrene standards at 5.000 mL/min appear to be about 0.025 mL larger than at lower flow rates, up to Mr_n = 1,860,000 Dalton. For higher *Mr*'s, these volumes increase significantly, indicating spurious effects possibly related to the influence of differential viscous drag on the conformation of the polymer backbone or, more probably, to viscous shear degradation of these

polymers. On the other hand, a reduction of the flow rate has no effect on the retention volumes of the polystyrene standards, except at high molecular masses. At flow rates of 0.050, 0.200 and 1.000 mL/min, the elution volumes of the standards up to 1,860,000 Dalton are independent of the velocity. However, the retention volumes of the three heaviest standards increase with increasing flow rate from 0.050 to 0.200 and 1.000 mL/min, demonstrating a larger exclusion degree and confirming the assumption of shear degradation at high flow rates. This is the justification for eliminating the corresponding data from the regression. In future studies, measurements made with polymers having more than 1,000,000 Dalton should be made at 0.100 mL/min or at a lower flow rate.

The total accessible pore volume inside the column, V_T, hence, the total column porosity is derived from the elution volume of benzene. Having derived successively the total and the external porosity, I can solve Eq. 3.8 for the internal porosity. The results are listed in Tables 3.1 to 3.4, as values of the internal and external porosities (Eqs. 3.6 and 3.7).

The values of the total porosity derived from the retention volume of uracil [see Chapter 2], $\epsilon_{T,u}$, are also listed in Tables 3.1 to 3.4. Uracil is commonly used as the non-retained compound in reverse phase liquid chromatography. The values of the total porosities derived from the retention volumes of benzene and uracil on all columns are nearly equal, the former being on average 2.7%, 0.1%, 1%, and 1.6% larger than the latter for KROMASIL, VYDAC, YMC, and ZORBAX, respectively. These differences are nearly constant for the five columns, with very small standard deviations. Thus, they may probably be explained by a difference in the differential amounts of methanol and methylene chloride adsorbed by the chemically bonded layers of octadecyl groups on the different phases and may relate to the structure of the layer of bonded alkyl chains. In order to distinguish between these two porosities, I call them *benzene and uracil*

total porosities, respectively [see Chapter 2].

The Pore Size Distributions of a Chromatographic Column

Based upon Eq. 3.3, the pore distribution inside the column can be expressed as the percentage of the total pore volume V_T accounted for by $\Delta V_{n+1,n}$, *i.e.*, the volume fraction occupied by the pores larger than ϕ_n and smaller than ϕ_{n+1} (*i.e.*, $\Delta V_{n+1,n}/V_T$, %). The results are listed in Tables 3.5 to 3.8. The first column gives the boundary of the fraction considered. The blank line indicates the separation between the internal and the external pore size distributions. For columns packed with the same ODS phase, there are some small but significant differences in the pore size distributions. As shown in Chapter 2, these differences are at the origin of the systematic column-to-column fluctuations observed for various parameters and the values of the external porosity derived from my measurements can be used as a basis for correction.

The average pore size distributions of the four phases are shown in Figures 3.6 (KROMASIL), 3.7 (VYDAC), 3.8 (YMC), and 3.9 (ZORBAX). These distributions are in good agreement with the pore distributions measured by the BET method, using nitrogen, which were performed by the manufacturers of the stationary phases studied here [private communications]. From the data in Tables 3.5 to 3.8, we see that the external porosity includes the fraction at 228 Å for KROMASIL and VYDAC but does not include it for YMC and ZORBAX. However, the contribution of this fraction to the total porosity is small, so this is a minor difference.

In all cases, the contribution to the total porosity of the pores having an average size equal to 228 Å or larger and equal to 3000 Å or lower is small, between 5.5% (ZORBAX) and 3.5% (KROMASIL). Data in Tables 3.5 to 3.8 show that the pores larger than 0.4 μm account for more than 91% of the external porosity for these spherical materials having all a nominal particle size

of 10 μm. The fact that these materials have different particle size distributions and different actual shapes [see Chapter 4] may explain the differences in the external pore size distributions in the low range. For reasons explained above in the discussion of Figure 3.5, it is doubtful that meaningful distributions of pores larger than 0.4 μm can be obtained by inverse SEC. Other methods, such as mercury porosimetry [Ritter *et al*, 1945] should be used. A comparison between the results obtained for the external psd using these different methods will be published shortly [Guan *et al*, in preparation].

Little is known about the relationships between the external porosity and the packing conditions [Guiochon *et al*, 1995], between the pore size distribution of the packing (*i.e.*, of the external pores), the particle shape, the average particle size, and the size distribution of the particles, or between any of these parameters and the column performance. Thus, my results open a new approach for the investigation of column properties and performance.

Conclusion

An accurate estimate of the values of the internal, external, and total porosities of a column, as well as of the external pore size distribution of that column can be derived from the retention volumes of a series of polystyrene standards with a wide range of known molecular masses. This method is faster and more accurate than the traditional methods used for the determination of the porosity on a solid phase. In a chromatographic laboratory, it does not require any special equipment.

The systematic measurements made demonstrate that there exist significant differences between the pore size distributions of individual columns in a series, even when they are packed successively with the same packing material. These differences may explain, at least in part, the

lack of reproducibility of the column performance which has been previously observed and reported for these columns [see Chapter 2]. Thermodynamic properties should depend only on the amount of surface area of stationary phase per unit volume of solvent. The external porosity measured as described in this work was used to correct satisfactorily for the deviation observed between the equilibrium isotherms measured for these columns [see Chapter 2].

In further work, the ISEC results obtained in this report will be compared to those obtained by other methods of investigation [Guan *et al*, in preparation].

CHAPTER 4.

STUDY OF THE PHYSICO-CHEMICAL PROPERTIES OF SOME PACKING MATERIALS.

II - GENERAL PROPERTIES OF THE PARTICLES

Introduction

The reproducibility of packed columns for chromatography has always been a problem of serious concern for practitioners [Kirkland, 1971]. So far, the reproducibility of the thermodynamic properties has attracted most of the attention. Progress made over the years in the manufacturing processes used to prepare silica particles and to derivitize them when needed has resulted in the present situation. Batch to batch repeatability of chromatographic separations performed with a given brand of packing is quite reasonable for neat silica and alkyl-bonded silica materials. There are still some significant fluctuations of the retention factors, much smaller variations for the separation factors. The results are generally less satisfactory for some nonconventional bonded phases, in which case there may be considerable batch-to-batch variations in the yield of the bonding reactions. Hence, the repeatability of some otherwise difficult separations is not assured [Welinder *et al*, 1995].

Until recently, the repeatability of the other column characteristics was not a topic of great interest. Provided the needed separations could be obtained, the analysts were satisfied and paid little attention to possible fluctuations of the column porosity, its permeability or even, to some extent, its efficiency nor to the possible consequences of these variations. In most cases, pumps

can deliver the mobile phase under pressures higher than needed, so changes in the column permeability are easily met with adjustments in the inlet pressure to keep the flow rate at the required level.

Recently, however, two new types of problems have arisen, both related to preparative chromatography, both requiring a much better control of the various column characteristics. Their importance is going to change the situation described above and to confer great benefit to the ability of closely reproducing the values of all the column parameters. First and foremost is the rapid development of the interest of separation chemists for Simulated Moving Bed separations (SMB). Second is the increasing economical importance of using physico-chemical parameters acquired with analytical columns for the scaling-up of industrial separations.

SMB is a continuous process of separation based on the ability of chromatographic columns to separate closely related components, *e.g.*, enantiomers [Ruthven *et al*, 1989; Ching *et al*, 1993]. It operates at relatively high concentrations, thus applies the considerable enhancement of separations that nonlinear effects related to competitive adsorption behavior may provide [Guiochon *et al*, 1994]. The process uses 12 or 16 identical columns, three or four of which constituting each column section at any given time. The columns are switched cyclically, in order to simulate the counter-current migration of the liquid and the solid phase. The performance of the whole column must remain constant from period to period. Cyclical perturbations in the flow rate or the retention pattern result from any difference between the packing density or the thermodynamic characteristics of the 12 or 16 individual columns. Such perturbations affect the stability of the steady-state operation of SMB and must be minimized. The production of batches of 16 nearly identical columns is not a simple problem, but must be achieved if the process is to become practical.

The selection of the design and operating parameters of an industrial scale separation is still often done using empirical methods, some merely based on the gut feelings of the chemist in charge. This approach is costly and wasteful of feed, solvent and packing material, even in the implausible case when it converges toward the actual set of optimum conditions. A more sound procedure consists in determining the competitive isotherms of the components to be separated and the correlation between the column efficiency and the mobile phase flow velocity on an analytical column and calculating the optimum conditions of the separation, given the proper objective function [Guiochon *et al*, 1994; Felinger *et al*, 1994]. The acquisition of competitive equilibrium isotherm, hydrodynamic, and efficiency data on analytical columns is rather straightforward as well as the calculation of optimum experimental conditions using simple models of chromatography [Guiochon *et al*, 1994]. However, the critical step is in the scaling-up of these data and results. Analytical and preparative columns are packed using quite different procedures and have significantly different packing densities [Guiochon *et al*, 1995; Sarker *et al*, in press]. As long as the characteristics of both types are not highly reproducible, it will be difficult to scale-up experimental conditions calculated for analytical columns to the design and operation of preparative columns.

The aim of this work is the study of the parameters which control the reproducibility of column performance. In this Chapter, I report the physico-chemical properties of four packing materials which are widely used in preparative chromatography.

Theory

I consider in this work the fractions of the column volumes occupied by different phases, or by phases having importantly different properties. They are listed in two groups as follows:

- The unaccessible volume fraction, ϵ_U, from which the mobile phase and the solutes traveling along the column are completely excluded. It contains three different fractions:

  - The skeleton made of solid silica, which occupies a volume fraction ϵ_s.

  - The bonded layer composed of alkyl chains chemically bonded to the surface, which occupies a volume fraction ϵ_a.

  - The closed pores, pores which have been formed during the synthesis of the material and have been closed at a later stage of particle growth. Their volume fraction, ϵ_c, is not accessible by chromatographic measurements.

- The volume fraction occupied by the mobile phase in the column, ϵ_T, or total porosity. It includes:

  - The volume fraction occupied by the pores inside the particles, also called internal pore volume, or internal porosity, ϵ_i.

  - The volume fraction of the voids between and around the particles, also called inter-particle, interstitial or external pore volume. This is the external porosity, ϵ_e.

While the external porosity is always reported to the geometrical column volume, the other porosities or volume fractions have been reported differently in chromatography and in chemical engineering. In the former area, the packing material is considered incompressible. So, these porosities have been conventionally reported to the geometrical column volume. In this case, the sum of all the porosities would be equal to 1. In chemical engineering, however, the internal porosity is conventionally reported to the actual volume of the particles. This has the advantage of giving a value of the internal porosity which remains constant in spite of any possible change in the packing density. We know now that the packing density may vary with the nature and

intensity of the stress applied during column packing [Guiochon *et al*, 1995; Sarker *et al*, in press]. For this reason, the volumes fractions of the skeleton, bonded layer and closed pores should also be reported to the actual volume of the particles. Accordingly, the closure relationship is written:

$$\epsilon_e + (1 - \epsilon_e)(\epsilon_i + \epsilon_c + \epsilon_s + \epsilon_d) = 1 \qquad (4.1)$$

This relationship will be helpful to assess the combined accuracy of the different methods used to determine the four volume fractions listed above. The convention described above has been used in the calculation of the data reported in Tables 4.2 and 4.3.

In the discussion of the methods of determination of the different volume fractions listed above, we must consider the definition of their boundaries. There are only three boundaries of importance, the column wall, the boundary between the external and internal pore volumes, and the interface between the internal pore volume and the inaccessible volume. The column wall is the only one which we can safely assumed to be a flat surface with a clear geometrical definition. The inner column wall is most often polished stainless steel, with a surface area exceeding little its geometrical surface area and which is orders of magnitude smaller than the surface area of the packing material in the column. The definition of the other two boundaries is fuzzy.

The external pores are bound to be larger on the average and far less numerous than the internal pores. However, a classification based on pore size cannot avoid some ambiguities. In principle, the mobile phase flows through the external pores, but this definition is equivalent to the former one: the permeability of the pores increases as the square of their size. Perfusion would use flow across large internal pores. Hydrodynamic chromatography is based on the exclusion of particles from the small external pores. The surface at which the mobile phase velocity is zero

would be a good definition of the boundary if there were any method of measurement based on its consideration. We shall use later a definition based on the pore size, but we must recognize that this introduces a model error in the very definition, albeit this error seems to be small.

The last boundary to consider is the solid-liquid interface. With conventional adsorbents (*e.g.*, silica, graphitized carbons), it is a surface which is not easy to define when liquid-solid adsorption is considered [Kováts, 1985]. With chemically bonded phases, the problem may be theoretically the same, but the error increases considerably. Furthermore, I use in this work different methods to measure the various porosities. Some methods take place in a low pressure gas phase where the bonded alkyl chains are most certainly collapsed, others in solution in organic solvents in which the alkyl bonded groups are well dispersed. This will introduce some discrepancies (see later). At any rate, since some of the methods used in this work are based on volume determinations and others on weight determination, I must handle separately the skeleton, with the density of silica, and the bonded alkyl chains, which will be assumed to have the density of liquid octadecane.

Experimental

Equipment

The chromatographic measurements were carried out using a Hewlett-Packard (Palo Alto, CA) HP1090M liquid chromatograph, equipped with a diode-array UV detector, an automatic sampling system, and a computerized data acquisition system. It has been reported previously [El Fallah *et al*, 1991] that the solvent delivery system of this equipment is highly stable and accurate. Accordingly, the reproducibility of retention volumes measurements was better than 0.1% and their accuracy between 0.1 and 0.2%.

Columns

Empty stainless steel tubes (10 cm long, 0.46 cm i.d.) were purchased from Alltech (Deerfield, IL). Samples of 10 μm spherical C_{18} ODS packing materials were obtained, KROMASIL from Eka-Nobel (Stratford, CT), VYDAC from The Separation Group (Hesperia, CA), YMC from YMC (Wilmington, NC), and ZORBAX from BTR (Wilmington, DE). Each material was packed into five columns by conventional slurry packing [Bristow, 1978], under the pressure recommended by the packing manufacturer. All the columns containing the same phase were packed on the same day, starting with column #1 and ending with column # 5. The lot numbers of each material and the column packing conditions are listed in Table 2.1.

The weight of packing material in the column is reported and discussed separately, together with the porosity data (see Table 4.2). It was determined from the difference between the weight of the column tubing measured before packing it, and the weight of the dry column. After completion of a series of measurements by inverse size exclusion chromatography [see Chapter 3], the columns were full of methylene chloride. They were emptied into a waste container, dried under a stream of nitrogen at 50 °C for eight hours and finally weighed.

Chemicals

Methylene chloride (J.T. Baker, Phillipsburg, NJ) was used both as the mobile phase and the sample solvent. Benzene (Mr = 78.11) was purchased from EM Science (Gibbstown, NJ). Unless specified otherwise, all chromatographic measurements were carried out with UV detection at 254 nm, at a mobile phase flow rate of 1.000 mL/min.

Measurement of the Apparent Density of the Packing Materials

The apparent density of the packing materials were determined by pycnometry, using an ACCUPYC 1330 (Micromeritics, Norcross, GA). The test method is based on a determination of the porosity in which the accessible volume of a sample is determined by application of Boyle's law. The apparatus consists of two cylinders of known volume connected by a valve. One of the cylinders, the calibrated sample cell volume, has an accessible chamber for insertion of the test specimen and is connected to a source of dry gas, preferably helium as used in this work. The pressure in the sample cell volume is increased to a predetermined pressure and the exact value of the pressure, P_1, is noted. The valve between the two cylinders is then opened and the second, lower pressure, P_2, is again noted. The ratio of these pressures, P_1/P_2, is directly related to the volume of the calibrated sample cell volume displaced by the unaccessible volume of the sample. This procedure provides the volume of solid material (including the volume of non-connected pores) actually contained in the sample. The apparent density of the solid material of the particles and the specific unaccessible volume of the particles are given in Table 4.1. The unaccessible volume fraction, ϵ_U, of each column is given in Table 4.2, derived from these density data.

Scanning Electron Micrography (SEM) of the Packing Materials

A small amount of each packing material was deposited onto an adhesive layer on an aluminum SEM stub and densely distributed across the stub. Each specimen was sputter-coated with Au/Pd alloy to impart electrical conductivity. These samples were examined with the secondary electron detector of a Hitachi S-800 SEM, looking at a fairly wide area of the sample surface. Regions which appeared to best typify the particles observed were photographed at 1000x magnification. A part of each region was selected to include details of anomalous particles and

photographed at magnification 5000x. Two typical photographs were selected for each material. They are reproduced in Figures 4.1 to 4.4.

Results and Discussion

I present here a number of properties of the materials studied whose consideration will be useful later for the interpretations of other results. As explained above, the values of the particle internal porosity and other volume fractions (unaccessible pore volume, closed pore, silica or bonded group layer) should be referred to the total actual volume of the particles. This provides numbers which remain constant during consolidation of the particles, independent of the degree of consolidation of the packings [Guiochon *et al*, 1995; Sarker *et al*, in press]. However, it is necessary to know the value of the external porosity of the packing to derive these data from the measurements. The determination of the external porosity of chromatographic columns by inverse size exclusion chromatography [Halász *et al*, 1978] is described in Chapter 3 and will be validated by comparison with the results obtained using different other methods in a forthcoming publication [Guan *et al*, in preparation]. To present here consistent data, I have used the values of the external porosity derived in Chapter 3 for their calculation.

Visual Examination of the Particles

The particles of KROMASIL (Figure 4.1) are most spherical. The most irregular particle seen in this lot is in the center of Figure 4.1a. However, there are some very fine particles (Figures 4.1b). The ratio of the largest to the smallest particle in the field of the microscope is close to 2 (Figure 4.1b). Although the VYDAC particles (Figure 4.2) are generally spherical, there are a number of irregular-shaped particles, some in the shape of a wheat seed (Figure 4.2a),

others strongly chipped (Figure 4.2b). There are few fine particles. The connections between closely placed particles (*e.g.*, the line of four particles in the top left part of Figure 4.2b) might be an artifact of sample preparation, although this phenomenon was not found in the other materials. The YMC particles (Figure 4.3) are generally spherical (Figure 4.3a), with a few irregular aggregates of very small spheres and an occasional irregular particle (Figure 4.3b). The ZORBAX particles (Figure 4.4) are also generally spherical, but are often chipped (Figure 4.4a), and sometimes agglomerated by pairs with a few larger agglomerates (Figure 4.4b), and include some particles which seem to originate from the breakage of these agglomerates.

All these particles are too irregular in shape and/or size to allow their packing as a regular hexagonal assembly of atoms, ions, or molecules in a crystal. The structure of the column packings must be irregular and, fortunately, the external porosity will be much larger than the minimum theoretically possible in a dense packing of regular spheres [see Chapter 3].

Unaccessible Volume Fraction

Pycnometry gives an accurate value of the volume nonaccessible to helium in a sample of known weight of the material. From this data, the apparent density or the specific volume of the material is easily calculated (Table 4.1). The only assumption made is that helium is not adsorbed by the solid at a temperature slightly above room temperature and this is certainly valid. However, it is highly probable too that the alkyl chains are collapsed on the surface, thus blocking access to some of the smallest internal pores and leading to a slight overestimate of the unaccessible pore volume.

The unaccessible volume fraction, ϵ_U, corresponds to the volume occupied by the solid silica skeleton, the C_{18} chains chemically bonded to the silica, and the non-connected or closed

pores inside the skeleton, with[4]

$$\epsilon_U = \epsilon_s + \epsilon_c + \epsilon_a \tag{4.2}$$

With the restriction given above, this volume fraction is accurately known, irrespective of the density of the alkyl groups. It can be calculated for each column, from the weight of packing material, its specific unaccessible volume and the column geometrical volume. The result is given in Table 4.2. Note that the sum of the total porosity and the unaccessible volume fraction is not equal to 1. This is their combination following Eq. 4.1 which should close to 1, as seen when comparing the data in the columns of Table 4.2.

An estimate of the three components of the unaccessible volume fraction, the volume fractions of the silica skeleton, of the alkyl group layer and of the closed pores can be made from the known proportion of organic bonded material in the packing material, assuming the skeleton to have the same density as silica (2.33 g/cm^3), the alkyl groups to have the same density as octadecane (0.777 g/cm^3) and the closed pores to be filled of gas (density 0), since the last operation of the silica material, prior to its bonding, is a high temperature treatment. The corresponding fractions are reported in Table 4.3 for KROMASIL and ZORBAX, for which the percent carbon was available.

Solid Volume Fractions

KROMASIL contains 19.40% carbon (data given by the manufacturer), hence approximately 3.35% hydrogen and 77.25% silica. For ZORBAX these values are 11.04%, 1.98%, and 86.98%, respectively. From the weight of packing per column, the specific

[4] Note that sum $\epsilon_U + \epsilon_T$ is not equal to 1 with my conventions. From Eq. 4.1, we have: $\epsilon_e + (1 - \epsilon_e)(\epsilon_i + \epsilon_U) = 1$

unaccessible volume, the column volume, and the weight fraction of silica in the packing material, it is possible to calculate the volume fractions of the particles which is occupied by the silica. Knowing the weight fraction of the bonded C_{18} chains allows the calculation of the volume fraction occupied by the bonded layer in each column. The difference with the total unaccessible volume gives the closed pore porosity. The results are reported in Table 4.3. Densities of 2.33 g/cm^3 for silica and 0.777 g/cm^3 for the alkyl chains have been assumed.

There may be a slight, positive systematic error on both values. The mass of silica was obtained by drying and weighing the column after completion of the experiments and subtracting the weight of the empty column measured before packing. Although dry methylene chloride (B.P. 40 °C) was used as the mobile phase and the column was purged with an excess of nitrogen at 50 °C (until constant weight), the packing might not have been completely cleaned of adsorbed material. However, the column temperature cannot be raised too high while it is purged with nitrogen, the bonded material becoming then too sensitive to oxidation.

The volume fraction occupied by the solid stationary phase is nearly the same for KROMASIL and ZORBAX (43 and 42%, respectively), it is about 25% smaller for YMC and 10% smaller for VYDAC. For almost the same value of the external porosity as ZORBAX, KROMASIL has a 50% higher volume fraction of bonded layer.

Closed Pores Porosity

The closed pore porosity is very small, nearly negligible and could probably be neglected. It is of the order of 1% for KROMASIL and ZORBAX for which the relevant data were available. The significant value of the amount of bonded alkyl material is the cause for an apparent density of the solid material in the particles which is markedly lower than that of solid silica (Table 4.1).

Furthermore, the value of the closed porosity is indirectly and only weakly related to the column performance. It is just a wasted amount of space in the column. It contributes neither to the retention nor to the particle mechanical strength but has, otherwise, no direct effect on column performance.

Column Total Porosity

The total column porosity is derived from the retention volume of either benzene in methylene chloride or uracil in methanol. Both methods give results which are in close agreement, albeit slightly different (see below, Table 4.2, and Chapter 3).

It should be noted that the total porosity on the one hand, the inaccessible volume fraction on the other hand, are determined separately and independently. The former is derived from chromatographic data, the latter from pycnometric measurements. The combination of these two sets of data as indicated in Eq. 4.1 should be equal to 1. Deviation of this sum from unity reflects all the errors made in the determination processes. Except for two columns (YMC # 1 and 3), the deviation is between +2 and +3%, which is small, considering the different conditions under which the measurements of density (hence, ϵ_U) and column hold-up volume (hence, ϵ_T) are carried out. This excess would be divided by approximately 2 if the retention volume of uracil instead of benzene was used. Note also that the difference between the numbers in the far right column of Table 4.2 and 1 is nearly constant for each stationary phase, suggesting the possibility of a systematic error of measurements which would be related to the nature of the material used.

The most important sources of error seem to be associated with the definition of the interface volume and the way it is accounted for. First, a fraction of the volume accessible to helium may be unaccessible to the mobile phase used in liquid chromatography, whose molecules

are much larger than those of helium. Second, in the measurement of the inaccessible volume fraction, the packing material is dried under vacuum and the bonded alkyl chains are collapsed against the underlying silica surface. In the measurement of the total porosity, the packing material is impregnated with a solvent (methylene chloride) which wets well the solid and the alkyl chains swim in the mobile phase. The weight fraction of bonded organic material is of the order of 10-12% on the products used. An amount of liquid octadecane equal to the amount of bonded chain would account for approximately 6% of the column volume. Collapsed chains occupy a larger volume than independent ones; when collapsed they block the access of small pores, so it is possible that the volume accessible to helium is slightly lower than the volume accessible to methylene chloride in spite of the larger size of the latter molecules. Note that these two effects act in opposite directions and may compensate to some extent.

Finally, while the relative standard deviation (rsd) on the inaccessible volume fraction is ca 0.03%, the rsd on the total porosity is 1%. The relative difference between the values of the total porosity derived from the retention volumes of benzene in methylene chloride (*e.g.*, average $\epsilon_{T,b} = 0.599$, rsd = 1% for KROMASIL) and of uracil in methanol ($\epsilon_{T,u} = 0.582$, rsd = 0.35%, also for KROMASIL) is 2.8%, which is significant. This suggests that further interpretation of the porosity data reported here is not warranted until a better understanding of the behavior of the liquid--solid interface is reached. This question will be discussed again in a further publication [Guan *et al*, in preparation].

Conclusion

Highly consistent data are obtained for all four packing materials. The relative standard deviations for the different volume fractions calculated are of the order of 0.5%. The agreement

between the values of the unaccessible volume fraction derived from helium pycnometry and from the total porosity, itself obtained from the retention volumes of benzene in methylene chloride and uracil in methanol is excellent. The values obtained for the internal porosity and for the volume fractions of the particle skeleton, the closed pore and the bonded layer are constant, when corrected for the influence of the changes of the packing density, hence of the external porosity (Eq. 4.1). This demonstrates the consistency of the data and the advantage of the later correction. The next problem is the determination of the internal and external porosity and the study of the pore size and particle size determination. These issues are discussed in Chapter 3] and will be revisited in further work [Guan *et al*, in preparation].

CHAPTER 5.

EFFECT OF THE PACKING PRESSURE ON THE PERFORMANCE OF C_{18} REVERSED PHASE LIQUID CHROMATOGRAPHIC COLUMNS

Introduction

The optimization of the experimental conditions of a preparative separation based on the use of the theory of nonlinear chromatography has become a distinct possibility [Guiochon *et al*, 1994] and an attractive proposition [Felinger *et al*, 1994] because of the potential savings in time and chemicals over the more traditional empirical approaches. However, the calculation of optimum experimental conditions requires the prior acquisition of relevant data regarding the equilibrium isotherms of the sample component and their mass transfer kinetics. The results of band profile calculations will be valid only as far as the thermodynamic and kinetic data used account accurately for the behavior of the column prepared for the actual separation or purification.

To achieve the potential savings in time and chemicals afforded by a fundamental approach to optimization, the experimental data must be acquired using analytical columns, not columns having a size of the same order of magnitude as the column actually needed for the industrial separation. Measurements on this column should be carried out only a few times, for the fine tuning eventually required. A major practical problem then arises, how to achieve a high degree of column-to-column reproducibility of chromatographic data. It has been repeatedly reported in

the literature [Poole *et al*, 1993] that the reproducibility of the performance of columns packed with the same stationary phase is moderate at best, although such studies have been mainly carried out with analytical columns having practically all the same inner diameter [Guan *et al*, 1994b,c; see Chapters 2, 3]. The differences observed between equilibrium isotherms measured on chromatographic columns having different diameters can be important, precluding the use of a direct scale-up approach [Sarker *et al*, 1994].

One of the important reasons for explaining these differences is the fact that the procedures used to pack analytical and preparative scale columns are often quite different. The former are packed by dynamic compression of a slurry using the viscous shear of a high velocity stream as the source of the consolidation stress [Kennedy *et al*, 1972; Poole *et al*, 1993], while the latter are packed by applying directly to the packing a mechanical stress, under either radial [Little *et al*, 1976] or axial compression [Godbille *et al*, 1976]. Since stress does not convey homogeneously in a bed of pulverulent material [Train, 1957], this latter process may not produce a column bed of constant density. Conversely, since the local flow velocity is proportional to the local column permeability, itself inversely related to the local packing density, the viscous shear is higher where the packing density is lower, which tends to result in a more homogeneous packing. I note, however, that these rationales are valid for the bulk packing but do not necessarily apply close to the column wall. Since first reported by Kirkland [Kirkland, 1973] and Verillon [Martin *et al*, 1976], there is growing evidence that the wall smoothness has a positive influence on the quality of the column. This influence of the column wall cannot be the same for a 4.6 mm or for a 30 cm i.d. column. Thus, we should pay great attention to the possible difference in the packing densities of columns in comparing thermodynamic and kinetic data obtained with them. This is especially important when both analytical and preparative scale columns are involved.

In earlier studies [Guan *et al*, 1994b,c; see Chapters 2, 3], I have demonstrated that columns packed with the same stationary phase under the same conditions have different performance, related to different packing densities. These differences can be corrected, in part, by the ratio of the individual column external porosities, which, itself, can be determined by Inverse Size Exclusion Chromatography [Halász, 1975; Halász *et al*, 1978; Nikolov *et al*, 1980; Werner *et al*, 1980; Groh *et al*, 1981; Crispin *et al*, 1982] and which is found to vary significantly from one column to another. Several questions remain unsolved, however. For example, what is the direct link between the external porosity of the column and its packing density? The determination of the column external porosity by ISEC requires the accurate measurement of the retention volumes of polystyrene standards. These volumes are rather small and difficult to measure accurately. Therefore, it would be more practical, more precise and probably more accurate to correct the isotherm parameters otherwise than by using the individual column external porosity. The aim of this work is to show that the determination of the weight of packing material contained in the packed column affords a useful alternative approach.

Theory

Thermodynamics of Phase Equilibrium

Under linear conditions, *i.e.*, for infinitely diluted samples (see a more accurate definition later in this section), the band profiles are usually nearly symmetrical. They can be modeled precisely enough by a Gaussian curve and two parameters are commonly used to characterize these elution profiles, the column efficiency, N_0, and the retention factor, k'

$$N_0 = 5.54\left(\frac{t_R}{\Delta t_w}\right)^2 \qquad k' = \frac{t_R - t_0}{t_0} \tag{5.1}$$

where t_R is the retention time of the band and t_0 is the column hold-up time.

In preparative chromatography, a large sample is used, the stationary phase concentration is no longer directly proportional to the mobile phase concentration, the column is said to be overloaded, the band profiles are no longer Gaussian nor even symmetrical, and the chromatographic separation is carried out under conditions which are no longer linear. The nonlinear behavior of equilibrium isotherms must be taken into account. The isotherm model used in this work is the Langmuir isotherm

$$q = \frac{q_s b C}{1 + bC} \tag{5.2}$$

where q is the stationary phase concentration, C is the mobile phase concentration, q_s is the saturation capacity, and b is a numerical coefficient. As seen in Eq. 5.2, linear conditions can be defined as those under which $bC << 1$, so the denominator in the RHS of Eq. 5.2 can be replaced by unity. The band profiles of large samples can be predicted accurately from the equilibrium isotherms [Guiochon *et al*, 1992; Guiochon *et al*, 1994].

The methods most commonly used for the experimental determination of isotherms are Elution by Characteristic Points (ECP) [Huber *et al*, 1971; Gerritse *et al*, 1972; Guiochon *et al*, 1994] and Frontal Analysis (FA) [Schay *et al*, 1954; James *et al*, 1954; Huber *et al*, 1971; Gerritse *et al*, 1972; Eltekov *et al*, 1985; Eltekov *et al*, 1986]. In ECP, the amount adsorbed at equilibrium with concentration C is

$$q = \frac{1}{V_p} \int_0^C (V - V_0)\, \delta_i C \tag{5.3}$$

where V_p is the volume of packing, V_0 is the column hold-up volume, V is the retention volume of

the point at concentration C on the diffuse boundary, and $\delta_i C$ is the concentration increment ($\sum \delta_i C = C$). This equation is derived from the ideal model of chromatography, which assumes an infinite column efficiency. In order to limit the consequences of this model error, a column efficiency of no fewer than 2000 plates is required for the column [Guan *et al*, 1994a].

In FA, the amount adsorbed at equilibrium with concentration C is calculated as

$$q_{i+1} = q_i + \frac{(C_{i+1} - C_i)\ (V_{F,i+1} - V_0)}{V_p} \tag{5.4}$$

where $V_{F,i+1}$ is the retention volume of the $i+1$th concentration step, q_i and q_{i+1} are the stationary phase concentrations in equilibrium with the ith and $i+1$th steps which have mobile phase concentrations of C_i and C_{i+1}, respectively. The major advantage of FA is that the results obtained with this method are independent of the column efficiency [Schay *et al*, 1954; James *et al*, 1954; Huber *et al*, 1971; Gerritse *et al*, 1972; Eltekov *et al*, 1985; Eltekov *et al*, 1986]. However, recent studies have shown that this is not true when the retention volume of the breakthrough front is derived using the most conventional methods of measurement of this volume. A column efficiency exceeding approximately one hundred theoretical plates is required [Sajonz *et al*, submitted; Sajonz *et al*, to be submitted] in order to avoid a systematic error.

Note that the coefficient b in Eq. 5.2 has the dimension of the inverse of a mobile phase concentration. The product bq_s, however, may or may not be dimensionless, depending on what units are chosen for the denominator V_p in Eqs. 5.3 and 5.4. V_p is commonly taken as the volume of stationary phase in the column. The apparent column volume or its geometrical volume, V_t, is also used in some cases. Then, the product bq_s is dimensionless. However, if I use the column packing weight W_p instead, the product bq_s has the units of *mL of solvent per mg of packing*.

Inverse Size Exclusion Chromatography (ISEC)

Samples of polymer standards of known molecular weights were successively injected into a chromatographic column. There is a correlation between the average molecular weight of the n-th sample, Mr_n, and its molecular size, ϕ_n. For polystyrene dissolved in methylene chloride, we have [Halász *et al*, 1978]

$$Mr_n = 2.25\ \phi_n^{1.7} \tag{5.5}$$

where ϕ_n is in angstrom (Å) units. This correlation is the basis of the determination of molecular size and molecular weight by size exclusion chromatography (SEC). In ISEC, the molecular weights of the polymeric samples are known and Eq. 5.5 is used to derive the integral pore volume distribution of the packing material from the retention volume distribution of the samples [see Chapter 3].

The total volume of a chromatographic column, V_k, can be written as the sum of four contributions

$$V_k = V_e + V_i + V_s + V_c \tag{5.6}$$

where V_e is the inter-particle or external pore volume, V_i is the intra-particle or internal pore volume, V_s is the stationary phase solid volume, and V_c is the closed-pore volume. This fourth term is accessible only if an assumption is made regarding the density of the solid silica.

Determination of the Different Volume Fractions

The volume fraction or porosity, ϵ_n, corresponding to a retention volume V_n, hence a certain pore size, ϕ_n, is defined by

$$\epsilon_n = \frac{V_n}{V_k} \tag{5.7}$$

According to this definition, the external porosity ϵ_e or total volume of the pores around the particles is

$$\epsilon_e = \frac{V_e}{V_k} \tag{5.8}$$

The internal porosity ϵ_i' is often defined in chromatography as the fractional column volume occupied by the internal pores

$$\epsilon_i' = \frac{V_i}{V_k} \tag{5.9}$$

The sum of these two porosities gives the total accessible porosity, ϵ_T, *i.e.*,

$$\epsilon_T = \epsilon_e + \epsilon_i' \tag{5.10}$$

This last definition leads to serious difficulties and may cause inconsistencies when the properties of beds of packing material consolidated to a different extent are compared. Then, the external porosity decreases with increasing value of the external stress applied to the column, while the true internal porosity of the particles decreases only slightly, the compressibility of the particle skeleton, made of solid silica, being limited [Guiochon *et al*, 1995]. Thus, it is more logical to define, as is commonly done in chemical engineering, the internal porosity as the fraction of the particle volume which is accessible to the mobile phase:

$$\epsilon_i = \frac{\epsilon_i'}{(1 - \epsilon_e)} \tag{5.11}$$

Then, the total column porosity becomes

$$\epsilon_T = \epsilon_e + \epsilon_i (1 - \epsilon_e) = \epsilon_e + \epsilon_i - \epsilon_i \epsilon_e \tag{5.12}$$

The accurate and precise determination of the internal and external porosities becomes a key to a better understanding of the packing behavior.

Experimental

Equipment

All experiments were made with a Hewlett-Packard (Palo Alto, CA) HP1090M liquid chromatograph equipped with a diode-array UV detector and a computerized data acquisition system. Retention factors, column efficiencies and ECP measurements were carried out at a detector wavelength of 250 nm. Frontal analysis (FA) was run at 270 nm. Porosity measurements by ISEC were run at 254 nm.

Columns

The empty stainless steel columns were purchased from Alltech (Deerfield, IL). All columns are 10 cm long and 0.46 cm I.D. Two 10 μm spherical C_{18} ODS packing material, one from KROMASIL® (Eka-Nobel, Stratford, CT, USA) with Lot No. DT0132 and pore size 100 Å and the other from ZORBAX® (BTR, Wilmington, DE, USA) with Lot No. B32161 and pore size 150 Å, were obtained. Each material was slurry packed into 10 columns in our laboratory.

The slurry solvent used was chloroform and the pushing solvent was methanol. The packing pressure used was 1,000 psi for the 1st column of each group, 2,000 psi for the 2nd column, ..., and 10,000 psi for the 10th column.

Chemicals

For thermodynamic studies, Uracil (Cat. No. 13078-8), m-Cresol (Cat. No. C8572-7, 99%), Benzyl alcohol (Cat. No. B1620-8, >99%), Methyl benzoate (Cat. No. M2990-8, 99%) and 2,6-Dimethyl phenol (Cat. No. D17500-5, 99%) were purchased from Aldrich (Milwaukee, WI); Acetone (Cat. No. AX0120-8, >99.5%) was purchased from EM Science (Gibbstown, NJ); Benzyl acetate (Cat. No. 45850, >99%), 2-Isopropyl phenol (Cat. No. 59720, >98%), and 3-Phenyl-1-propanol (Cat. No. 79000, >98%) were purchased from Fluka (Buchs, Switzerland). Both the mobile phase and the solvent used to dissolve the compounds listed above were a 45/55 (v/v) methanol/water solution. Methanol (Cat. No. 9093-33) was purchased from J. T. Baker (Phillipsburg, NJ). Water was freshly bidistilled/deionized in the laboratory, using a Thermolyne (Barnstead, Dubuque, IA) water-deionizing system consisting of two cartridges, one HN high-capacity DI cartridge (Cat. No. D8901) and one HG organic-removal cartridge (Cat. No. D8904). All samples and solvents were filtered on 0.45 μm pore size filters before use.

For porosity measurements, polystyrene standards with molecular weights ranging from 2,000 to 1,860,000 Daltons were purchased from SUPELCO (Bellefonte, PA). Polystyrene standards with molecular weights of 456, 1,050 and 3,840,000 Daltons were purchased from TOSOH (Tokyo, JAPAN). Benzene (Mr = 78.11 D) was purchased from EM Science (Gibbstown, NT). Methylene chloride (J.T. Baker, Phillipsburg, NJ) was used both as the mobile phase and the sample solvent.

Procedures

The amounts of samples used for the measurements of k' and N_o were 25 μg each of acetone, benzyl acetate, benzyl alcohol, m-cresol, 2,6-dimethyl phenol, methyl benzoate, 3-phenyl-1-propanol, and uracil. Uracil was also used for the determination of the system hold-up time, the stationary phase volume, and the average total porosity of the column, data which were later used for the equilibrium isotherm determinations.

To determine the equilibrium isotherm, the ECP measurements were made by injecting 0.120 mL of 35 mg/mL 3-phenyl-1-propanol solutions into each column. The FA measurements were made by having the liquid chromatograph solvent delivery system run a dedicated gradient program requiring 20 successive concentration step changes. Two pumps, one for the 45/55 (v/v) methanol/water mobile phase and the other one for a 20 mg/mL solution of 3-phenyl-1-propanol in the same solvent, were used for this purpose. The isotherm data obtained were fitted to a Langmuir isotherm model (Eq. 5.2) and the best coefficients were derived by applying the non-linear regression routine available at the University of Tennessee Computing Center (UTCC). The band profiles were calculated by applying the isotherm coefficients to the equilibrium-dispersive model solved by the Rouchon algorithm [Guiochon *et al*, 1994].

To apply ISEC, a total of 15 polystyrene standards with molecular weights ranging from 456 to 3,840,000 Dalton were injected into each column. Benzene was used for calibration and for the determination of the total accessible porosity, ϵ_T, of the column, which is practically equal to that measured with uracil in reversed phase liquid chromatography [see Chapter 3]. Each injection was repeated three times and the results listed are the average. Plots of the logarithm of the molecular weights of the probes versus their retention volumes showed a bimodal pore size distribution for each column. The external pore volume was derived from the intermediate point

between the two modes of the pore size distributions [Guiochon *et al*, 1994]. The total column volume, V_k, was calculated from the geometrical dimensions of the column tubing

$$V_k = \pi r^2 l \tag{5.13}$$

where r is the column radius (here $r = 0.23$ cm) and l the column length (here $l = 10.0$ cm). The external porosity, ϵ_e, was calculated from Eq. 5.8. Knowing ϵ_T and ϵ_e, the internal porosity, ϵ_i, is calculated from Eq. 5.12.

The empty weight of each column, W, was obtained prior to the packing procedure being applied. After the ISEC experiments, the column (filled with methylene chloride) was connected to a Hewlett Packard 5840A Gas Chromatography system, emptied and dried with a stream of ultra pure, dry nitrogen flowed through the column at an inlet pressure of 30 psi. The column was heated to 80 °C at a rate of 5 °C/minute and kept at this temperature, under the nitrogen stream, for at least 20 hours. After this step, the column was considered to be dried and its weight was measured as W^*. The packing weight, W_p, is then

$$W_p = W^* - W \tag{5.14}$$

An independent investigation has shown that under these experimental conditions, the column is dried to constant weight [Stanley *et al*, in preparation].

Detector Calibration

ECP requires detector calibration in order to allow the translation of the detector signal (mAu) into the solute concentration (mg/mL). Calibration was performed by pumping solutions of known concentration directly into the detector cell until a stable signal was obtained. A third-

order polynomial gave an excellent fit to the experimental data. The best coefficients of the fit were obtained by applying the polynomial regression in SigmaPlot (Jandel, San Rafael, CA) to the experimental data points.

Results and Discussion

Linear Chromatography Data

The chromatography data obtained under linear conditions are presented in Figures 5.1 and 5.2, in the format of the sample retention factors, k' (Figure 5.1), or the column efficiency at infinite dilution, N_0 (Figure 5.2), versus the packing pressure. For both packing materials, the values of both parameters, k' and N_0, tend to increase with increasing packing pressure. The retention factor for each compound tends to be larger on the KROMASIL® columns (Figure 5.1a) than on the ZORBAX® ones (Figure 5.1b), in agreement with the lower average pore size and larger surface area of the former material. The relative standard deviation (rsd) of the ten values of the retention factors of each of the compounds studied here is of the order of 3%, regardless of the column used. By contrast, the rsd for columns packed under the same experimental conditions is between 1 and 2% [see Chapter 2].

The rsd of the column efficiencies is much larger. The column efficiency increases rapidly with increasing retention factor. Note that the efficiency was measured at a single flow rate, which limits the validity of such comparison. For the KROMASIL® columns (Figure 5.2a), this rsd is on the order of 13%, comparable to the one observed for columns packed under the same pressure. On the other hand, for the ZORBAX® columns (Figure 5.2b) this rsd is around 11%, twice as much as for columns packed under the same pressure [see Chapter 2]. These results show that columns packed with the same stationary phase but under different packing

pressures may give performance which are quite significantly different.

Chromatograms

Eight of the ten chromatograms obtained are shown in Figures 5.3 (KROMASIL®) and 5.4 (ZORBAX®). Not shown for the sake of clarity of the figures are two chromatograms which are too close to some of those shown. These chromatograms are reported first as plots of the mobile phase concentration C versus the retention time (Figures 5.3a and 5.4a), as commonly done. The relative difference between the retention times of the earliest and the last eluted chromatograms exceeds slightly 10%. The plots of C versus the dimensionless retention factor, k', are illustrated in Figures 5.3b and 5.4b. They are at least as different and scattered as the previous ones. If I change the x-axis into the ratio of the sample retention factor k' and the column phase ratio F, *i.e.*, if I plot C versus the first parameter of the isotherm, the chromatograms become much closer for both packing materials, as shown in Figures 5.3c (KROMASIL®) and 5.4c (ZORBAX®). This suggests that a normalization of the isotherm data by a proper function of the porosity could correct for column-to-column fluctuations of the packing density.

Equilibrium Isotherms

The equilibrium isotherms of 3-phenyl-1-propanol on each column (not shown) were determined by both ECP and FA methods. The coefficients of the best Langmuir isotherm (Eq. 5.2) were derived using the SAS non-linear regression routine available at UTCC. The denominator, V_p, in both Eqs. 5.3 and 5.4 was first substituted by the column geometrical volume V_t (Eq. 5.13), then by the stationary phase volume, V_p . Tables 5.1 (KROMASIL®) and 5.2 (ZORBAX®) list the FA results obtained from V_t (rows $q_{s,vt}$ and b_{vt}) and both the ECP and FA

results obtained from V_p (rows $q_{s,Vp}$ and b_{Vp}). As shown by these Tables, $q_{s,Vt}$ is much smaller than $q_{s,Vp}$, while the coefficient b remains the same. There is also an excellent agreement between the isotherm coefficients obtained by both ECP and FA.

In Figure 5.5, the band profiles calculated with the isotherm coefficients obtained above are shown for the 10th column in each group. The agreement between the experimental chromatogram (symbols) and the band profile calculated with the isotherm coefficients derived from V_p and the experimental data on the same column (solid line) is excellent. The band profile calculated from the isotherm coefficients derived from V_t (long-chain line) is grossly incorrect. Figure 5.5 compares also the chromatograms calculated with the isotherm coefficients derived from V_p and the experimental data obtained on another column (column #1 in this case), without any modification or normalization (short-chain line). The agreement between the experimental profile (symbols) and this calculated band profile is poor. It is considerably improved when the isotherm data are corrected for the weight of packing (dotted line), as explained later.

Column Volume Fractions

The column total accessible volume was derived from the retention volumes of uracil in a 45/55 (v/v) methanol/water solution ($V_{T,w}$) and of benzene in methylene chloride ($V_{T,b}$). The results are listed in Tables 5.3 (KROMASIL®) and 5.4 (ZORBAX®). The agreement between these two sets of results is excellent, despite the systematic smaller value of $\epsilon_{T,w}$. This difference (ca 1.5%) could be explained by the partial or total collapse of the C_{18} chains onto the silica surface in the methanol/water solution while these chains are dissolved and extended in methylene chloride. Solvated chains leave between them a larger volume accessible to the mobile phase and to an unretained tracer than collapsed chains between which there are unaccessible cavities.

Indeed, $V_{T,a}$ is smaller than $V_{T,b}$ (Tables 5.3 and 5.4) which shows that the unaccessible volume is larger in methanol/water solution than in methylene chloride solution. In Figure 5.6, the column total porosity derived from the retention volume of benzene in methylene chloride, $\epsilon_{T,b}$, calculated from Eq. 5.8 is plotted versus the column packing pressure. A linear relationship is observed.

The column external porosity was determined by ISEC, using the procedure previously described [see Chapter 3]. The values of the column external porosity, ϵ_e, are listed in Tables 5.3 and 5.4 and plotted in Figure 5.6 versus the packing pressure. As the column total porosity, the external porosity decreases linearly with increasing packing pressure, showing that the space between the packing particles becomes smaller as the external stress resulting from viscous shear becomes larger.

The column internal porosity, ϵ_i, is derived by difference between the column total and external porosities, from Eq. 5.12. The results are also listed in Tables 5.3 and 5.4 and plotted in Figure 5.6. As expected, the packing pressure has little effect on the column internal porosity.

Packing Material Density

The weight of the packing material inside each column, W_p, the stationary phase volume, V_p, determined by injecting uracil in a 45/55 (v/v) methanol/water solution, the ratio of W_p and V_p, *i.e.*, the packing material actual density, d_p, and its apparent density, W_p / V_t, are listed in Table 5.5. As expected, both W_p and V_p increase in general as the packing pressure increases, while the ratio of these two quantities remains nearly constant. As a result, the higher the packing pressure, the more adsorbent particles are packed into the column, the heavier the packing material inside the column, the higher the apparent packing density, and the smaller the space between the particles, *i.e.*, the external porosity. This agrees with the above external porosity data. The

constancy of the actual density of the packing material is in agreement with that of the internal porosity.

Isotherm Correction by Packing Weight

As discussed earlier, the denominator in Eqs. 5.3 and 5.4 can be substituted by other stationary phase parameters than the column volume. I have found out that the isotherm coefficients derived by use of V_p give much more accurate result than that of V_t (Figure 5.5). However, in practice, it is more difficult to determine accurately a volume than a weight. Therefore, I now use the packing weight, W_p, obtained above to calculate the isotherm coefficients. The results are also listed in Tables 5.1 and 5.2 (rows $q_{s,w}$ and b_w). As expected, the coefficient b remains constant in all cases while q_s depends on which stationary phase parameter is used in the isotherm calculation.

Given the dispersion of the chromatograms obtained with the different columns of the batch studied (Figures 5.3 and 5.4), it is necessary to find out an easy way to unify the isotherm coefficients so that, after simple modification, the data measured on one column can be easily applied to the prediction of the chromatograms observed on another one. Considering the ease of measuring the weight of packing in a column, I considered normalizing the isotherm coefficients ($q_{s,w}$ and b_w) by the packing weight in the column. If I want to apply the results obtained from column I to column j, I write

$$q_{s,w,j} = q_{s,w,i} \frac{W_{p,j}}{V_{p,j}} \tag{5.15}$$

By applying this procedure, I used the modified isotherm parameters obtained from

column #1 onto #10 in both the KROMASIL® and the ZORBAX® column groups and recalculated the band profiles. The results are shown in Figure 5.5 (dotted line). As we can see, the difference between the simulated band profile and the experimental chromatogram is minimal in this case.

Conclusion

Accurate and dependable measurements of the porosity of liquid-chromatography columns can be made with inverse size exclusion chromatography. The data derived from these measurements demonstrate that the column packing density is directly affected by the packing procedure. The higher the packing pressure, the more particles of packing material can be packed inside the column, the larger the column packing density, the smaller the column external porosity, and the lower its permeability [Guiochon *et al*, 1995].

The isotherm coefficients measured on a column and reported to its geometrical volume cannot be used to predict accurately the band profiles obtained on another column because the apparent density of the packing varies from column to column. However, satisfactory results are obtained when the isotherm data are reported to the actual volume of stationary phase held in the column or to the weight of packing used. Considering the difficulties encountered in accurate volume determinations, the normalization procedure that uses the column packing weight offers the most practical solution.

CHAPTER 6.

STUDY OF THE MASS TRANSFER KINETICS OF BSA ON TSK-GEL DEAE-5PW ANION EXCHANGER IN A WIDE CONCENTRATION RANGE

Introduction

In recent years, preparative scale liquid chromatography has become an important technique for the large scale separation and purification of biopolymers such as peptides and proteins [Chang *et al*, 1976; Kato *et al*, 1982a,b; Regnier, 1987; Guiochon *et al*, 1987; Huang *et al*, 1989; Fulton *et al*, 1991; Liapis, 1993; Horvath *et al*, 1994]. The stationary phases most commonly used at present include both non-silica based polymers [Kato *et al*, 1982a,b; Fulton *et al*, 1991; Liapis, 1993] and silica based materials [Chang *et al*, 1976; Horvath *et al*, 1994]. The former (polyacrylamides, polysaccharides and related compounds) tend to be gentler on the tertiary structure of proteins and to cause less denaturation than the latter. However, polymeric phases suffer from two major drawbacks, their mechanical strength is weak and their mass transfer resistances are high. The poor mechanical strength prevents the use of the high pressures required for operating high efficiency columns[5]. Large particle sizes are needed to avoid crushing the bed under the intense stress caused by the viscous friction of the mobile phase stream and the associated high pressure gradient. This, in turn exacerbates the mass transfer resistance problem

[5] These columns have to be packed with fine particles (20 μm or smaller), to be relatively long (10 cm or longer), and to be operated at relatively high velocities (0.01 to 0.1 cm/sec) which may require inlet pressures between 10 and 100 atm, depending on the mobile phase viscosity and on the values of the column length and particle size.

by preventing the use of fine particles.

To break this vicious circle and achieve reasonable efficiencies under economically acceptable experimental conditions (*e.g.*, moderate flow rates), material scientists have tried to prepare particles having a strong skeleton, shielded from contact with the feed components and supporting a layer of a biocompatible polymer, which would provide retention and separation without significant degradation. There are two main contenders for the skeleton material, porous silica and polystyrene crossed-linked with divinylbenzene. These two lines of products, together with the conventional gel particles, are available to the separation scientist who is faced with a difficult choice and little reliable, basic information.

Although numerous publications discuss the behavior of these stationary phases, most are focussed on the thermodynamics (retention behavior) and on the biochemical characteristics (ability to denature). By contrast, little effort has been invested into systematic investigations of the mass transfer kinetics of proteins on these stationary phases, although several kinetic models of liquid chromatography are available [Hiester *et al*, 1958; Guiochon *et al*, 1994]. These models allow the derivation from experimental breakthrough curves of precise values of the axial dispersion coefficient and of a lumped rate coefficient for the mass transfer kinetics, a constant which includes contributions of all the mass transfer processes. Some investigations indicate a significant dependence of the diffusion [Gallagher *et al*, 1989; Marlowe *et al*, 1990] or the axial dispersion coefficient of proteins on their concentration in solution [Lederer *et al*, 1990]. Similar results have also been obtained with smaller molecules [*e.g.*, Trõger's base enantiomers on cellulose microcrystalline triacetate, Seidel-Morgenstern *et al*, 1993].

Among the stationary phases developed for HPLC, the TSK gels are among the most popular [Kato *et al*, 1982a,b]. This material is a weak anion exchanger made of semi-rigid porous

polymer beads. We have previously acquired isotherm data for several proteins on this material [Huang *et al*, 1990, 1991]. It appeared most suitable for a first investigation. The goal of the present work is the study of the mass transfer kinetics of a typical protein, Bovine Serum Albumin (BSA) on this same material.

Theory

The study of the profiles of breakthrough curves provides a useful method for characterizing both the equilibrium isotherm and the mass transfer kinetics of a solute on a stationary phase.

For a series of n successive steps, from initial solution concentration 0 to final concentration C_n, the stationary phase concentration, q_i at equilibrium with the mobile phase concentration C_i, is given by

$$q_i = \frac{C_i \, (V_{F,i} - V_0)}{V_p} \tag{6.1}$$

where $V_{F,i}$ is the retention volume of the ith breakthrough curve, V_0 is the column void volume, and V_p is the volume of stationary phase contained inside the column.

The isotherm data (sets of values of C_i and q_i acquired under the same experimental conditions) can be plotted in the isotherm format, *i.e.*, as plots of q versus C, and fitted to one of the classical isotherm models, or plotted in the Scatchard plot format (plots of q/C versus q). The two models used in this work are the Langmuir isotherm model

$$q = \frac{a\,C}{1 + b\,C} \tag{6.2}$$

where a and b are numerical coefficients, and the bi-Langmuir isotherm model

$$q = \frac{a_1 C}{1 + b_1 C} + \frac{a_2 C}{1 + b_2 C} \tag{6.3}$$

where a_1, b_1, a_2 and b_2 are numerical coefficients. In the former case (Eq. 6.2), the Scatchard plot is linear ($q/C = a - b\,q$). If the Scatchard plot is curved with a downward convexity, the latter model (Eq. 6.3) should be used. It suggests the existence of two types of non-cooperative, independent adsorption sites on the stationary phase [Andrade, 1985; Jacobson *et al*, 1990].

However, breakthrough curves contain more information than their mere retention time used to determine adsorption isotherms. Their profile depends on the mass transfer kinetics across the column and provides a way to determine its characteristics. I used a lumped kinetic model, coupling the conventional mass balance equation of ideal liquid chromatography

$$\frac{\partial C}{\partial t} + F\frac{\partial Q}{\partial t} + u\frac{\partial C}{\partial z} = 0 \tag{6.4}$$

(where F is phase ratio which is equal to $(1 - \epsilon_T)/\epsilon_T$; ϵ_T is total column porosity; Q, is actual stationary phase concentration; and u is mobile phase velocity) and the Solid Film Linear (SFL) driving force kinetic model [Hiester *et al*, 1958; Guiochon *et al*, 1994; Vermeulen *et al*, 1984], given by

$$\frac{\partial Q}{\partial t} = k_f (q - Q) \tag{6.5}$$

where k_f is the mass transfer coefficient or rate coefficient and q is the equilibrium concentration given by Eq. 6.2 or 6.3. The justification for the use of this simple model is in the relatively high efficiency of the column for a nonretained solute (see later), indicating a low value of the axial

dispersion, and the very low value of this efficiency for the protein studied, indicating slow mass transfer kinetics. There are no analytical solutions to this model. An asymptotic solution, however, assuming constant pattern behavior, has been derived by Glueckauf *et al* (1947).

Previous experimental results suggest that the rate coefficient of the mass transfer kinetics, k_f, is a function of the mobile phase concentration. This complicates the determination, as the data directly accessible from any given breakthrough profile is an average of the rate coefficient during the experiment. Recent theoretical studies [Sajonz *et al*, 1995] have shown how this problem can be solved.

Experimental

Column

A 7.5 x 0.75 cm stainless steel column (Cat. No. 07164) packed with TSK-Gel DEAE-5PW (No. S0116) was obtained from TOSOHAAS (Montgomeryville, PA). According to the manufacturer's data, this column contains a stationary phase volume, V_p, of 0.73 mL and has a void volume, V_o, of 2.58 mL. For 0.002 mg cytidine-5'-monophosphate injection at a flow rate of 1.0 mL/min of an eluent containing 35 mM NaCl in 20 mM Tris-HCl buffer at pH = 8.0, the column has an efficiency of 2,800 theoretical plates.

Materials

The pH standard solutions (pH = 4.0, 7.0 and 9.0) were purchased from BAXTER (Deerfield, IL). Bovine Serum Albumin (BSA) (Cat. No. A-4378), Tris (Cat. No. T-1503), and Bis-Tris (Cat. No. B-9754) were purchased from SIGMA (St. Louis, MO). Hydrochloric acid (Cat. No. 5620-02) and acetonitrile (Cat. No. 9017-03) were purchased from J. T. Baker

(Phillipsburg, NJ). Sodium chloride (Cat. No. 7581) was purchased from Mallinckrodt Specialty Chemicals Co. (Paris, KY). Sodium hydroxide solution (Cat. No. SX0607H-1) was purchased from EM Science (Gibbstown, NJ). Water was freshly bidistilled/deionized in the laboratory, using a Thermolyne (Barnstead, Dubuque, IA) water-deionizing system consisting of two cartridges, one HN high-capacity DI cartridge (Cat. No. D8901) and one HG organic-removal cartridge (Cat. No. D8904).

Equipments

An American pH II pH meter was used to measure the pH of the prepared buffers. A Sartorius balance was used for weighing the samples. A Perkin-Elmer (Norwalk, CT) series 400 pump system was used for the solvent and sample delivery. A SpectraFlow SF 757 UV detector connected with a Spectra-Physics SP 4270 integrator was used for recording data files during the experiments.

Sample Preparation

The buffer with pH = 7.5 was prepared by dissolving Tris into water to make up 50 mM concentration followed by the titration of HCl to reach the desired pH value. The buffer with pH = 6.0 was prepared by dissolving Bis-Tris into water to make up 25 mM concentration followed by the titration of HCl to reach the desired pH value. The pH meter was first calibrated using the three pH standard solutions and then used to measure the buffer pH during the titration. The prepared buffers were later used as the mobile phases and the solvents for the experiments.

The BSA sample solution for each experiment was prepared freshly by first weighing the dry BSA and then dissolving it into the same solvent as the one to be used as the mobile phase for

the experiment, in the amount needed to make up the desired sample concentration. For my experiments, neither the mobile phase nor the solvent used for dissolving the BSA sample contained any NaCl in order to maximize the column dynamic loading capacity.

A NaCl solution (> 1.0 M) was prepared by dissolving NaCl crystals into the same solvent as the one to be used as the mobile phase for the experiment. This solution was used to condition the column before each run and to elute the remaining protein from the column after each run.

Procedures

Four experimental conditions were chosen for obtaining the breakthrough curves: pH = 7.5 at 1.0 mL/min, and pH = 6.0 at 1.0, 2.0 and 3.0 mL/min flow rates. Under each condition, solutions were prepared with BSA sample concentrations ranging from ca. 0.2 to 3 mg/mL.

Once the buffer pH and the flow rate were chosen for a run and before starting the experiment, the column was conditioned by flowing through it ca. 20 mL NaCl solution and then equilibrated by flowing ca. 20 mL of mobile phase. These two solutions were pre-stored in two separate solvent reservoirs. Then a third pump started pumping the BSA sample solution through the column until the concentration plateau came out. Immediately afterward, the column was washed by ca. 20 mL of NaCl buffer solution.

All solvents and samples were filtered with 0.2 μm cellulose acetate filters before application.

Detector Calibration

During my experiments, the wavelength was set at 280 nm. The detector calibration was

made by pumping the known protein solution directly into the detector flow cell until a stable signal was obtained. A parabolic function was found to best fit the calibration data points. However, the detector response at 280 nm was saturated for the 3 mg/mL concentration.

Column Regeneration

After each series of measurements, the column was regenerated before making further experiments under new experimental conditions. The mobile phase solution used for this purpose was a 30/70 (v/v) acetonitrile/buffer mixture. It was pumped through the column at a flow rate of 0.5 mL/min for ca. 30 min. In between 0.25 mL of 0.2 M NaOH solution was injected into the column in 5 increments. The column was then conditioned and equilibrated.

Results and Discussion

Adsorption Isotherms

The adsorption isotherms of BSA were determined by applying Eq. 6.1 to each breakthrough curve. The classical isotherm plots are shown in Figure 6.1. At low flow rates (1.0 and 2.0 mL/min), the plots are well-behaved, while at 3.0 mL/min, the isotherm data points are very scattered (see inset) and the high concentration limit is much lower. This confirms the importance of carrying out isotherm determinations at low mobile phase flow velocities, as pointed out by Jacobson *et al* (1984). Even when the theoretically accurate integration method is used [Sajonz *et al*, 1995], there is a systematic error due to the noise recorded by the detector on the concentration plateau. This noise caused the integration to be stopped too early. Accordingly, these data were not used further in my work. Even at lower flow rates, significant instabilities of the plateau recorded by the detector are observed, as is almost always the case with proteins. This

practically forces to use the retention time at half-height of the step for the isotherm determination. This choice gives precise results which are still sufficiently accurate, as shown by Sajonz *et al* (1995). The isotherms obtained for pH=6.0 at the two different flow rates used (1 and 2 mL/min) are very close (Figure 6.1). This shows that the isotherm data obtained are thermodynamic equilibrium data, in spite of the relatively slow mass transfer kinetics [Jacobson *et al*, 1984; Guiochon *et al*, 1994].

It should be noted that the equilibrium concentration in the stationary phase at 0.15 mg/mL, the lowest mobile phase concentration used, is already high. This fact and the results of earlier studies [Huang *et al*, 1990, 1991] suggested that the bi-Langmuir isotherm model could represent well the isotherm data. The Scatchard plots, Figure 6.2, have the downward convexity indicative of this model (Eq. 6.3). The best isotherm coefficients for the bi-Langmuir model were calculated by use of an SAS non-linear regression routine available at the University of Tennessee Computer Center (UTCC). It turned out, however, that, after optimization, the value for b_2 remained zero. The isotherm obtained is a special case of the bi-Langmuir isotherm model; it is actually a single Langmuir isotherm (Eq. 6.2) plus a linear term (a_2C). The physical interpretation of the result is not straightforward. It may suggest aggregation of the proteins in the sorbed phase. However, the most probable explanation is a mixed retention mechanism. Ionized proteins interact with ion exchangers as ions but a significant contribution to their retention arises from molecular interactions between the hydrophobic patches on their surface and the polystyrene chains of the resin matrix. A similar type of isotherm has been found by Jandera *et al* (1991) for cholesterol and cholesteryl acetate on C_{18} silica and by Charton *et al* (1995) for chiral separations. This isotherm model is in agreement with the nature of the Scatchard plot in Figure 6.2 [Andrade, 1985; Jacobson *et al*, 1984; Jacobson *et al*, 1990; Huang *et al*, 1990, 1991]. Still, the isotherm

obtained should be considered as empirical at this stage.

Nevertheless, this isotherm accounts well for the experimental results, as demonstrated by the agreement between the lines in Figure 6.1 (best fitted isotherms) and the symbols (data points). The isotherm parameters are listed in Table 6.1. Finally, the lines in the inset of Figure 6.1 show the best fitted Langmuir equation (with coefficients also listed in Table 6.1). The agreement with the experimental data is less satisfactory, especially for the data collected at pH=6.0 and 1 mL/min, which justifies the use of the more complex model. It is important to reduce the isotherm model error since both isotherm and mass transfer kinetics control the width of the breakthrough curves. The residuals are listed in Table 6.1. They show that the experimental isotherm data fit the bi-Langmuir model better than the Langmuir model. This is another reason in favor of the more complex model.

Mass Transfer Kinetics Data

A computer program using a finite difference algorithm was used to calculate numerical solutions of the lumped kinetic model. Because the column efficiency measured for a nonretained component is relatively high (2800 theoretical plates) while the breakthrough profiles are wide, the axial dispersion term was neglected [Guiochon *et al*, 1994]. Thus, the profiles obtained depend only on one parameter, the rate coefficient of the mass transfer kinetics, which can be adjusted to best fit any given experimental curve. With a column length of 7.5 cm and values of the mobile phase flow velocities of 0.048 cm/s (with k_f between 1.3 and 15.0 x 10^{-3} s^{-1}) or 0.097 cm/s (with k_f between 1.7 and 26.7 x 10^{-3} s^{-1}), the Stanton number ($St=k_f l/u$) is between approximately 0.1 and 2.3, values which are extremely low. This justifies neglecting the contribution of axial dispersion to band broadening. In these calculations, the whole set of data point is shifted (by

adjustment of the flow rate, hence the retention time), so as to bring its mass center at the center of the calculated curve. This allows the use of a simple optimization program minimizing the distance between the calculated curve and the experimental profile. The shift was only a few percents for my experimental data.

First, I assumed the rate coefficient of the mass transfer kinetics, k_f, to be independent of the concentration and determined its optimum value for the best fit of the first breakthrough curve, the one corresponding to the lowest concentration step. Then, using this constant value and the isotherm obtained above, I calculated the breakthrough curves. Figures 6.3 to 6.5 compare the results of these calculations (lines) and the experimental profiles (symbols), for the three series of experiments obtained with pH = 7.5 and 1.0 mL/min (Fig. 6.3), pH = 6.0 and 1.0 mL/min (Fig. 6.4), and pH = 6.0 and 2.0 mL/min (Fig. 6.5). These figures demonstrate that only at low concentrations (C < 0.5 mg/mL, see Figs. 6.3, 6.4, and 6.5) do the calculated curves match reasonably well the experimental ones. At high concentrations, the experimental curves are much steeper than the calculated ones, showing that the rate coefficient must be higher than estimated. Obviously, the breakthrough curves cannot be fitted properly to the profiles calculated with a constant value of k_f. Thus, the rate coefficient of the mass transfer kinetics on TSK-Gel DEAE-5PW is concentration dependent. This increase of the rate coefficient with increasing concentration enhances the self-sharpening behavior of breakthrough curves observed in the case of convex downward isotherms.

In a second step, I calculated for each breakthrough curve the best value of the rate coefficient, the value which minimizes the distance between calculated and experimental profiles. An example of the fitting procedure followed, as described above, is given for the lowest concentration step in the inset of Fig. 6.6. In this case, the time shift made was - 6 minutes,

smaller than 2 % of the retention time. The calculation procedure assumes the rate coefficient to be constant for each single breakthrough curve but to vary from one breakthrough curve to the next as a function of the concentration plateau. This procedure is not accurate because it gives an *average rate coefficient* k_f, relative to the average concentration of each breakthrough curve, but it gives an approximate value of the concentration dependence. However, this estimate turns out to be accurate enough in the present case, as we see later. The error would increase with increasing rate of variation of the rate coefficient, dk_f/dC. The calculated curves (solid lines) are compared with the experimental results (symbols) in Figures 6.6 (pH = 7.5 at 1.0 mL/min), 6.7 (pH = 6.0 at 1.0 mL/min), and 6.8 (pH = 6.0 at 2.0 mL/min). The agreement is considerably improved compared to the use of a constant value of k_f, especially at high concentrations. The precision in the estimation of the best value of the rate coefficient was approximately ± 10 %. The choice of the best average rate coefficient was somehow arbitrary since the upper part of the breakthrough curves did not fit very well in a number of cases. In these cases, the value of the rate coefficient was optimized for the best fit of approximately the lower two thirds of the breakthrough curve. This is illustrated in the inset of Figure 6.6.

The values obtained for the average rate coefficients are listed in Table 6.2. Figure 6.9 shows plots of these values as a function of the average sample concentration. The rate coefficient increases nearly linearly with increasing concentration. The consequence of such a dependence has been studied theoretically by Sajonz *et al* (1995). The data measured at different values of the pH are very close. By contrast, the values of the rate coefficient obtained for the higher flow rate of 2 mL/min appear to be somewhat higher than those found at 1 mL/min. However, no general conclusions can be derived from these limited results at this stage. Systematic experiments should be carried out in a wider range of flow rates. However, as shown above, results obtained at high

velocities are unreliable (Fig. 6.1, inset), while results at lower velocities take a prohibitively long time.

Finally, I calculated band profiles using the same nondispersive lumped kinetic model as earlier but with a rate coefficient which is a linear function of the concentration, with the numerical coefficients in Table 6.2. The profiles calculated are shown in Figures 6.6 to 6.8 (dashed lines). There are no great differences between the two sets of calculated profiles in the Figures. Those corresponding to a rate coefficient increasing linearly with increasing concentration are, expectedly, somewhat steeper than those for an average rate coefficient remaining constant for a given plateau concentration. However, both sets agree well with the experimental data. This justifies the procedure used here in order to take into account the concentration dependence of the rate coefficient.

Conclusion

The excellent agreement between the experimental profiles of the breakthrough curves of Bovine Serum Albumin on TSK-Gel DEAE-5PW anion exchange resin and the profiles calculated using a simple nondispersive lumped kinetic model is due to the extremely slow process of mass transfer observed in this case.

The conclusion that the rate coefficient changes by more than one order of magnitude when the BSA concentration increases 15-fold is important. It confirms previous reports by different authors who have all observed important increases of the rate coefficient of the mass transfer kinetics with increasing concentrations. Further investigations of the mass transfer kinetics are in progress on other stationary phases, in an effort to assess the importance and the generality of the phenomenon.

CHAPTER 7.

STUDY OF THE REPRODUCIBILITY AND MASS TRANSFER KINETICS OF BSA ON TWO IDENTICAL RESOURCE-Q COLUMNS

Introduction

The use of preparative chromatography for the separation and purification of biochemicals has become increasingly popular in the recent past [Chang *et al*, 1976; Kato *et al*, 1982a; Kato *et al*, 1982b; Regnier, 1987; Guiochon *et al*, 1987; Huang *et al*, 1989; Fulton *et al*, 1991; Liapis, 1993; Horvath *et al*, 1994]. Both non-silica based polymers [Kato *et al*, 1982a; Kato *et al*, 1982b; Fulton *et al*, 1991; Liapis, 1993] and silica based materials [Chang *et al*, 1976; Horvath *et al*, 1994] have been used as the stationary phases. Most of the many publications that discuss the behavior of these stationary phases are focussed on a description of the results achieved, a discussion of the biochemical characteristics of these phases or the determination of their thermodynamic properties.

In previous studies [see Chapters 2, 3, 4, and 5], I have reported that, albeit nearly identical in nature, columns packed with a given stationary phase could have quite different values for the parameters of their properties. Most of these differences appear to originate from differences in the packing density, causing differences in the permeability, efficiency, and isotherm parameters. These studies were carried out on C_{18} columns, which are commonly used in Reversed Phase Liquid Chromatography (RPLC). Little attention has been paid to the same aspect in Ion Exchange Liquid

Chromatography (IXLC). A high degree of reproducibility of column properties is important to achieve because it is necessary to satisfy current Good Manufacturing Practice (cGMP) requirements, because it is useful for scale-up from laboratory to industrial scale separations, and because the operation of Simulated Moving Bed separators requires a rather large number of nearly identical columns.

I determined the main characteristics of two RESOURCE-Q anion exchange columns (Pharmacia Biotech Inc., Piscataway, NJ, USA). This includes the phase ratio, the isotherm data and the rate coefficient of the mass transfer kinetics for Bovine Serum Albumin (BSA). This stationary phase is made of rigid, monodisperse 15 μm beads whose matrix consists of polystyrene cross-linked with divinyl benzene. The results will also be compared with those previously obtained for a similar material [see Chapter 6].

Theory

The equilibrium isotherms in this study were determined by Frontal Analysis (FA), using a series of steps. For each one in a series of n successive concentration steps, a breakthrough curve is obtained. In this series, each sigmoidal profile ranges from the initial mobile phase concentration, usually 0, to a final concentration plateau, C_n. At the end of the ith step, the stationary phase concentration q_i is in equilibrium with the mobile phase concentration C_i. It can be calculated by

$$q_i = \frac{C_i \, (V_{F,i} - V_0)}{V_p} \tag{7.1}$$

where $V_{F,i}$ is the retention volume of the ith breakthrough curve, V_0 is the column void volume, and V_p is the volume of stationary phase contained inside the column.

The isotherm data points (q_i and C_i) obtained can be fitted to an isotherm model. In this study, a special format of the bi-Langmuir isotherm model was used, *i.e.*,

$$q = \frac{a_1 C}{1 + b_1 C} + \frac{a_2 C}{1 + b_2 C} \tag{7.2}$$

where a_1, b_1, a_2, and b_2 are numerical coefficients. This model suggests the existence of two types of non-cooperative, independent adsorption sites on the stationary phase [Andrade, 1985; Jacobson *et al*, 1990]. One of them is certainly the ion exchanger groups bonded to the aromatic rings in the polystyrene chains. The other is probably the matrix of the resin itself, interacting with the hydrophobic patches at the surface of the protein molecules. It turns out that the best value of the fourth coefficient for the experimental data is very small, practically negligible, so the second term of the isotherm model reduces to a linear term.

The mass transfer kinetics was studied by combining the conventional mass balance equation of ideal liquid chromatography

$$\frac{\delta C}{\delta t} + F \frac{\delta Q}{\delta t} + u \frac{\delta C}{\delta z} = 0 \tag{7.3}$$

(where F is the phase ratio, which can be determined from the column total porosity ϵ_T, $F = (1 - \epsilon_T)/\epsilon_T$, and u is the mobile phase velocity) and the Solid Film Linear (SFL) driving force kinetic model [see Chapters 2 and 3; Hiester *et al*, 1958]

$$\frac{\delta Q}{\delta t} = k_f (q - Q) \tag{7.4}$$

where k_f is the mass transfer coefficient or rate constant, Q is the actual stationary phase concentration, and q is the equilibrium concentration given by the equilibrium isotherm (Eq. 7.2).

Experimental

Columns

Two RESOURCE-Q anion exchange columns were obtained from Pharmacia Biotech Inc. (Piscataway, NJ, USA). Both columns have the same catalog number but different lot numbers. The column information is summarized in Table 7.1.

Materials

The pH standard solutions (pH = 4.0, 7.0 and 9.0) were purchased from BAXTER (Deerfield, IL). Bovine Serum Albumin (BSA) (Cat. No. A-4378), Tris (Cat. No. T-1503), and Bis-Tris (Cat. No. B-9754) were purchased from SIGMA (St. Louis, MO). Hydrochloric acid (Cat. No. 5620-02) and acetonitrile (Cat. No. 9017-03) were purchased from J. T. Baker (Phillipsburg, NJ). Sodium chloride (Cat. No. 7581) was purchased from Mallinckrodt Specialty Chemicals Co. (Paris, KY). Sodium hydroxide solution (Cat. No. SX0607H-1) was purchased from EM Science (Gibbstown, NJ). Water was freshly bidistilled/deionized in the laboratory, using a Thermolyne (Barnstead, Dubuque, IA) water-deionizing system consisting of two cartridges, one HN high-capacity DI cartridge (Cat. No. D8901) and one HG organic-removal cartridge (Cat. No. D8904).

Equipments

An American pH II pH meter was used to measure the pH of the prepared buffers. A Sartorius balance was used for weighing the samples. A Perkin-Elmer (Norwalk, CT) series 400 pump system was used for the solvent and sample delivery. A SpectraFlow SF 757 UV detector (Kratos, Ramsey, NJ) connected with a Spectra-Physics SP 4270 (San Jose, CA) integrator was used for recording data files during the experiments.

Sample Preparation

A pH = 6.0 buffer was prepared by dissolving Bis-Tris into water to make up a 25 mM concentration solution which was titrated with HCl to reach the desired pH value. The pH meter was first calibrated using the three pH standard solutions and then used to measure the buffer pH during the titration. The prepared buffers were later used as the mobile phases and the solvents for the experiments.

The BSA sample solution for each experiment was prepared freshly by first weighing the dry BSA and then dissolving it into the same solvent as the one to be used as the mobile phase for the experiment, in the amount needed to make up the desired sample concentration. For my experiments, neither the mobile phase nor the solvent used for dissolving the BSA sample contained any NaCl in order to maximize the column dynamic loading capacity.

A NaCl solution (> 1.0 M) was prepared by dissolving NaCl crystals into the same solvent as the one to be used as the mobile phase for the experiment. This solution was used to condition the column before each run and to elute the remaining protein from the column after each run.

Procedures

The experiments for obtaining the breakthrough curves were made with the pH = 6.0 buffer as the mobile phase, at 1.0 mL/min flow rate. Solutions were prepared with BSA in concentrations ranging from 0 to 4 mg/mL. All solvents and samples were filtered with 0.2 μm cellulose acetate filters before application.

The stationary phase volume inside each column, V_p, was determined by injecting a diluted uracil solution in the buffer used as the mobile phase. Acetone was found to be slightly retained. The system hold-up time (due to extra-column volumes) was measured and corrected for in all the

retention time determinations. The values of V_p, hence, of the phase ratio F for each column are listed in Table 7.1 (last two rows).

Before starting the acquisition of the breakthrough curves, the column was conditioned by flowing through it ca. 20 mL of the NaCl solution. Then it was equilibrated by flowing ca. 20 mL of mobile phase. These two solutions were pre-stored in two separate solvent reservoirs. A third pump was used to pump the BSA sample solution throughout the column until the concentration plateau came out. Immediately afterward, the column was washed by ca. 20 mL of NaCl buffer solution. After that, a second breakthrough curve could be acquired.

Detector Calibration

During my experiments, the wavelength was set at 260 nm. The detector calibration was made by pumping known protein solutions directly into the detector flow cell until a stable signal was obtained. A parabolic function was found to best fit the calibration data points.

Results and Discussion

Column Phase Ratio

The stationary phase volume, V_p, of each column is listed in Table 7.1. Although the two columns studied are supposed to be packed with the same material, but admittedly with different lot numbers, the stationary phase volume for the first column, hence the amount of stationary phase that it contains, is nearly 64% higher than that of the second one. Knowing the column geometrical volume is 0.965 mL, the phase ratio, F, for each column can be calculated, as listed in the last row of Table 7.1. Due to the difference in the stationary phase volumes, the phase ratios of these two columns differ by nearly 83%. This result confirms that columns packed with the same stationary

phase do not necessarily have the same properties. This observation had been reported previously in reversed phase liquid chromatography [see Chapters 2, 3, 4, and 5]. It seems that the column to column variations are much larger still in ion exchange liquid chromatography.

Adsorption Isotherms

The adsorption isotherm data points of BSA on each column were determined by applying Eq. 7.1 to each breakthrough curve. The results are shown in Figure 7.1 (symbols). A bi-Langmuir isotherm model (Eq. 7.2) was found to best fit the experimental data points. The isotherm coefficients were calculated by applying the SAS non-linear regression routine available at the University of Tennessee Computing Center (UTCC). The results are listed in Table 7.2 and plotted in Figure 7.1 (lines). This figure illustrates the large difference between the adsorption isotherms on the two columns. For the second column (Table 7.2), the third isotherm coefficient, a_2, is near zero, suggesting that this isotherm is close to the Langmuir model. This is not the case for the first column, whose a_2 value is much larger (ca. 15 times). This difference shows that the thermodynamic properties of the two columns are quite different.

Although the difference in volume of the stationary phase contained in the two columns could be easily explained by a difference in degree of consolidation, a property certainly difficult to reproduce with soft particles, as opposed to silica particles, this does not explain the differences between the isotherm coefficients. The retention factors at infinite dilutions ($k' = F(a_1 + a_2)$) on the two columns are quite similar. Retention is approximately 25% larger on the first column, the one which has the largest amount of stationary phase. However, the saturation capacity on the second column is nearly 70% larger, while the amount of stationary phase is nearly 64% smaller. This could rather be explained by differences in the matrix density and the degree of substitution of

the aromatic rings by the ionizable groups.

Mass Transfer Kinetics - Rate Coefficient Independent of the Concentration

The average rate of the mass transfer kinetics was determined for each breakthrough curve. The value of the rate coefficient obtained corresponds to the average concentration range of the corresponding step. A computer program using a finite difference algorithm allows the calculation of the numerical solutions of the lumped kinetic model for any value of the rate coefficient, whether constant or a function of the BSA concentration [see Chapter 6]. By identification of the experimental and the calculated breakthrough curve, the best value of the rate coefficient is obtained. The precision is approximately 10% [see Chapter 6].

In Figures 7.2 (column # 1) and 7.3 (column # 2), the rate coefficient, k_f, determined for the lowest concentration breakthrough curve was used to calculate the other breakthrough curves, regardless of the height of the concentration step. The agreement between calculated and experimental breakthrough curves is poor on these figures. It degrades when the BSA concentration increases. This indicates that the rate coefficient of the mass transfer kinetics changes with the sample concentration. This confirms previous findings on TSK-Gel [see Chapter 6].

Mass Transfer Kinetics - Rate Coefficient Concentration Dependence

The best value of the rate coefficient for each breakthrough curve was determined as explained in a previous section. The calculated breakthrough curve that best fits each experimental breakthrough curve so that the deviation between experimental and calculated curves is minimal, is shown in Figures 7.4 (column # 1) and 7.5 (column # 2). The agreement is generally very good. In a few instances, a slight adjustment of the retention time of the breakthrough curve had to be

done. The corresponding values of the rate coefficient for each breakthrough curve are listed in Table 7.3.

In Figure 7.6, the rate coefficient, k_f, is plotted versus the average concentration of BSA, C_{ave}, which is equal to half the height of the concentration step. As seen in the figure, the rate coefficient increases linearly with increasing sample concentration for both columns. The linear relationships are represented by the straight lines in the figure. These lines nearly go through the origin of coordinates. The coefficients of the linear regression are reported in Table 7.3 for each column. The slope observed for the first column is nearly three times as large as that for the second column. At constant BSA concentration, the rate constant for the first column is much larger than that for the second column. It is difficult to explain such a result by a difference between the packing densities of the two columns, although such a difference could not be ruled out. A difference in density of cross-linking of the polystyrene matrix and possibly in the bonding density of ionizable groups is much more probable.

Conclusion

The column-to-column reproducibility of the packing material studied seems to be insufficient at this stage for the safe development of industrial applications. All the properties studied, phase ratio, packing density, equilibrium thermodynamics of BSA between the packing and the buffer solution used as the mobile phase, rate coefficient of the mass transfer kinetics, all seem to be quite different on the two columns. This points to major efforts which should be made in the future if preparative liquid chromatography is to become a major technique of separation in the pharmaceutical industry.

CHAPTER 8.

CONCLUSIONS

In summary, the conclusions drawn during this study are:

1. Liquid chromatographic columns packed with the same stationary phase may not have the same performance, appearing to be different equilibrium isotherms, retention factors, column efficiencies, and external pore size distributions, *etc.*

2. The externa, internal and total porosities of a column and its external pore size distribution can be determined by Inverse Size Exclusion Chromatography (ISEC). Helium pycnometry results suggest that the closed pore porosity of the packing material is 1 to 2 % at most therefore negligible. There is an excellent agreement between the values derived from helium pycnometry and from ISEC.

3. High resolution Scanning Electron Microscopy (SEM) pictures show that the particles of liquid chromatographic packing material are not as spherical as they are claimed to be by the individual manufacturers.

4. The column packing density is directly affected by the packing procedure. The higher the packing pressure, the more particles of packing material can be packed inside the column, the larger the column packing density, the smaller the column external porosity.

5. The isotherm coefficients measured on a column and reported to its actual volume of stationary phase held in the column or to the weight of packing can be used to predict accurately the band profiles obtained on another column. Considering the difficulties encountered in accurate volume determination, the normalization procedure that uses the

column packing weight offers the most practical solution.

6. The rate coefficient of mass transfer kinetics between the protein sample and ion exchanger resins increases linearly with increasing sample concentrations.

LIST OF REFERENCES

Adkins, B.D.; Davis, B.H. *J. Phys. Chem.*, **90**, 4866(1986).

Afeyan, N.B.; Gordon, N.F.; Mazsaroff, I.; Varady, L.; Fulton, S.P.; Yang, Y.B.; Regnier, F.E. *J. Chromatogr.*, **519**, 1(1990).

Afeyan, N.B.; Fulton, S.P.; Regnier, F.E. *J. Chromatogr.*, **544**, 267(1991).

Andrade, J.D. *Surface and Interfacial Aspects of Biomedical Polymers*, Plenum Press, New York, **2**, 1(1985).

Bambrick, W.E.; Geoghegan, J.T. *Anal. Chem.*, **41**, 1516(1969).

Bhattacharja, S.; D'Orazio, F.; Tarczon, J.C.; Halperin, W.P.; Gerhardt, R. *J. Am. Ceram. Soc.*, **72**, 2126(1989).

Bonmati, R.; Chapelet-Letourneux, G.; Guiochon, G. *Separat. Sci. Technol.*, **19**, 113 (1984).

Brace, W.F.; Silver, E.; Hadley, K.; Goetze, C. *Science*, **17**, 162(1972).

Bristow. P.A. *J. Chromatogr.*, **149**, 13(1978).

Brunauer, S.; Emmett, P.H.; Teller, E. *J. Am. Chem. Soc.*, **60**, 309(1938).

Chang, S.H.; Gooding, K.M.; Regnier, F.E. *J. Chromatogr.*, **125**, 103(1976).

Charton, F.; Nicoud, R.M. *J. Chromatogr. A.*, **702**, 97(1995).

Ching, C.B.; Lim, B.G.; Lee, E.J.D.; Ng, S.C. *J. Chromatogr.*, **634**, 215 (1993).

Colin, H.; Ward, N.; Guiochon, G. *J. Chromatogr.*, **149**, 169 (1978a).

Colin, H.; Guiochon, G. *J. Chromatogr.*, **158**, 183(1978b).

Colin, H; Diez-Masa, J.C.; Guiochon, G. *J. Chromatogr.*, **167**, 41(1978c).

Courant, R.; Friedrichs, K.O.; Lewy, H. *Math. Ann.*, **100**, 32(1928).

Craig, L.C. *J. Biol. Chem.*, **155**, 519(1944).

Crispin, T.; Halász, I. *J. Chromatogr.*, **239**, 351(1982).

Cuatrecasas, P.; Anfinsen, C.B. *Methods in Enzymology*, Academic Press, New York, NY, 1971.

Czok, M.; Guiochon, G. *Anal. Chem.*, **62**, 189(1990).

Davies, S.; Packer, K.J. *J. Appl. Phys.*, **67**, 3163(1990).

Deen, W.M.; Bohrer, M.P.; Epstein, N.B. *AIChE J.*, **27**, 952(1981).

Delage, P.; Altcin, P. *Ind. Eng. Chem. (Prod. Res. Dev.)*, **22**, 286(1983).

DeVault, D. *J. Am. Chem. So.*, **65**, 532 (1943).

Do, D.D. *AIChE J.*, **30**, 849(1984).

Donnet, J.B.; Kobel, L.; Sevenster, A. *Ind. Eng. Chem. (Fundam.)*., **13**, 83(1974).

El Fallah, M.Z.; Guiochon, G. *Anal. Chem.*, **63**, 859, 2244(1991).

Eltekov, Y.A.; Kazakevitch, Y.V.; Kiselev, A.V.; Zhuchkov, A.A. *Chromatographia*, **20**, 525(1985).

Eltekov, Y.A.; Kazakevitch, Y.V. *J. Chromatogr.*, **365**, 213(1986).

Felch, D.E.; Shuck, F.O. *Ind. Eng. Chem. (Fundam.)*, **10**, 299(1971).

Feldman, R.F. *J. Am. Ceram. Soc.*, **67**, 30(1984).

Felinger, A.; Guiochon, G. *AIChE J.*, **40**, 594 (1994).

Fulton, S.P.; Afeyan, N.B.; Gordon, N.F.; Regnier, F.E. *J. Chromatogr.*, **547**, 452(1991).

Gallagher, H.W.; Woodward, C.K. *Biopolymers*, **28**, 2001(1989).

Gerritse, R.E.; Huber, J.F.K. *J. Chromatogr.*, **71**, 173(1972).

Gethner, J.S. *J. Appl. Phys.*, **59**, 1068(1986).

Giddings, J.C. *Dynamics of Chromatography*, M.Dekker, New York, NY, 1965.

Giddings, J.C. *Unified Separation Science*, Wiley, New York, NY (1991).

Glinka, C.J.; Sander, L.C.; Wise, S.A.; Hunnicutt, M.L.; Lochmuller, C.H. *Anal.*

Chem., **57**, 2079(1985).

Glueckuf, E.; Coates, J.A. *J. Chem. Soc.*, 1315(1947).

Godbille, E.; Devaux, P. *J. Chromatogr.*, **122**, 317(1976).

Golshan-Shirazi, S.; Guiochon, G. *Anal. Chem.*, **60**, 2364(1988).

Golshan-Shirazi, S.; Guiochon, G. *J. Phys. Chem.*, **93**, 4143(1989).

Golshan-Shirazi, S.; Guiochon, G. *J. Phys. Chem.*, **94**, 495(1990).

Greyson, R.I.; Patch, A.M. *J. Chromatogr.*, **242**, 349(1982).

Groh, R.; Halász, I. *Anal. Chem.*, **53**, 1325(1981).

Grushka, E. *Bonded Stationary Phases in Chromatography*, Ann Arbor Sci. Publ., Ann Arbor, MI, 1974.

Guan, H.; Stanley, B.J.; Guiochon, G. *J. Chromatogr. A*, **659**, 27(1994a).

Guan, H.; Guiochon, G. *J. Chromatogr. A*, **687**, 179(1994b).

Guan, H.; Guiochon, G. *J. Chromatogr. A*, **687**, 201(1994c).

Guan, H.; Guiochon, G. Gulakowski, K.; Davis, E.; Smith, D.W. *J. Chromatogr. A*, in preparation.

Guiochon, G.; Katti, A.M. *Chromatographia*, **24**, 165(1987).

Guiochon, G; Golshan-Shirazi, S.; Jaulmes, A. *Anal. Chem.*, **60**, 1856(1988).

Guiochon, G.; Katti, A.M.; Diack, M.; El Fallah, M.Z.; Golshan-Shirazi, S.; Jacobson, S.C.; Seidel-Morgenstern, A. *Acc. Chem. Res.*, **25**, 366(1992).

Guiochon, G.; Golshan-Shirazi. S.; Katti, A.M. *Fundamentals of Preparative and Nonlinear Chromatography*, Academic Press, Boston, MA, 1994.

Guiochon, G.; Sarker, M. *J. Chromatogr. A*, **704**, 237 (1995).

Haarhoff, P.C.; Van Der Linde, H.J. *Anal. Chem.*, **38**, 573(1966).

Halász, I. *Ber. Bunsenges Phys. Chem.*, **79**, 731(1975).

Halász, I.; Martin, K. *Angew. Chem. Int. Ed. Engl.*, **17**, 901(1978).

Haring, R.E.; Greenkorn, R.A. *AIChE J.*, **16**, 477(1970).

Hashimoto, K.; Silveston, P.L. *AIChE J.*, **19**, 368(1973).

Herino, R.; Bomchil, G.; Barla, K.; Bertrand, C. *J Electrochem. Soc.*, **134**, 1994(1987).

Hiester, N.K.; Vermeulen, T. *Chem. Eng. Prog.*, **48**, 505(1958).

Horvath, J.; Boschetti, E.; Guerrier, L.; Cooke, N. *J. Chromatogr. A*, **679**, 11(1994).

Howard, A.J.; Carta, G.; Byers, C.H. *Ind. Eng. Chem. Res.*, **27**, 1873(1988).

Huang, J.X.; Guiochon, G. *J. Chromatogr. Review*, **492**, 431(1989).

Huang, J.X.; Schudel, J.; Guiochon, G.; *J. Chromatogr.*, **504**, 335(1990).

Huang, J.X.; Schudel, J.; Guiochon, G. *J. Chromatogr. Sci.*, **29**, 122(1991).

Huber, J.F.K.; Gerritse, R.E. *J. Chromatogr.*, **58**, 138(1971).

Hudak, P.F. *Environ. Geo.*, **24**, 140(1994).

Jacobson, J.; Frenz, J.; Horvath, Cs. *J. Chromatogr.*, **316**, 53(1984).

Jacobson, S.C.; Golshan-Shirazi, S.; Guiochon, G. *J. Am. Chem. Soc.*, **112**, 6492(1990).

James, D.H.; Phillips, C.S.G. *J. Chem. Soc.*, 1066(1954).

Jandera, P.; Guiochon, G. *J. Chromatogr.*, **588**, 1(1991).

Kaizuma, H. *Anal. Chem.*, **56**, 638(1984).

Kathawalla, I.A.; Anderson, J.L. *Ind. Eng. Chem. (Res.)*, **27**, 866(1988).

Kato, Y.; Nakamura, K.; Hashimoto, T. *J. Chromatogr.*, **245**, 193(1982a).

Kato, Y.; Nakamura, K.; Hashimoto, T. *J. Chromatogr.*, **253**, 219(1982b).

Kennedy, J.G.; Knox, J.H. *J. Chromatogr. Sci.*, **10**, 549(1972).

Kerch, H.M.; Gerhardt, R.A.; Grazul J.L. *J. Am. Ceram. Soc.*, **73**, 2228(1990).

King, C.B.; Chu, K.H.; Hidajat, K.; Uddin, M.S. *AIChE J.*, **38**, 1744 (1992).

Kirkland, J.J. *Modern Practice of Liquid Chromatography*, Wiley, New York, NY (1971).

Kirkland, J.J. *J. Chromatogr.*, **83**, 149(1973).

Kirkland, J.J.; Snyder, L.R. *Modern Practice of Liquid Chromatography*, Academic Press, New York, NY, 1984.

Knox, J.H.; Saleem, M. *J. Chromatogr. Sci.*, **12**, 614(1969).

Knox, J.H.; Scott, H.P. *J. Chromatogr.*, **316**, 311(1984).

Knox, J.H.; Ritchie, H.J. *J. Chromatogr.*, **387**, 65(1987).

Kocirik, M.; Zikanova, A. *Ind. Eng. Chem. (Fundam.)*, **13**, 347(1974).

Komiyama, H.; Smith, J.M. *AIChE J.*, **20**, 1110(1974).

Kováts, E. *The Science of Chromatography*, F.Bruner Ed., Journal of Chromatography Library #32, Elsevier, Amsterdam, The Netherlands (1985).

Krueger, S.; Long, G.G.; Black, D.R.; Minor, D.; Jamian, P.R.; Nieman, G.W.; Page, R.A. *J. Am. Ceram. Soc.*, **74**, 2538(1991).

Lathe, G.H.; Ruthven, C.R.J. *Biochem. J.*, **62**, 665(1956).

Lederer, K.; Amtmann, I.; Vijayakumar, S.; Billiani, J. *J. Liquid Chromatogr.*, **13**, 1849(1990).

Li, Z.; Giese, R.F.; van Oss, C.J.; Kerch, H.M.; Burdette, H.E. *J. Am. Ceram. Soc.*, **77**, 2220(1994).

Liapis, A.I.; McCoy, M.A. *J. Chromatogr. A*, **599**, 87(1992).

Liapis, A.I. *Math. Modeling and Sci. Computing*, **1**, 397(1993).

Lin, B.C.; Guiochon, G. *Sep. Sci. Technol.*, **24**, 31(1989).

Locke, D.C. *J. Chromatogr. Sci.*, **11**, 120(1973).

Little, J.N.; Cotter, R.L.; Prendergast, J.A.; McDonald, P.D. *J. Chromatogr.*, **126**, 439(1976).

Ma, Z.; Guiochon, G. *Comput. Chem. Eng.*, **15**, 415(1991).

Mair, B.J.; Montjar, M.J.; Rossini, F.D. *Anal. Chem.*, **28**, 56 (1956).

Majors, R.E. *Int. Lab.*, **July-August**, 25(1972).

Marlowe, R.L.; Jackson, H.E. *Spectroscopy Letters*, **23**, 1203(1990).

Martin, A.J.P.; Synge, R.L.M. *Biochem. J.*, **35**, 1359(1941).

Martin, M.; Eon, C.; Guiochon, G. *J. Chromatogr.*, **110**, 213(1975).

Martin, M.; Verillon, F.; Eon, C.; Guiochon, G. *J. Chromatogr.*, **125**, 17(1976).

McCoy, M.A.; Liapis, A.I.; Unger, K.K. *J. Chromatogr. A*, **644**, 1(1993).

Merrill, M.R. *AIChE J.*, **40**, 1262(1994).

Meyer, B.A.; Smith, D.W. *Ind. Eng. Chem. (Fundam.)*, **24**, 360(1985).

Miller, N.T. *J. Chromatogr.*, **550**, 301(1991).

Mishra, B.K.; Sharma, M.M. *AIChE J.*, **34**, 684(1988).

Murakata, T.; Sato, S.; Ohgawara, T.; Watanabe, T.; Suzuki, T. *J. Mater. Sci.*, **27**, 1567(1992).

Nicoud, R.M.; Fuchs, G.; Adam, P.; Bailley, M.; Kusters, E.; Antia, F.; Reuille, R.; Schmid, E. *Chirality*, **5**, 267 (1993).

Nikolov, R.; Werner, W.; Halász, I. *J. Chromatogr. Sci.*, **18**, 207(1980).

Northrop, D.M.; Scott, R.P.W.; Martire, D.E. *Anal. Chem.*, **63**, 1350(1991).

Novak, L.T.; Coulman, G.A. *Can. J. Chem. Eng.*, **53**, 60(1975).

Ogan, K.; Katz, E.; Slavin, W. *Anal. Chem.*, **51**, 1315(1979).

Ogan, K.; Katz, E. *J. Chromatogr.*, **188**, 115(1980).

Olsson, M.; Sander, L.C.; Wise, S.A. *J. Chromatogr.*, **477**, 277(1989).

Ouchlyama, N.; Tanaka, T. *Ind. Eng. Chem. (Fundam.)*, **23**, 490(1984).

Pakula, R.J.; Greenkorn, R.A. *AIChE J.*, **17**, 1265(1971).

Pedersen, K.O. *Arch. Biochem. Biophys. Suppl.*, **1**, 157(1962).

Phillips, M.W.; Subramania,n G.; Cracer, S.M. *J. Chromatogr.*, **454**, 1(1988).

Poole, C.F.; Poole, S.K. *Chromatography Today*, Elsevier, Amsterdam, The Netherlands, 1993.

Regnier, F.E. *J. Chromatogr.*, **418**, 115(1987).

Rice, R.W. *J. Am. Ceram. Soc.*, **77**, 2232(1994).

Ritter, H.L.; Drake, L.C. *Ind. Eng. Chem. (Anal.)*, **17**, 782 (1945).

Rogers, L.B. In S. Siggia, Ed., *Survey of Analytical Chemistry*, McGraw-Hill, New York, 1968, Chapter 11.

Roos, J.R.; Celis, J.P.; Fan, C. *J. Electrochem. Soc.*, **137**, 1096(1990).

Rouchon, P.; Schönauer, M.; Valentin, P.; Guiochon, G. *Separat. Sci. Technol.*, **22**, 1793(1987).

Roumeliotis, P.; Unger, K.K. *J. Chromatogr.*, **149**, 211(1978).

Roz, B.; Bonmati, R.; Hagenbach, G.; Valentin, P.; Guiochon, G. *J. Chromatogr. Sci.*, **14**, 367(1976).

Ruckenstein, E.; Tsai, M.C. *AIChE J.*, **27**, 697(1981).

Ruthven, D.M.; Ching, C.B. *Chem. Eng. Sci.*, **44**, 1011 (1989).

Sajonz, P.; Zhong, G.M.; Guiochon, G. *J. Chromatogr. A*, 1995, submitted.

Sajonz, P.; Zhong, G.M.; Guiochon, G. *J. Chromatogr. A*, 1995, to be submitted.

Sakodynskii, K. *J. Chromatogr.*, **49**, 2(1970).

Sakodynskii, K. *J. Chromatogr.*, **73**, 303(1972).

Sander, L.C.; Wise, S.A. *J. Chromatogr.*, **316**, 163(1984).

Sarker, M.; Guiochon, G. *LC-GC*, **12(4)**, 300(1994).

Sarker, M.; Katti, A.M.; Guiochon, G. *J. Chromatogr. A*, in press.

Schay, G.; Szekely, G. *Acta Chim. Hung.*, **5**, 167(1954).

Seidel-Morgenstern, A.; Jacobson, S.C.; Guiochon, G. *J. Chromatogr.*, **637**, 19(1993).

Semonian, B.P.; Manes, M. *Anal. Chem.*, **49**, 991(1977).

Sing, K.S.W. *Chem. & Ind.*, **17**, 475(1982).

Skoog, D.A.; West, D.M.; Holler, F.J. *Fundamentals of Analytical Chemistry*, 5th ed., W.B.Saunders, New York, 1988, Chapters 23-25.

Smillie, R.D.; Wang, D.T., Merez, O. *J. Environ. Sci. Health*, **A13**, 47(1978).

Smith, D.M. *AIChE J.*, **32**, 1039(1986).

Somonian, B.P.; Manes, M. *Anal. Chem.*, **49**, 991(1977).

Spedding, F.H.; Voight, A.F.; Gladrow, E.M.; Sleight, N.R.; Powel, J.E.; Wright, J.M; Butler, T.A.; Figard, P. *J. Am. Chem. Soc.*, **69**, 2786 (1947).

Stanek, V.; Szekely, J. *The Canadian Journal of Chemical Engineering*, **50**, 9(1972).

Stanley, B.; Foster, C.; Guiochon, G. In Preparation.

Stegeman, G.; Kraak, J.C.; Poppe, H. *J. Chromatogr.*, **550**, 721(1991).

Stegeman, G.; Kraak, J.C.; Poppe, H.; Tijssen, R. *J. Chromatogr. A*, **657**, 283(1993).

Strobel, H.A.; Heineman, W.R. *Chemical Instrumentation: A Systematic Approach*, 3rd ed., Wiley, New York, 1989, Chapters 24-26.

Su, J.L.; Perlmutter, D.D. *AIChE J.*, **31**, 973(1985).

Talu, O.; Guo, C.; Hayhurst, D.T. *J. Phys. Chem.*, **93**, 7294(1989).

Ternan, M.; Fuller, O.M. *Can. J. Chem. Eng.*, **51**, 106(1973).

Ternan, M.; Packwood, R.H.; Buchanan, R.M.; Parsons, B.I. *Can. J. Chem. Eng.*, **60**, 33(1982).

Tiller, F.M.; Yeh, C.S. *AIChE J.*, **31**, 1241(1985).

Train, D. *Trans. Instn. Chem. Engrs.*, **35**, 258(1957).

Tswett, M.S. *Tr. Protok. Varshav. Obshch. Estestvoistpyt., Otd. Biol.*, **14** (1905).

Unger, K.K.; Messer, W.; Krebs, K.F. *J. Chromatogr.*, **149**, 1(1978).

Van Deemter, J.J.; Zuiderweg, F.J.; Klinkenberg, A. *Chem. Eng. Sci.*, **5**, 271(1956).

Vermeulen, T.; LeVan, M.D.; Hiester, N.K.; Klein, G. *Handbook of Chemical Engineering*, Perry Ed., McGrawHill, New York, 6th edition, 1984.

Verzele, M.; Dewaele, C. *Preparative High Performance Liquid Chromatography*, TEC, Gent, Belgium, 1986, Chapter I.

Wang, Q.C.; Hosoya, K.; Svec, F.; Frechet, J.M.J. *Anal. Chem.*, **64**, 1232(1992).

Wang, Y.J.; Wu, T.C.; Chiang, C.L. *AIChE J.*, **35**, 1551(1989).

Welinder, B.S.; Kornfelt, T.; Sorensen, H.H. *Anal. Chem*, **67**, 39A(1995).

Werner, W.; Halász, I. *J. Chromatogr. Sci.*, **18**, 277(1980).

Whitaker, S. *AIChE J.*, **13**, 420(1967).

Wicke, E. *Kolloid Z.*, **86**, 295(1939).

Willard, H.H.; Merritt, Jr., L.L.; Dean, J.A.; Settle, Jr., F.A. *Instrumental Methods of Analysis*, 7th ed., Wadsworth, Belmont, CA, 1988, Chapter 1.

Wise, S.A.; May, W.E. *Anal. Chem.*, **55**, 1479(1983).

Wilson, J.N. *J. Am. Chem. Soc.*, **62**, 1583(1940).

Wotzak, G.P. *AIChE J.*, **20**, 197(1974).

Yau, W.W.; Kirkland, J.J.; Bly, D.D. *Modern Size-Exclusion Liquid Chromatography: Practice of Gel Permeation and Gel Filtration Chromatography*, Wiley, New York, 1979.

Yau, W.W.; Kirkland, J.J.; Bly, D.D. *Chem. Anal.*, **98**, 277(1989).

Yu, Q.; Wang, N.H.L. *Comput. Chem. Eng.*, **13**, 915(1989).

Zhang, J.; Gungor, M.N.; Lavernia, E.J. *J. Mater. Sci.*, **28**, 1515(1993).

Zhao, J.; Harmer, M.P. *J. Am. Ceram. Soc.*, **75**, 830(1992).

Zheng, J.; Reed, J.S. *J. Am. Ceram. Soc.*, **72**, 810(1989).

APPENDIX

Table 2.1 Column Packing Conditions (10 μm particles); Column Dimension 10 cm x 0.46 cm i.d.

Brand	KROMASIL	VYDAC	YMC	ZORBAX
Lot No.	DT 0080	920714-28-1	EC 16717	B 32110
Pore Size (Å)	100	90	120	150
Slurry Solvent	30 % Methylene Chloride and 70 % Isopropanol	60 % Chloroform and 40 % Acetone	Methylene Chloride	30 % Methylene Chloride and 70% Isopropanol
Pushing Solvent	same as above	33 % Isopropanol and 67 % Methanol	Methanol	same as above
Pressure Increase	Direct	Step Gradient	Direct	Direct
Maximum Pressure (psi)	10,000	7,000	4,000	8,000
Packing Time (min)	5	20	10	5
Settle Time (min)	5	30	5	5

Table 2.2 Column Characteristics

Columns		#1	#2	#3	#4	#5
KROMASIL	V_p	0.684	0.698	0.690	0.697	0.696
	V_o	0.978	0.964	0.972	0.965	0.966
	$\epsilon_{T,M}$	0.588	0.580	0.585	0.581	0.581
	ϵ_e	0.383	0.370	0.371	0.366	0.368
	F	0.645	0.675	0.672	0.681	0.681
VYDAC	V_p	0.608	0.611	0.601	0.609	0.597
	V_o	1.054	1.051	1.061	1.053	1.065
	$\epsilon_{T,M}$	0.634	0.632	0.638	0.634	0.641
	ϵ_e	0.372	0.368	0.369	0.366	0.366
	F	0.570	0.580	0.575	0.577	0.575
YMC	V_p	0.502	0.497	0.504	0.503	0.499
	V_o	1.160	1.165	1.158	1.159	1.163
	$\epsilon_{T,M}$	0.698	0.701	0.697	0.697	0.700
	ϵ_e	0.394	0.394	0.393	0.393	0.396
	F	0.414	0.416	0.422	0.418	0.416
ZORBAX	V_p	0.676	0.673	0.681	0.674	0.681
	V_o	0.986	0.989	0.981	0.988	0.981
	$\epsilon_{T,M}$	0.593	0.595	0.590	0.594	0.590
	ϵ_e	0.399	0.401	0.395	0.398	0.398
	F	0.658	0.650	0.669	0.658	0.667

Table 2.3 KROMASIL: k' and N_0 Measurements

Samples		Columns					Ave. ± Std.
		#1	#2	#3	#4	#5	
URA 0.7 μg	N_0	1552	1926	2278	2256	2177	2038±305
ACE 76 μg	k'	0.291	0.300	0.300	0.303	0.300	0.299±0.004
	N_0	1666	2247	2765	2848	2571	2419±480
MCR 25 μg	k'	4.516	4.645	4.701	4.707	4.680	4.650±0.079
	N_0	2133	3057	3562	3502	3484	3148±602
BAL 25 μg	k'	2.044	2.106	2.120	2.132	2.116	2.104±0.035
	N_0	2144	2888	3438	3377	3355	3040±547
MBE 25 μg	k'	10.143	10.446	10.496	10.543	10.471	10.420±0.159
	N_0	2672	3767	4329	4083	4264	3823±679
BAC 25 μg	k'	9.921	10.226	10.243	10.313	10.225	10.186±0.152
	N_0	3708	3865	4568	4054	4328	4105±347
DPH 25 μg	k'	9.181	9.479	9.463	9.571	9.432	9.425±0.146
	N_0	2284	3275	3859	3695	3910	3405±674
PPR 25 μg	k'	7.583	7.832	7.799	7.900	7.783	7.779±0.119
	N_0	2301	3254	3705	3710	3779	3350±622

Table 2.4 VYDAC: k' and N_0 Measurements

Samples		Columns					Ave. ± Std.
		#1	#2	#3	#4	#5	
URA 0.7 μg	N_0	1185	1353	1169	1284	1012	1201 ± 129
ACE 76 μg	k'	0.287	0.291	0.289	0.290	0.280	0.287 ± 0.004
	N_0	1277	1529	1385	1533	1617	1468 ± 136
MCR 25 μg	k'	3.419	3.420	3.450	3.472	3.440	3.440 ± 0.022
	N_0	1063	1469	1143	1158	959	1158 ± 191
BAL 25 μg	k'	1.650	1.658	1.649	1.650	1.634	1.648 ± 0.009
	N_0	1270	1565	1400	1525	1577	1467 ± 131
MBE 25 μg	k'	8.496	8.493	8.427	8.371	8.355	8.428 ± 0.066
	N_0	1793	2530	2237	2405	2572	2307 ± 316
BAC 25 μg	k'	8.104	8.112	8.035	8.003	7.977	8.046 ± 0.060
	N_0	1909	3676	3394	3677	3717	3275 ± 774
DPH 25 μg	k'	6.511	6.519	6.517	6.588	6.536	6.534 ± 0.031
	N_0	1162	1741	1266	1469	1497	1432 ± 226
PPR 25 μg	k'	5.633	5.658	5.617	5.630	5.603	5.628 ± 0.020
	N_0	1430	1749	1637	1784	1853	1691 ± 165

Table 2.5 YMC: k' and N_0 Measurements

Samples		Columns					Ave. ± Std.
		#1	#2	#3	#4	#5	
URA 0.7 μg	N_0	2650	2878	2548	2745	2664	2697 ± 123
ACE 76 μg	k'	0.232	0.228	0.230	0.230	0.226	0.229 ± 0.002
	N_0	3066	3385	3144	3602	3366	3313 ± 213
MCR 25 μg	k'	3.796	3.796	3.843	3.756	3.691	3.776 ± 0.057
	N_0	3149	3397	3281	3197	3442	3293 ± 126
BAL 25 μg	k'	1.760	1.756	1.770	1.745	1.715	1.749 ± 0.021
	N_0	3207	3471	3315	3462	3460	3383 ± 118
MBE 25 μg	k'	8.632	8.629	8.693	8.518	8.353	8.565 ± 0.134
	N_0	3602	4035	3931	4015	4034	3923 ± 185
BAC 25 μg	k'	8.421	8.421	8.473	8.318	8.152	8.357 ± 0.128
	N_0	4254	5446	5154	6083	5572	5302 ± 675
DPH 25 μg	k'	7.494	7.483	7.534	7.401	7.255	7.433 ± 0.111
	N_0	3248	3636	3445	3676	3592	3519 ± 175
PPR 25 μg	k'	6.329	6.322	6.355	6.246	6.118	6.274 ± 0.096
	N_0	3437	3579	3449	3593	3573	3526 ± 76

Table 2.6 ZORBAX: k' and N_0 Measurements

Samples		Columns					Ave. ± Std.
		#1	#2	#3	#4	#5	
URA 0.7 μg	N_0	2546	2671	2630	2666	2745	2652±72
ACE 76 μg	k'	0.219	0.218	0.221	0.220	0.223	0.220±0.002
	N_0	3222	3237	3201	3242	3339	3248±53
MCR 25 μg	k'	2.994	3.061	3.041	3.033	3.102	3.046±0.040
	N_0	3200	3141	3206	3276	3193	3203±48
BAL 25 μg	k'	1.428	1.447	1.443	1.442	1.474	1.447±0.017
	N_0	3258	3266	3269	3311	3224	3266±31
MBE 25 μg	k'	7.752	7.877	7.845	7.891	8.098	7.893±0.127
	N_0	3980	3884	3840	3911	4524	4028±282
BAC 25 μg	k'	7.405	7.508	7.472	7.533	7.729	7.529±0.121
	N_0	4484	4018	4791	4322	4269	4377±286
DPH 25 μg	k'	5.959	6.054	6.018	6.093	6.272	6.079±0.118
	N_0	3473	3374	3402	3451	3414	3423±39
PPR 25 μg	k'	5.191	5.264	5.237	5.303	5.450	5.289±0.099
	N_0	3378	3347	3422	3408	3365	3384±31

Table 2.7 Isotherm Studies on KROMASIL Columns

		Columns				
		#1	#2	#3	#4	#5
ECP	*a*	11.608 ±0.003	11.791 ±0.002	12.326 ±0.001	11.965 ±0.001	11.907 ±0.001
		Average of all 5 columns: 11.919±0.265				
	b (mL/mg)	0.0690± 0.0001	0.0689± 0.0001	0.0707± 0.0001	0.0681± 0.0000	0.0681± 0.0000
		Average of all 5 columns: 0.0690±0.0011				
FA	*a*	10.763 ±0.075	11.099 ±0.089	11.652 ±0.114	11.302 ±0.098	11.211 ±0.102
		Average of all 5 columns: 11.205±0.322				
	b (mL/mg)	0.0548± 0.0008	0.0572± 0.0010	0.0587± 0.0012	0.0570± 0.0011	0.0569± 0.0011
		Average of all 5 columns: 0.0569±0.0014				
k'_i / k'_{ave}		0.975	1.007	1.003	1.015	1.000
k' - ECP	*a*	11.318 ±0.003	11.873 ±0.002	12.363 ±0.001	12.145 ±0.001	11.907 ±0.001
		Average of all 5 columns: 11.921±0.391				
	b (mL/mg)	0.0690± 0.0001	0.0689± 0.0001	0.0707± 0.0001	0.0681± 0.0000	0.0681± 0.0000
$\epsilon_{e,i} / \epsilon_{e,ave}$		1.030	0.995	0.997	0.984	0.989
ϵ_e - ECP	*a*	11.957 ±0.003	11.732 ±0.001	12.289 ±0.001	11.774 ±0.001	11.776 ±0.001
		Average of all 5 columns: 11.906±0.231				
	b (mL/mg)	0.0690± 0.0001	0.0689± 0.0001	0.0707± 0.0001	0.0681± 0.0000	0.0681± 0.0000
$a = k' / F$		11.757	11.603	11.606	11.601	11.429
		Average of all 5 columns: 11.599±0.116				

Table 2.8 Isotherm Studies on VYDAC Columns

		Columns				
		#1	#2	#3	#4	#5
ECP	*a*	10.827 ±0.004	10.739 ±0.003	10.917 ±0.003	10.790 ±0.003	11.040 ±0.003
		Average of all 5 columns: 10.863±0.119				
	b (mL/mg)	0.0483± 0.0001	0.0462± 0.0001	0.0457± 0.0001	0.0454± 0.0001	0.0457± 0.0001
		Average of all 5 columns: 0.0463±0.0012				
FA	*a*	10.442 ±0.072	10.420 ±0.061	10.561 ±0.069	10.448 ±0.054	10.693 ±0.068
		Average of all 5 columns: 10.513±0.115				
	b (mL/mg)	0.0417± 0.0007	0.0411± 0.0006	0.0402± 0.0007	0.0401± 0.0005	0.0402± 0.0007
		Average of all 5 columns: 0.0407±0.0007				
k'_i / k'_{ave}		1.001	1.005	0.998	1.000	0.996
k' - ECP	*a*	10.837 ±0.004	10.792 ±0.003	10.895 ±0.003	10.790 ±0.003	10.996 ±0.003
		Average of all 5 columns: 10.862±0.086				
	b (mL/mg)	0.0483± 0.0001	0.0462± 0.0001	0.0457± 0.0001	0.0454± 0.0001	0.0457± 0.0001
$\epsilon_{e,i} / \epsilon_{e,ave}$		1.011	1.000	1.003	0.995	0.995
ϵ_e - ECP	*a*	10.946 ±0.004	10.739 ±0.003	10.950 ±0.003	10.736 ±0.003	10.985 ±0.003
		Average of all 5 columns: 10.871±0.108				
	b (mL/mg)	0.0483± 0.0001	0.0462± 0.0001	0.0457± 0.0001	0.0454± 0.0001	0.0457± 0.0001
$a = k' / F$		9.882	9.755	9.769	9.757	9.744
		Average of all 5 columns: 9.781±0.057				

Table 2.9 Isotherm Studies on YMC Columns

		Columns				
		#1	#2	#3	#4	#5
ECP	*a*	16.026 ±0.002	16.153 ±0.003	15.981 ±0.003	15.750 ±0.003	15.539 ±0.002
		Average of all 5 columns: 15.890±0.244				
	b (mL/mg)	0.0573± 0.0001	0.0569± 0.0001	0.0569± 0.0001	0.0558± 0.0001	0.0546± 0.0001
		Average of all 5 columns: 0.0563±0.0011				
FA	*a*	15.478 ±0.142	15.723 ±0.136	15.320 ±0.121	15.298 ±0.133	15.027 ±0.107
		Average of all 5 columns: 15.369±0.256				
	b (mL/mg)	0.0526± 0.0011	0.0534± 0.0010	0.0528± 0.0009	0.0528± 0.0010	0.0519± 0.0008
		Average of all 5 columns: 0.0527±0.0005				
k'_i / k'_{ave}		1.009	1.008	1.013	0.995	0.975
k' - ECP	*a*	16.170 ±0.003	16.282 ±0.003	16.189 ±0.003	15.671 ±0.003	15.151 ±0.002
		Average of all 5 columns: 15.893±0.478				
	b (mL/mg)	0.0573± 0.0001	0.0569± 0.0001	0.0569± 0.0001	0.0558± 0.0001	0.0546± 0.0001
$\epsilon_{e,i} / \epsilon_{e,ave}$		1.000	1.000	0.997	0.997	1.005
ϵ_e - ECP	*a*	16.026 ±0.003	16.153 ±0.003	15.933 ±0.003	15.702 ±0.003	15.617 ±0.002
		Average of all 5 columns: 15.886±0.223				
	b (mL/mg)	0.0573± 0.0001	0.0569± 0.0001	0.0569± 0.0001	0.0558± 0.0001	0.0546± 0.0001
$a = k' / F$		15.287	15.197	15.059	14.943	14.707
		Average of all 5 columns: 15.039±0.227				

Table 2.10 Isotherm Studies on ZORBAX Columns

		Columns				
		#1	#2	#3	#4	#5
ECP	*a*	8.381 ±0.001	8.562 ±0.001	8.404 ±0.002	8.632 ±0.001	8.812 ±0.001
		Average of all 5 columns: 8.558±0.177 Average of columns 1,2,4,5: 8.597±0.178				
	b (mL/mg)	0.0648± 0.0000	0.0666± 0.0001	0.0662± 0.0001	0.0661± 0.0000	0.0677± 0.0000
		Average of all 5 columns: 0.0663±0.0010				
FA	*a*	8.025 ±0.097	8.128 ±0.102	8.076 ±0.092	8.280 ±0.104	8.326 ±0.101
		Average of all 5 columns: 8.167±0.130				
	b (mL/mg)	0.0602± 0.0015	0.0608± 0.0016	0.0613± 0.0014	0.0612± 0.0016	0.0612± 0.0015
		Average of all 5 columns: 0.0609±0.0005				
k'_i / k'_{ave}		0.981	0.995	0.990	1.003	1.030
k' - ECP	*a*	8.222 ±0.001	8.519 ±0.001	8.320 ±0.002	8.658 ±0.001	9.076 ±0.001
		Average of all 5 columns: 8.559±0.335				
	b (mL/mg)	0.0648± 0.0000	0.0666± 0.0001	0.0662± 0.0001	0.0661± 0.0000	0.0677± 0.0000
$\epsilon_{e,i} / \epsilon_{e,ave}$		1.002	1.007	0.992	1.000	1.000
ϵ_e - ECP	*a*	8.398 ±0.001	8.622 ±0.001	8.336 ±0.002	8.632 ±0.001	8.812 ±0.001
		Average of all 5 columns: 8.560±0.193 Average of columns 1,2,4,5: 8.616±0.169				
	b (mL/mg)	0.0648± 0.0000	0.0666± 0.0001	0.0662± 0.0001	0.0661± 0.0000	0.0677± 0.0000
$a = k' / F$		7.889	8.098	7.828	8.059	8.171
		Average of all 5 columns: 8.009±0.145				

Table 3.1 KROMASIL Porosities

		Columns				
		#1	#2	#3	#4	#5
Intersection Coordinates	ϕ_e (Å)	153	149	147	147	147
	V_e (mL)	0.637	0.615	0.617	0.608	0.611
$\epsilon_{T,b}$		0.608	0.597	0.598	0.595	0.595
ϵ_i		0.365	0.360	0.361	0.361	0.359
ϵ_e		0.383	0.370	0.371	0.366	0.368
$\epsilon_{T,M}$		0.588	0.580	0.584	0.581	0.582

Table 3.2 VYDAC Porosities

		Columns				
		#1	#2	#3	#4	#5
Intersection Coordinates	ϕ_e (Å)	213	212	213	210	210
	V_e (mL)	0.619	0.612	0.613	0.608	0.609
$\epsilon_{T,b}$		0.637	0.633	0.635	0.634	0.635
ϵ_i		0.422	0.419	0.421	0.423	0.423
ϵ_e		0.372	0.368	0.369	0.366	0.366
$\epsilon_{T,u}$		0.634	0.632	0.638	0.634	0.641

Table 3.3 YMC Porosities

		Columns				
		#1	#2	#3	#4	#5
Intersection Coordinates	ϕ_c (Å)	253	252	256	252	253
	V_c (mL)	0.655	0.655	0.654	0.654	0.658
$\epsilon_{T,b}$		0.707	0.706	0.703	0.705	0.706
ϵ_i		0.516	0.515	0.509	0.514	0.513
ϵ_e		0.394	0.394	0.393	0.393	0.396
$\epsilon_{T,u}$		0.698	0.701	0.697	0.697	0.700

Table 3.4 ZORBAX Porosities

		Columns				
		#1	#2	#3	#4	#5
Intersection Coordinates	ϕ_c (Å)	272	275	268	272	257
	V_c (mL)	0.664	0.666	0.657	0.661	0.661
$\epsilon_{T,b}$		0.603	0.606	0.599	0.603	0.600
ϵ_i		0.338	0.342	0.337	0.340	0.335
ϵ_e		0.399	0.401	0.395	0.398	0.398
$\epsilon_{T,u}$		0.593	0.595	0.590	0.594	0.590

Table 3.5 Incremental Pore Distribution on KROMASIL Columns (% of Total Pore Volume)

$\Delta\phi$ (Å)	Columns				
	#1	#2	#3	#4	#5
8 - 22.7	9.33	9.50	9.53	9.67	9.57
22.7 - 37.1	5.47	5.87	5.87	6.03	5.93
37.1 - 54.2	8.01	8.12	8.19	8.32	8.25
54.2 - 81.5	5.37	5.67	5.80	5.86	5.90
81.5 - 131	5.93	6.31	6.04	6.17	6.13
131 - 228	4.35	4.13	4.06	4.01	4.04
228 - 292	0.00	0.07	0.20	0.10	0.10
292 - 349	0.33	0.24	0.03	0.24	0.17
349 - 508	0.33	0.13	0.27	0.24	0.27
508 - 831	0.43	0.64	0.54	0.54	0.51
831 - 1222	0.33	0.47	0.50	0.51	0.40
1222 - 1513	0.56	0.30	0.30	0.37	0.51
1513 - 1969	0.40	0.64	0.60	0.51	0.51
1969 - 3017	0.96	0.97	1.04	1.04	1.01
3017 - 4620	1.22	1.07	1.27	1.21	1.28
4620 -	56.99	55.86	55.75	55.17	55.42

Table 3.6 Incremental Pore Distribution on VYDAC Columns (% of Total Pore Volume)

$\Delta\phi$ (Å)	Columns				
	#1	#2	#3	#4	#5
8 - 22.7	8.15	8.24	8.15	8.35	8.53
22.7 - 37.1	6.17	6.24	6.13	6.39	6.19
37.1 - 54.2	7.78	7.86	7.87	7.94	7.90
54.2 - 81.5	5.57	5.61	5.69	5.60	5.75
81.5 - 131	5.86	5.96	6.01	6.07	5.94
131 - 228	7.87	7.95	7.93	7.94	8.00
228 - 292	0.63	0.70	0.66	0.60	0.54
292 - 349	0.72	0.57	0.66	0.63	0.66
349 - 508	0.50	0.41	0.32	0.38	0.44
508 - 831	0.50	0.63	0.54	0.57	0.41
831 - 1222	0.44	0.38	0.57	0.47	0.51
1222 - 1513	0.35	0.32	0.22	0.32	0.38
1513 - 1969	0.50	0.54	0.54	0.47	0.00
1969 - 3017	0.94	0.95	0.82	0.89	1.39
3017 - 4620	1.13	1.24	1.17	1.20	1.26
4620 -	52.87	52.42	52.72	52.17	52.09

Table 3.7 Incremental Pore Distribution on YMC Columns (% of Total Pore Volume)

$\Delta\phi$ (Å)	Columns				
	#1	#2	#3	#4	#5
8 - 22.7	8.23	8.21	8.30	8.39	8.07
22.7 - 37.1	5.99	5.80	5.68	5.60	5.94
37.1 - 54.2	7.77	7.65	7.62	7.90	7.59
54.2 - 81.5	5.59	5.94	5.85	5.83	5.82
81.5 - 131	6.21	6.14	6.08	6.11	6.08
131 - 228	9.96	9.84	9.96	9.95	9.91
228 - 292	0.77	0.82	0.74	0.77	0.77
292 - 349	0.77	0.68	0.71	0.63	0.68
349 - 508	0.06	0.31	0.37	0.26	0.28
508 - 831	0.71	0.45	0.43	0.54	0.45
831 - 1222	0.45	0.43	0.43	0.34	0.37
1222 - 1513	0.26	0.28	0.29	0.43	0.43
1513 - 1969	0.00	0.00	0.00	0.00	0.00
1969 - 3017	0.91	0.77	0.86	0.68	0.80
3017 - 4620	1.13	1.22	1.03	1.17	1.02
4620 -	51.21	51.45	51.67	51.41	51.79

Table 3.8 Incremental Pore Distribution on ZORBAX Columns (% of Total Pore Volume)

$\Delta\phi$ (Å)	Columns				
	#1	#2	#3	#4	#5
8 - 22.7	6.78	6.49	6.80	6.69	6.89
22.7 - 37.1	4.02	4.21	4.12	4.09	4.08
37.1 - 54.2	5.59	5.73	5.72	5.69	5.72
54.2 - 81.5	4.29	4.21	4.32	4.39	4.32
81.5 - 131	4.82	4.61	4.79	4.66	4.85
131 - 228	7.02	7.22	7.16	6.99	6.86
228 - 292	0.86	0.96	0.77	1.20	1.14
292 - 349	1.36	1.06	1.34	1.10	0.33
349 - 508	1.00	1.16	1.00	1.13	1.14
508 - 831	0.70	0.73	0.70	0.33	0.84
831 - 1222	0.43	0.43	0.54	0.90	0.67
1222 - 1513	0.43	0.03	0.40	0.33	0.43
1513 - 1969	0.00	0.00	0.00	0.00	0.00
1969 - 3017	0.96	1.16	1.14	1.10	1.30
3017 - 4620	1.30	0.76	1.07	1.13	0.00
4620 -	60.43	61.23	60.13	60.25	61.43

Table 4.1 Density of the Packing Materials

Material	Density (g/cm^3)	rsd (%)	Specific unaccessible volume (cm^3/g)
KROMASIL	1.5674	0.02	0.638
VYDAC	1.7589	0.02	0.568
YMC	1.6016	0.05	0.624
ZORBAX	1.8039	0.03	0.554

Table 4.2 Unaccessible and Total Porosities of the Columns Studied

Columns		W (g)	ϵ_U	$\epsilon_{T,b}$	$\epsilon_{T,u}$	$\epsilon_{T,b}+(1-\epsilon_e)\epsilon_U$
KROMASIL	#1	1.1070	0.689	0.608	0.588	1.033
	#2	1.1287	0.688	0.597	0.580	1.030
	#3	1.1331	0.692	0.598	0.584	1.033
	#4	1.1374	0.689	0.595	0.581	1.032
	#5	1.1302	0.686	0.595	0.582	1.029
VYDAC	#1	1.1269	0.614	0.637	0.634	1.022
	#2	1.1337	0.614	0.633	0.632	1.021
	#3	1.1132	0.603	0.635	0.638	1.016
	#4	1.1381	0.614	0.634	0.634	1.023
	#5	1.1277	0.608	0.635	0.641	1.021
YMC	#1	0.9037	0.560	0.707	0.698	1.046
	#2	0.8618	0.534	0.706	0.701	1.030
	#3	0.9557	0.591	0.703	0.697	1.062
	#4	0.8512	0.527	0.705	0.697	1.025
	#5	0.8641	0.537	0.706	0.700	1.031
ZORBAX	#1	1.2513	0.694	0.603	0.593	1.020
	#2	1.2583	0.701	0.606	0.595	1.026
	#3	1.2651	0.697	0.599	0.590	1.021
	#4	1.2804	0.709	0.603	0.594	1.030
	#5	1.2539	0.695	0.600	0.590	1.018

Note that the definition used in this work for the porosities of particle parts (*e.g.*, internal, skeleton) refers the corresponding void fractions to the actual volume occupied by the particles. See paragraph above Eq. 4.1.

Table 4.3 Volume Fractions Occupied by Silica, the Bonded Chains and the Closed Pores

Columns		ϵ_U	ϵ_s[a]	ϵ_a[b]	$\epsilon_C = \epsilon_U - (\epsilon_s + \epsilon_a)$
KROMASIL	#1	0.689	0.360	0.310	0.019
	#2	0.688	0.359	0.309	0.019
	#3	0.692	0.361	0.312	0.019
	#4	0.689	0.360	0.311	0.018
	#5	0.686	0.359	0.308	0.019
ZORBAX	#1	0.694	0.467	0.210	0.017
	#2	0.701	0.472	0.212	0.016
	#3	0.697	0.469	0.212	0.016
	#4	0.709	0.472	0.214	0.017
	#5	0.695	0.468	0.209	0.017

[a] ρ_s: 2.33 g/cm^3

[b] ρ_a: 0.777 g/cm^3

Table 5.1 Calculated Equilibrium Isotherm Coefficients on KROMASIL® Columns

		Columns									
		K1	K2	K3	K4	K5	K6	K7	K8	K9	K10
FA $-V_k$	$q_{s,vk}$	75.612 ±0.870	74.211 ±0.861	76.204 ±0.742	76.594 ±0.791	75.723 ±0.661	77.345 ±0.552	76.713 ±0.695	77.496 ±0.671	77.485 ±0.685	78.023 ±0.662
	b_{vk}	0.0582 ± 0.0012	0.0602 ± 0.0012	0.0587 ± 0.0010	0.0623 ± 0.0012	0.0593 ± 0.0009	0.0579 ± 0.0007	0.0593 ± 0.0009	0.0586 ± 0.0009	0.0597 ± 0.0009	0.0602 ± 0.0009
FA $-V_p$	$q_{s,vp}$	190.539 ±0.030	183.120 ±2.125	189.161 ±1.842	188.160 ±1.944	184.117 ±1.607	189.169 ±1.349	186.251 ±1.686	185.445 ±1.605	185.151 ±1.636	185.105 ±1.572
	b_{vp}	0.0582 ± 0.0008	0.0602 ± 0.0012	0.0587 ± 0.0010	0.0623 ± 0.0012	0.0593 ± 0.0009	0.0579 ± 0.0007	0.0593 ± 0.0009	0.0586 ± 0.0009	0.0597 ± 0.0009	0.0602 ± 0.0009
ECP $-V_p$	$q_{s,vp}$	160.049 ±0.267	157.077 ±0.259	161.011 ±0.249	164.247 ±0.181	161.012 ±0.217	164.609 ±0.192	163.072 ±0.209	160.293 ±0.289	163.042 ±0.166	164.235 ±0.148
	b_{vp}	0.0731 ± 0.0001	0.0726 ± 0.0001	0.0722 ± 0.0001	0.0717 ± 0.0001	0.0708 ± 0.0001	0.0709 ± 0.0001	0.0705 ± 0.0001	0.0711 ± 0.0001	0.0700 ± 0.0001	0.0712 ± 0.0001
FA $-W$	$q_{s,w}$	122.071 ±1.469	120.031 ±1.393	120.947 ±1.168	120.770 ±1.248	119.362 ±1.040	119.661 ±0.854	117.729 ±1.074	119.362 ±1.034	117.978 ±1.041	119.157 ±1.011
	b_w	0.0582 ± 0.0008	0.0602 ± 0.0012	0.0587 ± 0.0010	0.0623 ± 0.0012	0.0593 ± 0.0009	0.0579 ± 0.0007	0.0593 ± 0.0009	0.0586 ± 0.0009	0.0597 ± 0.0009	0.0602 ± 0.0009

$q_{s,vk}$ (mg: sample/mL: column) = 76.541±1.143 (rsd=1.49%) FA-$q_{s,vp}$ (mg: sample/mL: packing) = 186.622±2.476 (rsd=1.33%)
$q_{s,w}$ (mg: sample/mg: packing) = 119.707±1.325 (rsd=1.11%) b_{vk} = FA-b_{vp} = b_w = 0.0594±0.0013 (rsd=2.14%)

Table 5.2 Calculated Equilibrium Isotherm Coefficients on ZORBAX® Columns

		Columns									
		Z1	Z2	Z3	Z4	Z5	Z6	Z7	Z8	Z9	Z10
FA -V_k	$q_{s,Vk}$	52.215 ±0.582	52.843 ±0.513	52.855 ±0.524	53.573 ±0.539	53.956 ±0.482	55.117 ±0.535	54.554 ±0.490	54.994 ±0.582	55.044 ±0.471	54.948 ±0.526
	b_{Vk}	0.0611 ± 0.0012	0.0605 ± 0.0010	0.0610 ± 0.0011	0.0619 ± 0.0011	0.0607 ± 0.0010	0.0592 ± 0.0010	0.0589 ± 0.0009	0.0590 ± 0.0011	0.0616 ± 0.0009	0.0599 ± 0.0010
FA -V_p	$q_{s,Vp}$	135.061 ±1.505	135.839 ±1.318	135.035 ±1.340	135.618 ±1.366	136.378 ±1.217	137.640 ±1.337	136.029 ±1.221	136.511 ±1.445	136.228 ±1.167	136.806 ±1.310
	b_{Vp}	0.0611 ± 0.0012	0.0605 ± 0.0010	0.0610 ± 0.0011	0.0619 ± 0.0011	0.0607 ± 0.0010	0.0592 ± 0.0010	0.0589 ± 0.0009	0.0590 ± 0.0011	0.0616 ± 0.0009	0.0599 ± 0.0010
ECP -V_p	$q_{s,Vp}$	115.674 ±0.228	121.622 ±0.128	118.979 ±0.950		127.946 ±0.660	120.391 ±0.101	121.146 ±0.193		120.058 ±0.108	122.585 ±0.115
	b_{Vp}	0.0753 ± 0.0002	0.0705 ± 0.0001	0.0723 ± 0.0007		0.0664 ± 0.0004	0.0713 ± 0.0001	0.0689 ± 0.0001		0.0705 ± 0.0001	0.0716 ± 0.0001
FA -W	$q_{s,w}$	76.719 ±0.855	76.813 ±0.745	75.901 ±0.753	76.693 ±0.772	76.191 ±0.680	76.742 ±0.745	76.207 ±0.684	76.391 ±0.809	76.435 ±0.655	75.915 ±0.727
	b_w	0.0611 ± 0.0012	0.0605 ± 0.0010	0.0610 ± 0.0011	0.0619 ± 0.0011	0.0607 ± 0.0010	0.0592 ± 0.0010	0.0589 ± 0.0009	0.0590 ± 0.0011	0.0616 ± 0.0009	0.0599 ± 0.0010

$q_{s,Vk}$ (mg: sample/mL: column) = 54.010±1.083 (rsd=2.00%) FA-$q_{s,Vp}$ (mg: sample/mL: packing) = 136.114±0.792 (rsd=0.58%)
$q_{s,w}$ (mg: sample/mg: packing) = 76.401±0.340 (rsd=0.44%) b_{Vk} = FA-b_{Vp} = b_w = 0.0604±0.0011 (rsd=1.79%)

Table 5.3 Porosities of KROMASIL® Columns

	Columns									
	K1	K2	K3	K4	K5	K6	K7	K8	K9	K10
$V_{T,u}$	1.002	0.988	0.992	0.985	0.978	0.982	0.977	0.967	0.966	0.961
$V_{T,b}$	1.014	1.006	1.010	0.999	0.997	0.993	0.991	0.982	0.978	0.973
$\epsilon_{T,b}$	0.610	0.605	0.608	0.601	0.600	0.597	0.596	0.591	0.588	0.585
ϵ_e	0.402	0.400	0.404	0.390	0.389	0.389	0.384	0.386	0.372	0.374
ϵ_i	0.347	0.342	0.341	0.346	0.346	0.342	0.345	0.334	0.345	0.338

Table 5.4 Porosities of ZORBAX® Columns

	Columns									
	Z1	Z2	Z3	Z4	Z5	Z6	Z7	Z8	Z9	Z10
$V_{T,u}$	1.019	1.015	1.011	1.005	1.004	0.996	0.995	0.992	0.990	0.994
$V_{T,b}$	1.035	1.029	1.023	1.020	1.021	1.012	1.011	1.008	1.004	1.007
$\epsilon_{T,b}$	0.623	0.619	0.615	0.614	0.614	0.609	0.608	0.606	0.604	0.606
ϵ_e	0.434	0.428	0.428	0.424	0.418	0.408	0.409	0.404	0.405	0.399
ϵ_i	0.334	0.334	0.328	0.329	0.337	0.338	0.337	0.339	0.335	0.344

Table 5.5 Packing Density Data for KROMASIL® and ZORBAX® Columns

		Columns (V_t = 1.662 mL)									
		#1	#2	#3	#4	#5	#6	#7	#8	#9	#10
KROMASIL®	V_p (mL)	0.659	0.673	0.669	0.676	0.683	0.679	0.684	0.694	0.695	0.700
	W_p (g)	1.029	1.027	1.047	1.054	1.054	1.074	1.083	1.079	1.091	1.088
	W_p/V_t (g/mL)	0.619	0.618	0.630	0.634	0.634	0.646	0.652	0.649	0.656	0.655
	W_p/V_p (g/mL)	1.562	1.527	1.565	1.559	1.544	1.582	1.583	1.555	1.570	1.554
ZORBAX®	V_p (mL)	0.642	0.646	0.650	0.656	0.657	0.665	0.666	0.669	0.671	0.667
	W_p (g)	1.131	1.143	1.157	1.161	1.177	1.194	1.190	1.196	1.197	1.203
	W_p/V_t (g/mL)	0.680	0.688	0.696	0.698	0.708	0.718	0.716	0.720	0.720	0.724
	W_p/V_p (g/mL)	1.762	1.770	1.780	1.770	1.791	1.795	1.786	1.788	1.784	1.803

Table 6.1 Parameters of the bi-Langmuir and Langmuir Adsorption Isotherms of Bovine Serum Albumin (BSA) on TSK-Gel DEAE-5PW Column (b_2=0.0)

pH	Buffer	Flow Rate (mL/min)	a_1	b_1	a_2	Residuals (Sum of squares)
Bi-Langmuir						
7.5	50 mM Tris-HCl	1.0	3043.9 ±696.7	32.1 ±0.0	3.4 ±1.1	23.1
6.0	25 mM Bis-Tris-HCl	1.0	1380.5 ±316.0	17.3 ±0.0	11.9 ±1.7	46.1
6.0	25 mM Bis-Tris-HCl	2.0	1055.3 ±349.3	12.1 ±5.0	8.2 ±3.6	139.6
Langmuir						
7.5	50 mM Tris-HCl	1.0	2037.8 ±286.2	20.0 ±3.0		50.0
6.0	25 mM Bis-Tris-HCl	1.0	656.0 ±109.0	6.0 ±1.2		287.1
6.0	25 mM Bis-Tris-HCl	2.0	677.9 ±115.6	6.3 ±1.3		228.4

Table 6.2 Mass Transfer Rate Coefficient Concentration Dependence

pH	Flow Rate (mL/min)	C_{ave} (mg/mL)	Average k_f ±10% ($10^3 s^{-1}$)
7.5	1.0	0.08	1.3
		0.17	2.0
		0.23	5.0
		0.37	6.7
		0.45	7.5
		0.71	8.3
		0.93	10.0
		1.15	11.7
		1.38	15.0
6.0	1.0	0.08	1.7
		0.14	2.0
		0.21	1.6
		0.35	3.3
		0.45	5.0
		0.68	8.3
		0.92	10.0
		1.16	11.7
		1.39	13.3
6.0	2.0	0.08	1.7
		0.14	3.3
		0.21	5.0
		0.34	6.7
		0.44	7.5
		0.68	13.0
		0.93	18.3
		1.41	26.7

Table 7.1 RESOURCE-Q Columns Characteristics

	RESOURCE-Q #1	RESOURCE-Q #2
Lot Number	227922	226436
Code Number	17-1177-01	
Column Dimension	30 mm x 6.4 mm i.d.	
Column Geometrical Volume (mL)	0.965	
Base Matrix	Monodisperse polystyrene/divinyl benzene beads	
Particle Size	15 μm	
Pore Size	200 - 10,000 Å	
Stationary Phase Volume V_s (mL)	0.215	0.131
Phase Ratio F	0.287	0.157

Table 7.2 Adsorption Isotherm Coefficients for the two RESOURCE-Q Columns (pH = 6.0, flow rate = 1.0 mL/min)

	RESOURCE-Q #1	RESOURCE-Q #2
a_1	4906.7	7215.4
b_1 (mL/mg)	35.7	31.0
a_2	15.0	0.1

Table 7.3 Mass Transfer Rate Coefficient Concentration Dependence (pH=6.0, flow rate = 1.0 mL/min).

	C_{ave} (mg/mL)	Average k_f ±10% ($10^3 s^{-1}$)
Column #1: $k_f = 0.0329 * C_{ave} + 0.0016$	0.04	2.5
	0.08	4.2
	0.17	7.5
	0.27	10.8
	0.36	13.3
	0.45	15.8
	0.71	25.0
	0.94	33.3
	1.22	41.7
	1.48	50.0
	1.73	58.3
	1.97	66.7
Column #2: $k_f = 0.0111 * C_{ave} + 0.0011$	0.01	0.8
	0.03	1.0
	0.05	1.7
	0.12	2.5
	0.17	3.3
	0.31	5.0
	0.39	5.8
	0.49	6.7
	0.76	10.0
	1.02	12.5
	1.27	15.0
	1.55	18.3

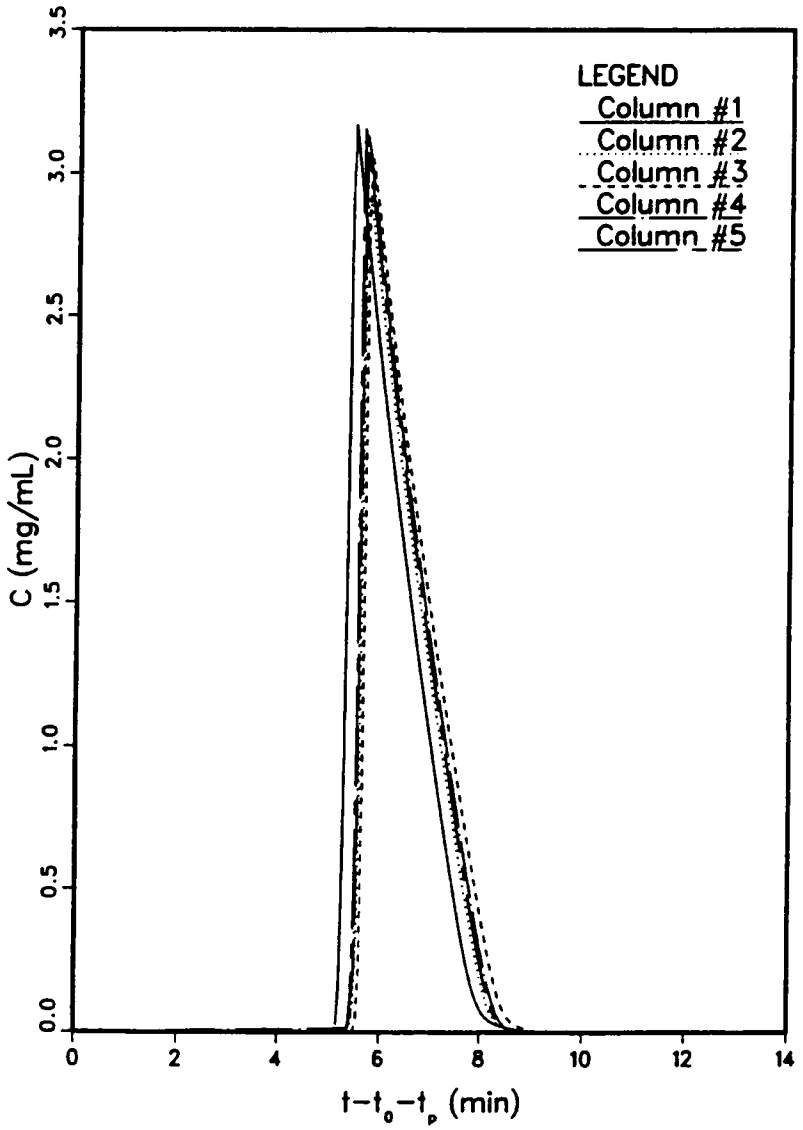


Figure 2.1 Band profiles used for the determination of the isotherm by ECP. KROMASIL columns.

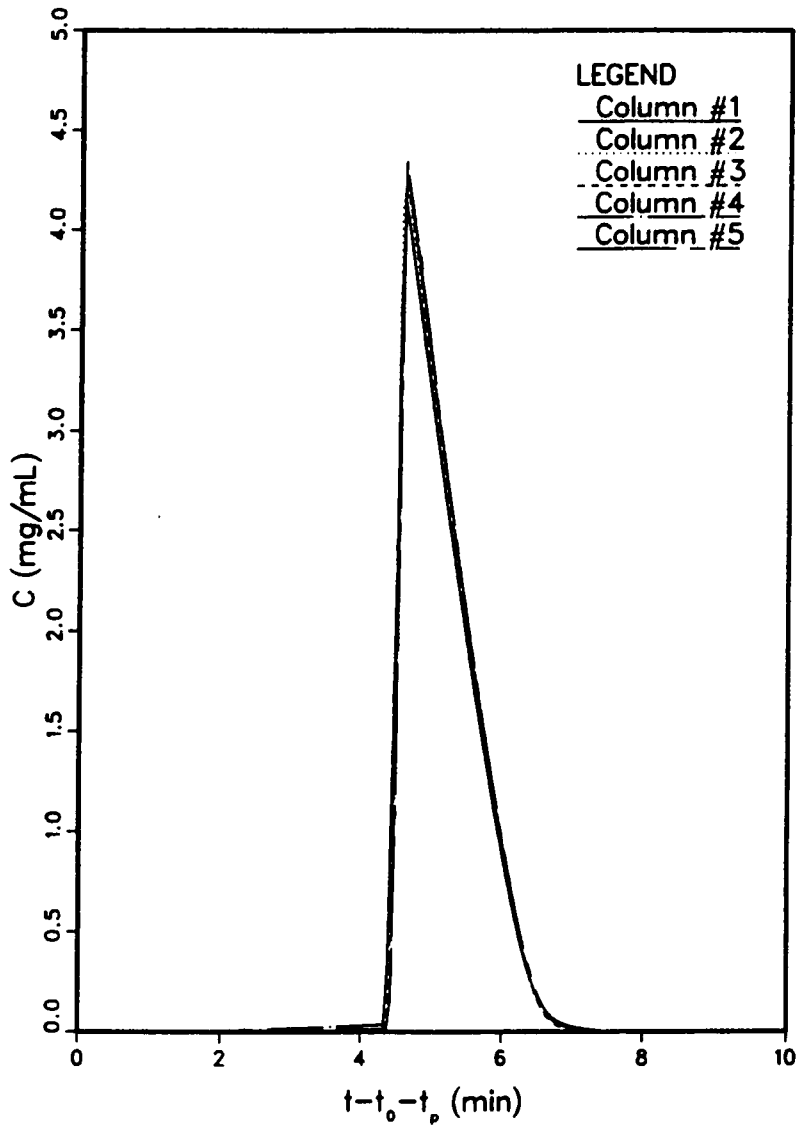


Figure 2.2 Band profiles used for the determination of the isotherm by ECP. VYDAC columns.

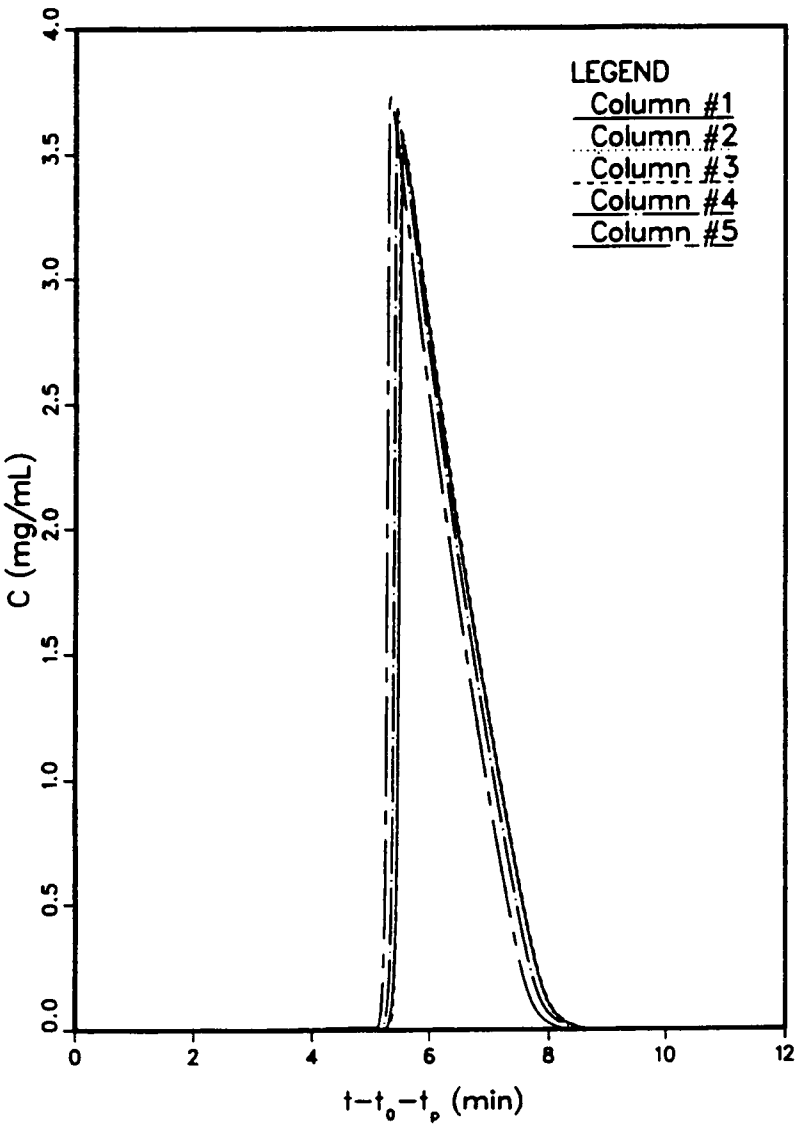


Figure 2.3 Band profiles used for the determination of the isotherm by ECP. YMC columns.

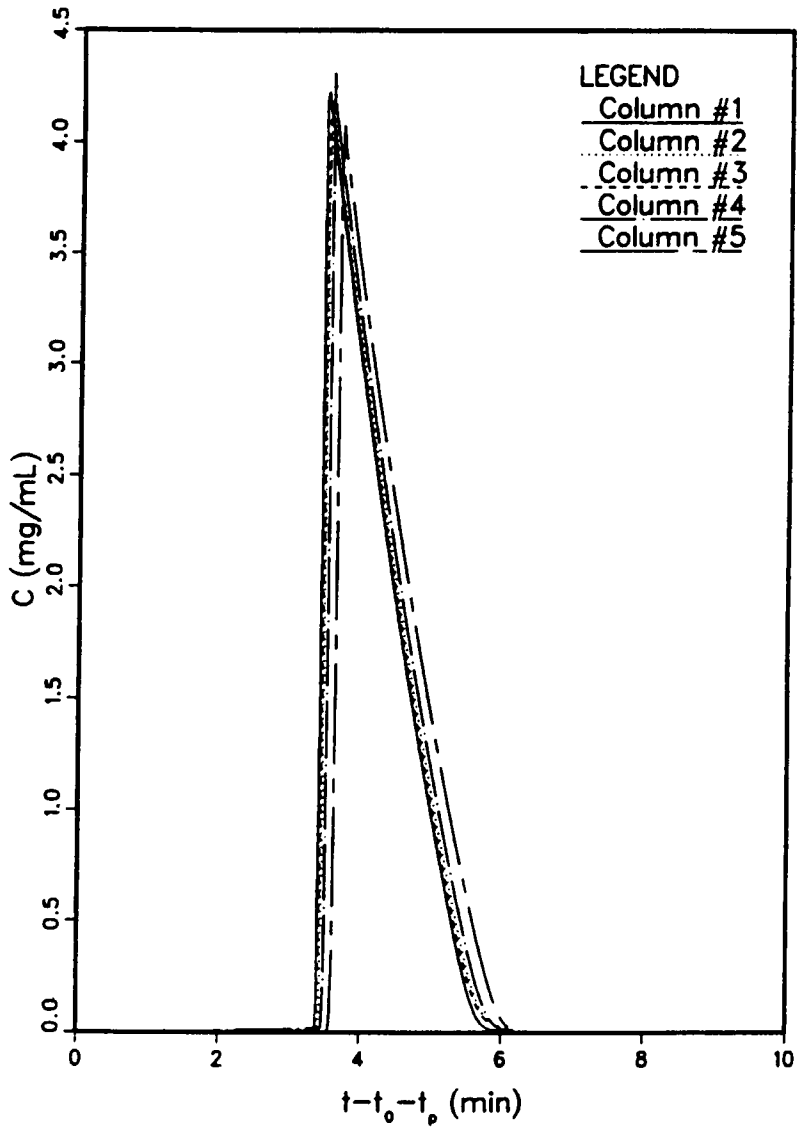


Figure 2.4 Band profiles used for the determination of the isotherm by ECP. ZORBAX columns.

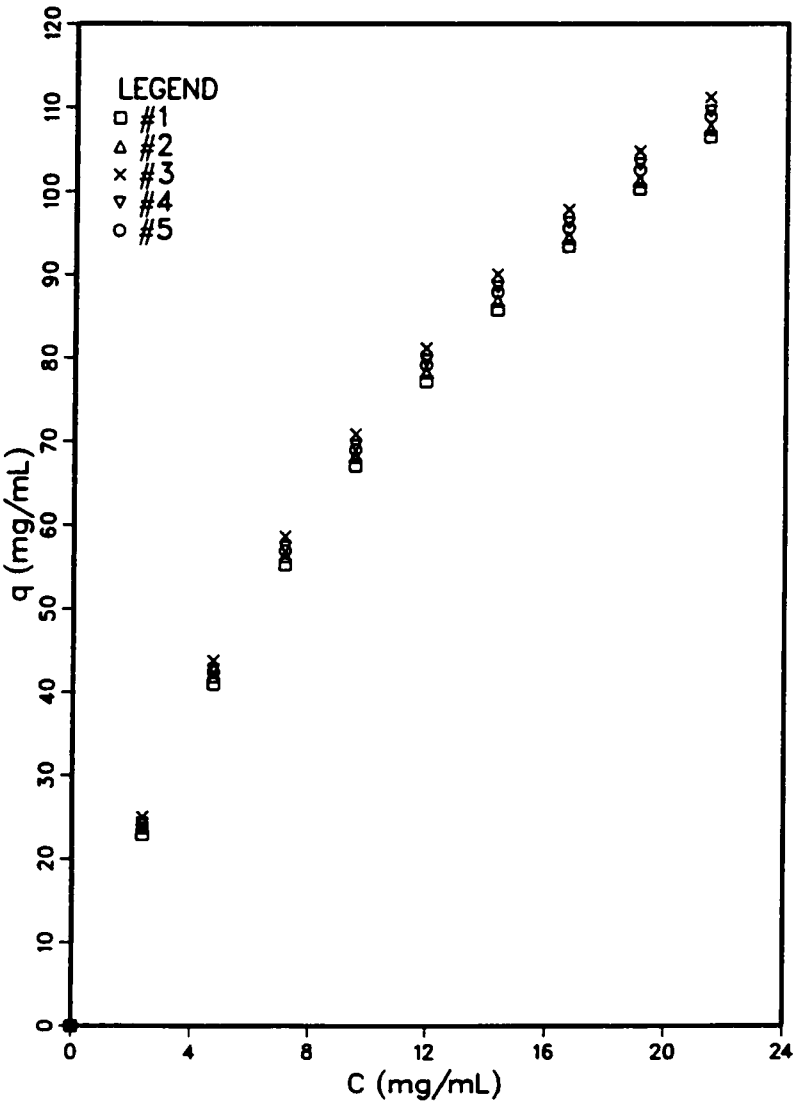


Figure 2.5 FA isotherms of 3-phenyl-1-propanol on KROMASIL.

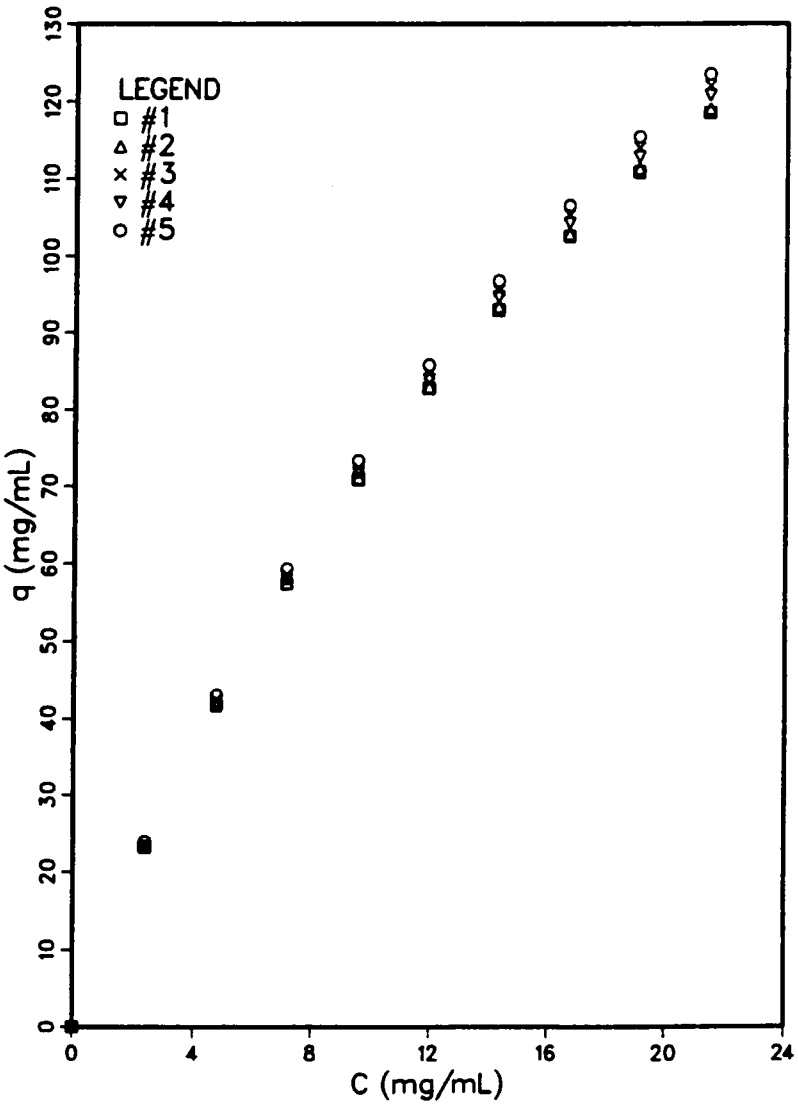


Figure 2.6 FA isotherms of 3-phenyl-1-propanol on VYDAC.

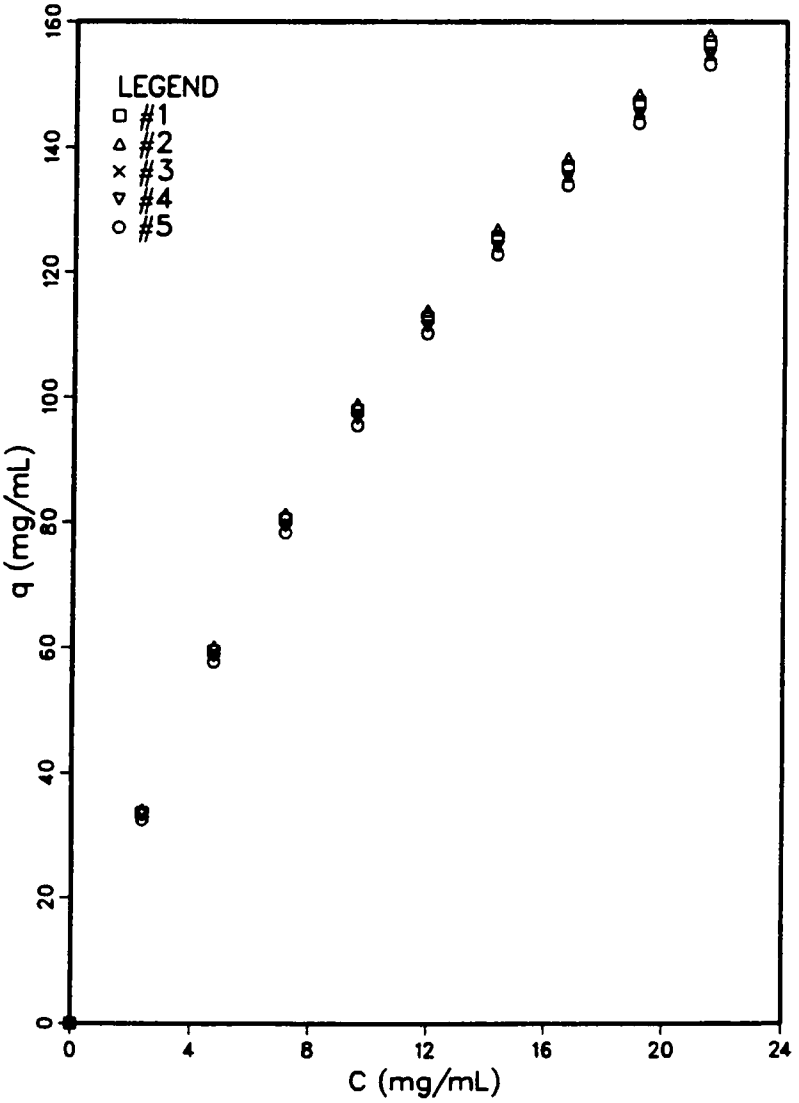


Figure 2.7 FA isotherms of 3-phenyl-1-propanol on YMC.

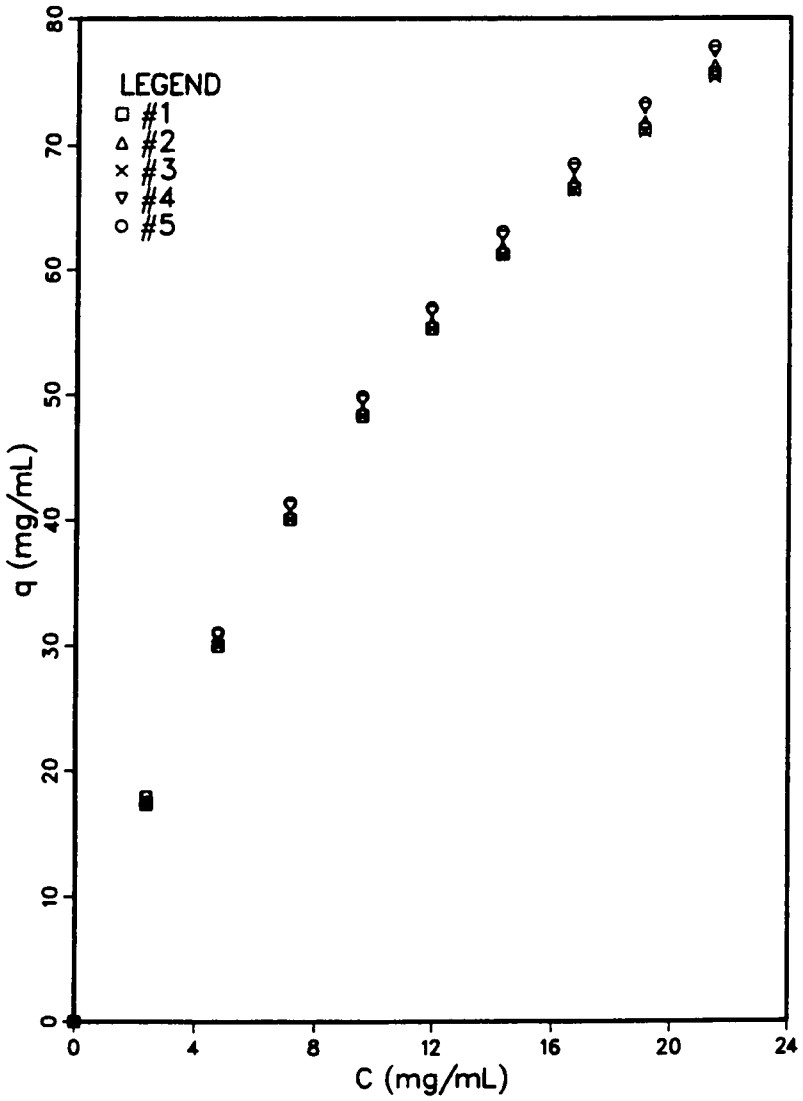


Figure 2.8 FA isotherms of 3-phenyl-1-propanol on ZORBAX.

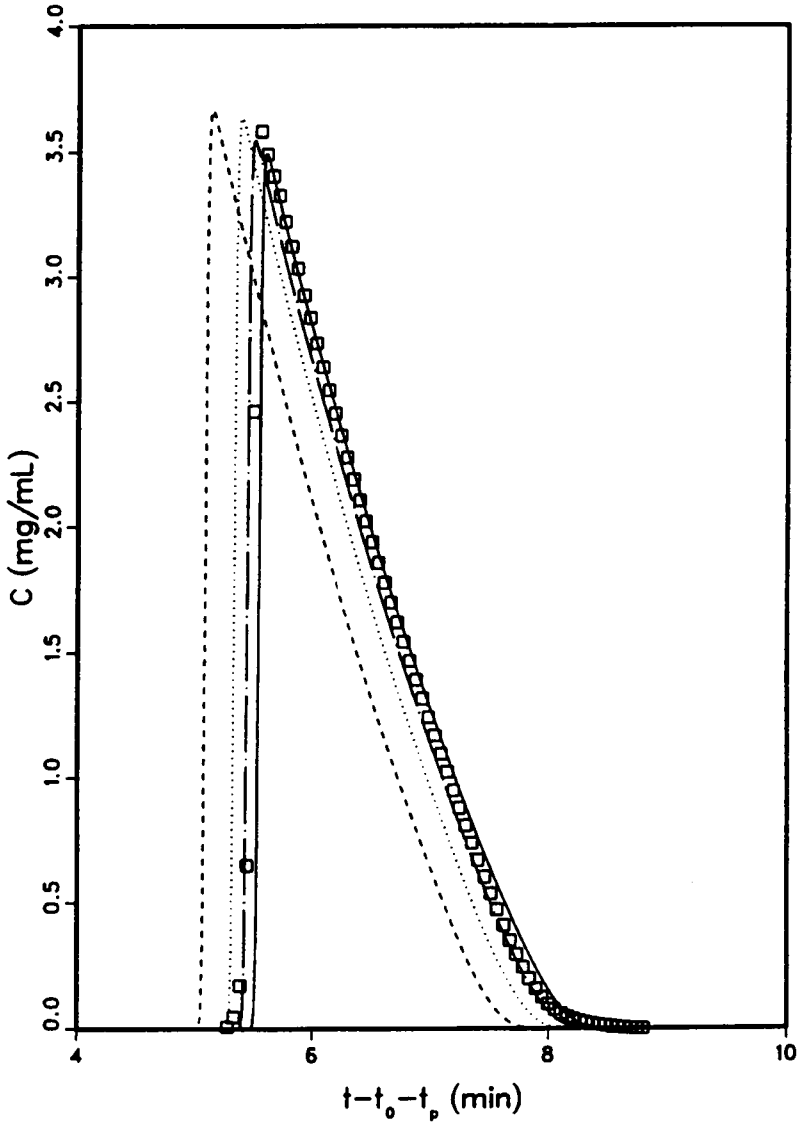


Figure 2.9 Comparison between experimental (symbols) and calculated (lines) band profiles for column YMC #2. Profiles calculated with the isotherm measured on the same column (solid line), with the isotherm measured on column #5 (dotted line), with the isotherm obtained by taking the average values of a ($a = k'/F$, Table 2.9, last row) (dashed line), and with the isotherm obtained by taking the average values of a and b after being corrected by the porosity (Table 2.9, row ϵ_e-ECP) (chain dot line).

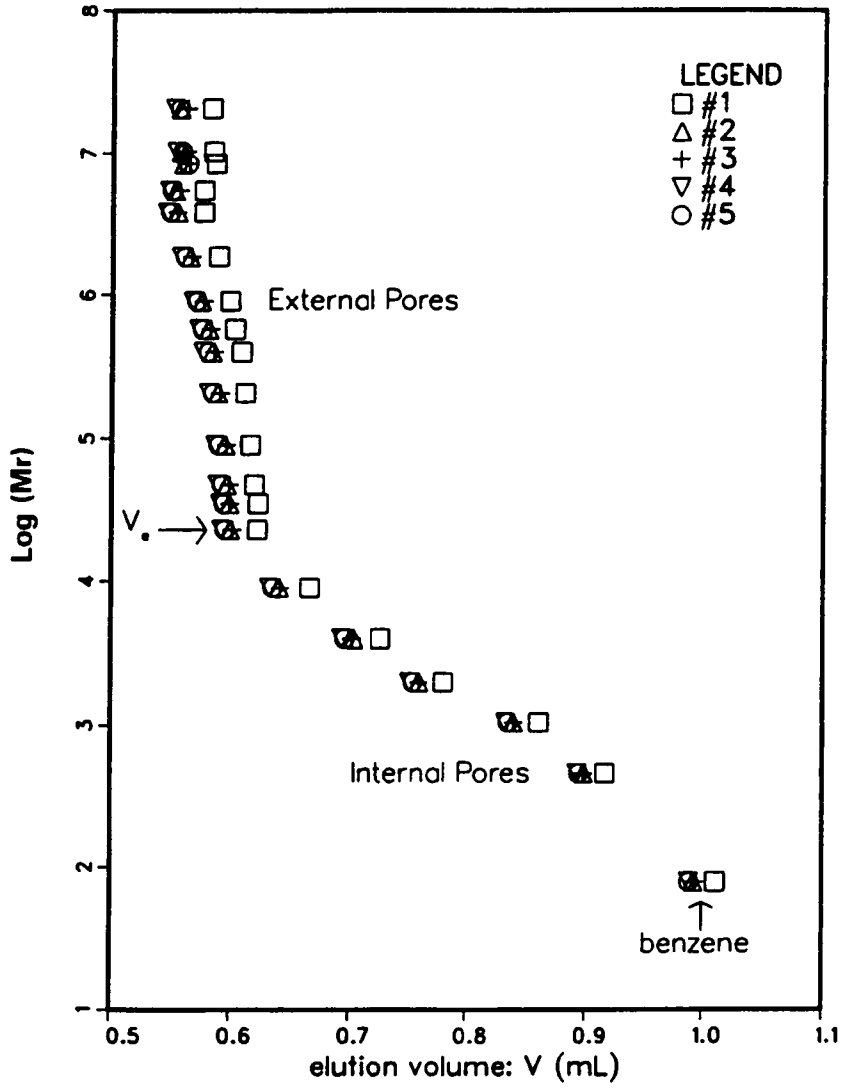


Figure 3.1 Plot of the logarithm of molecular masses of the polystyrene standards injected versus their elution volumes @ 1.000 mL/min flow rate of methylene chloride. KROMASIL columns. □ column #1; △ column #2; + column #3; ▽ column #4; ○ column #5.

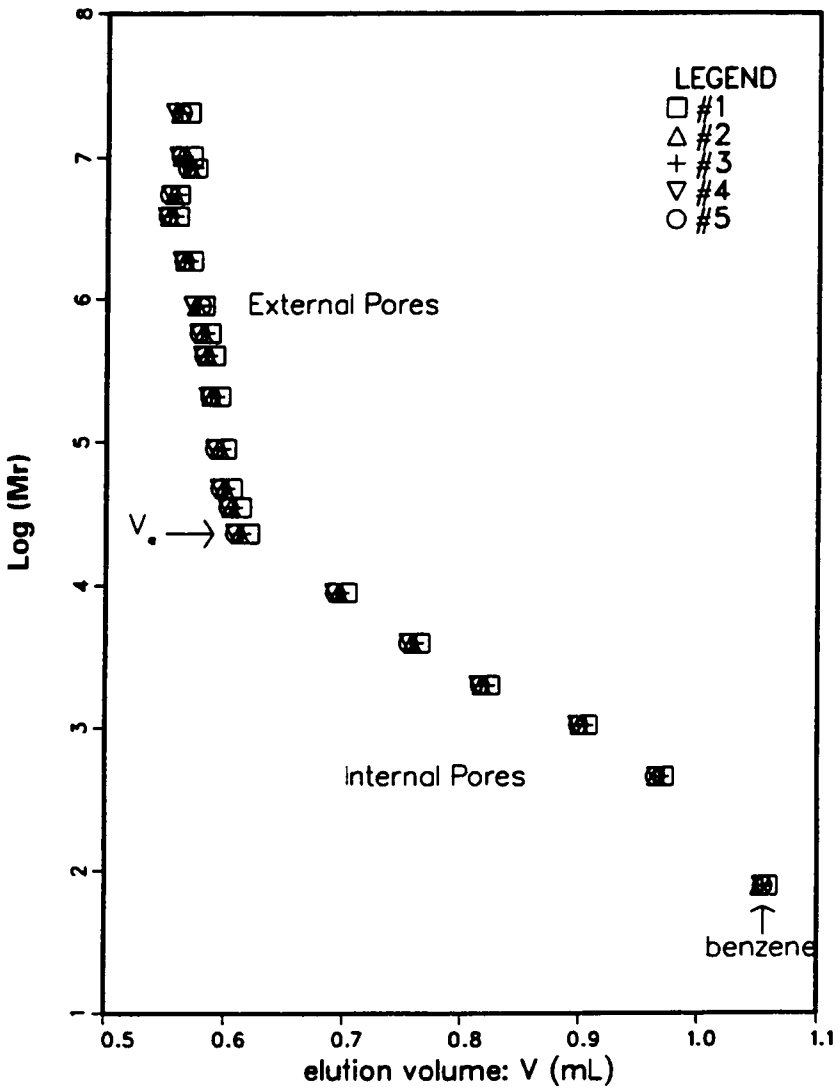


Figure 3.2 Plot of the logarithm of molecular masses of the polystyrene standards injected versus their elution volumes @ 1.000 mL/min flow rate of methylene chloride. VYDAC columns. Symbols, see Figure 3.1.

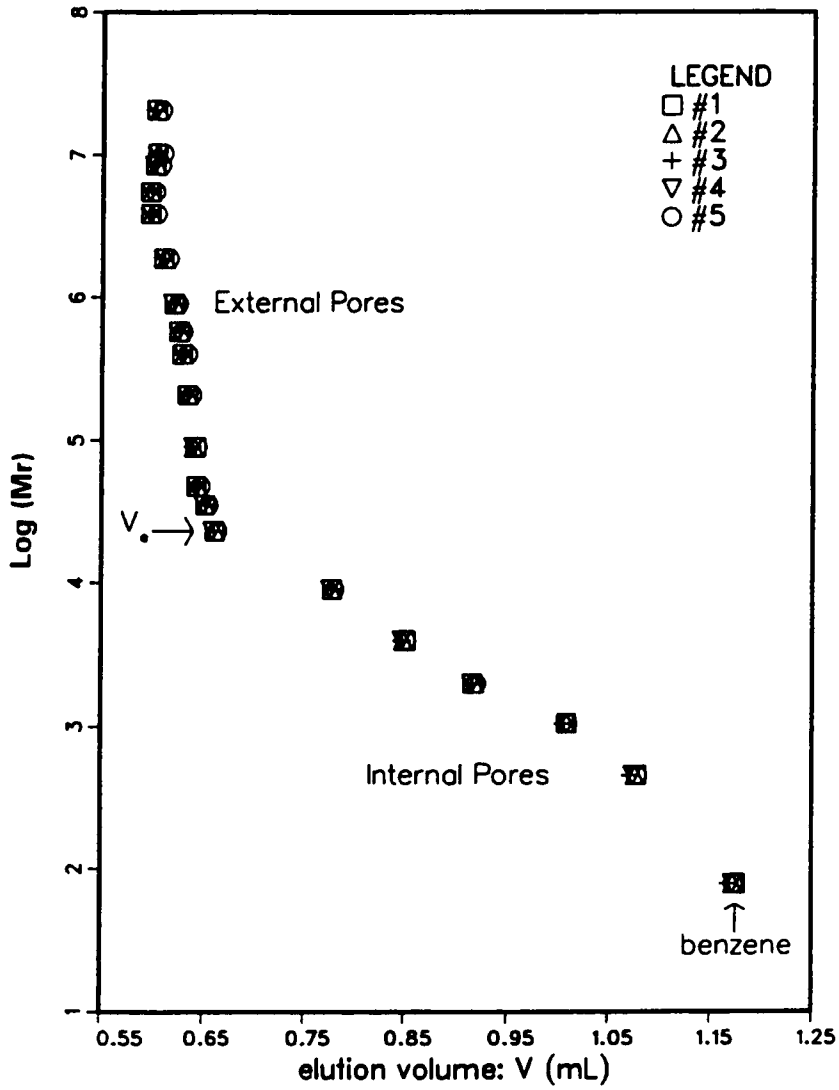


Figure 3.3 Plot of the logarithm of molecular masses of the polystyrene standards injected versus their elution volumes @ 1.000 mL/min flow rate of methylene chloride. YMC columns. Symbols, see Figure 3.1.

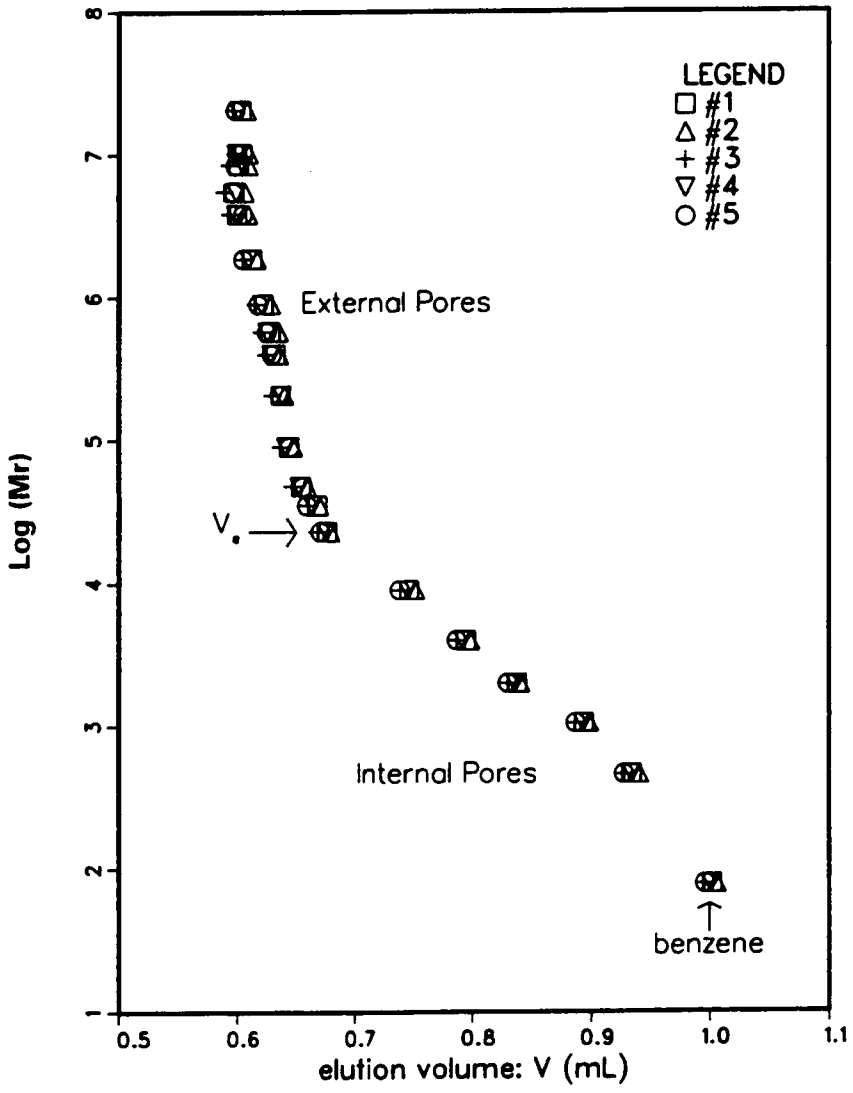


Figure 3.4 Plot of the logarithm of molecular masses of the polystyrene standards injected versus their elution volumes @ 1.000 mL/min flow rate of methylene chloride. ZORBAX columns. Symbols, see Figure 3.1.

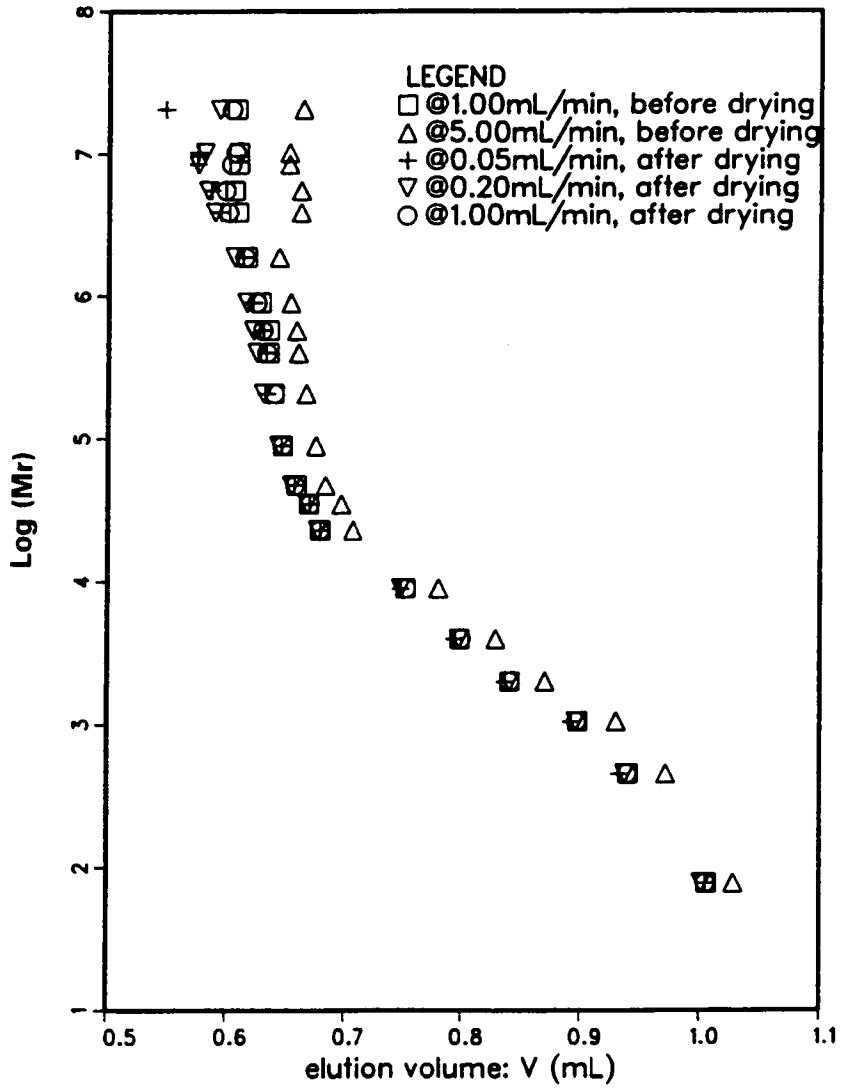


Figure 3.5 Plot of the logarithm of molecular masses of the polystyrene standards injected versus their elution volumes @ 0.050, 0.200, 1.000, and 5.000 mL/min flow rates. ZORBAX column #2.

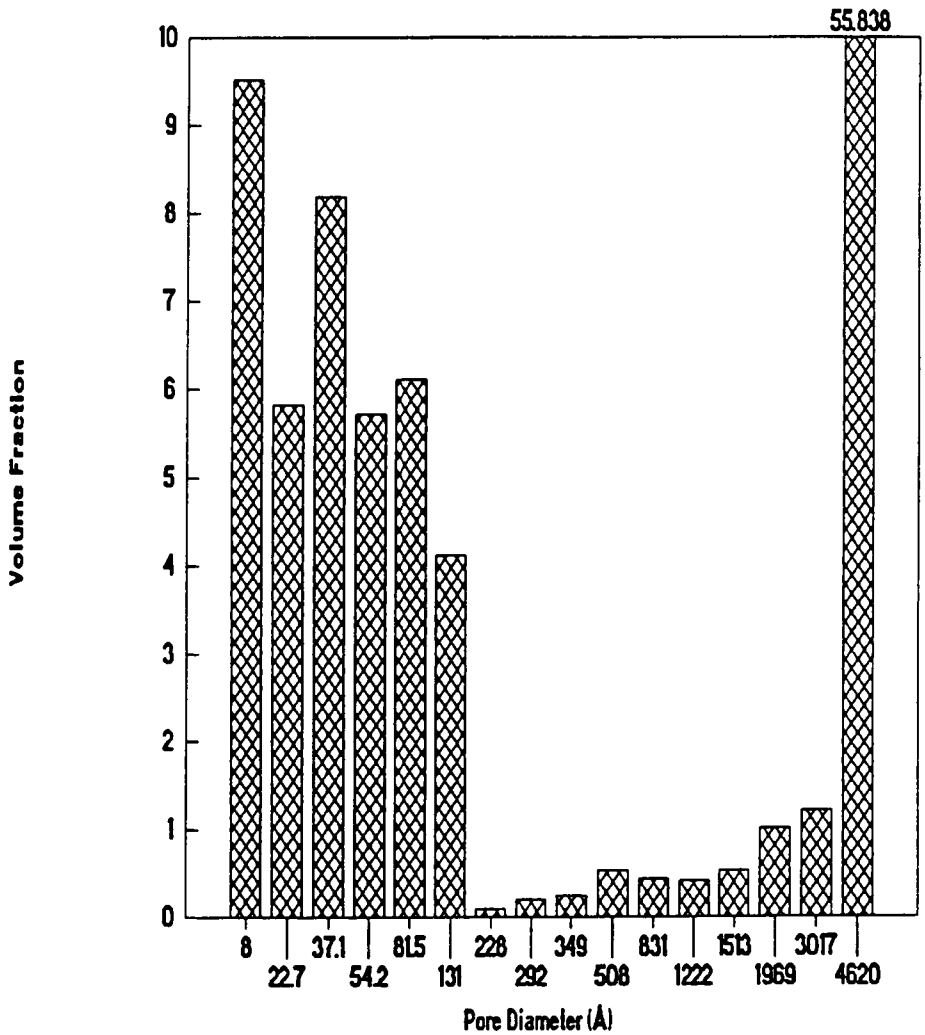


Figure 3.6 Average pore size distribution of KROMASIL columns.

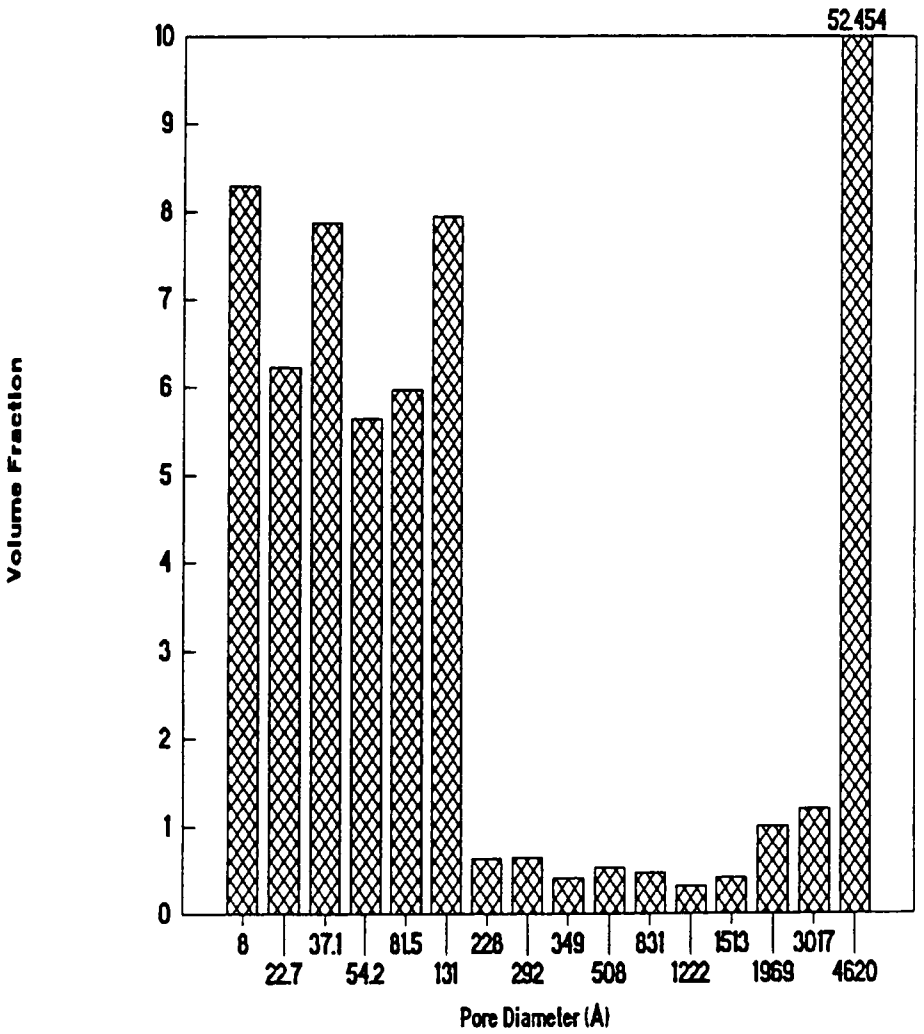


Figure 3.7 Average pore size distribution of VYDAC columns.

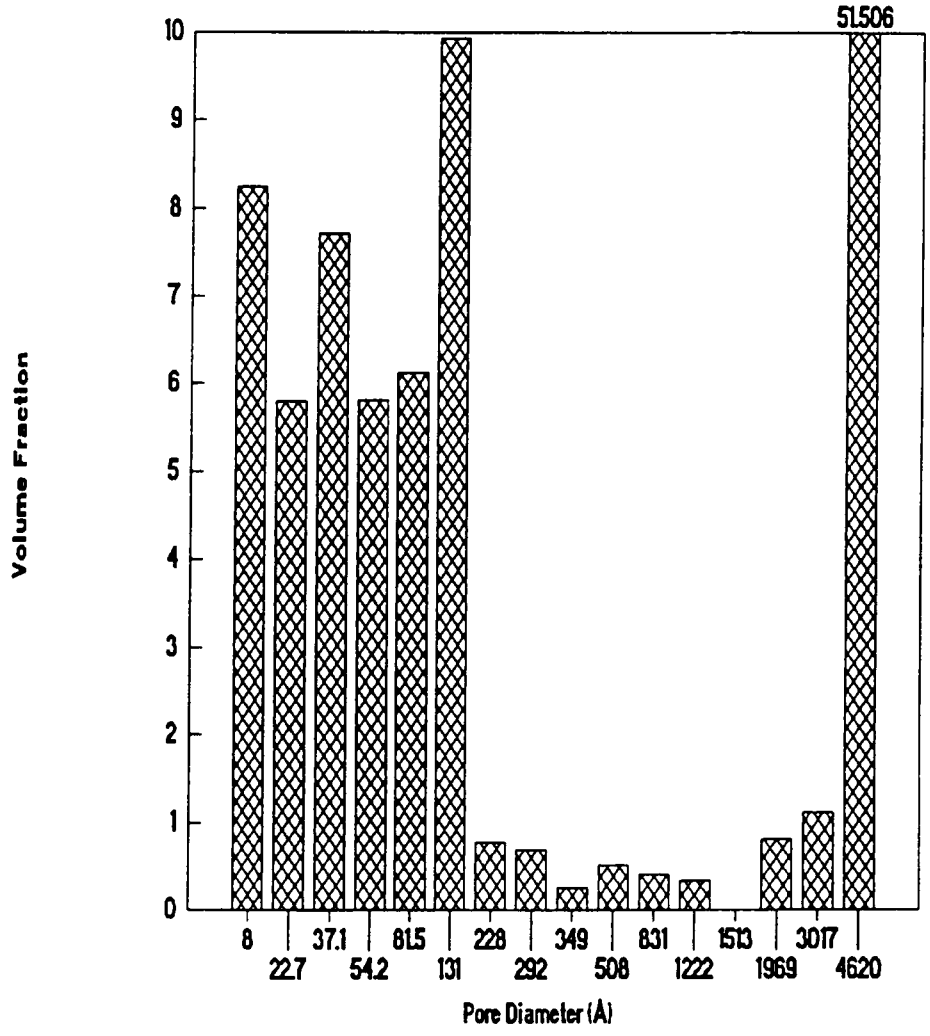


Figure 3.8 Average pore size distribution of YMC columns.

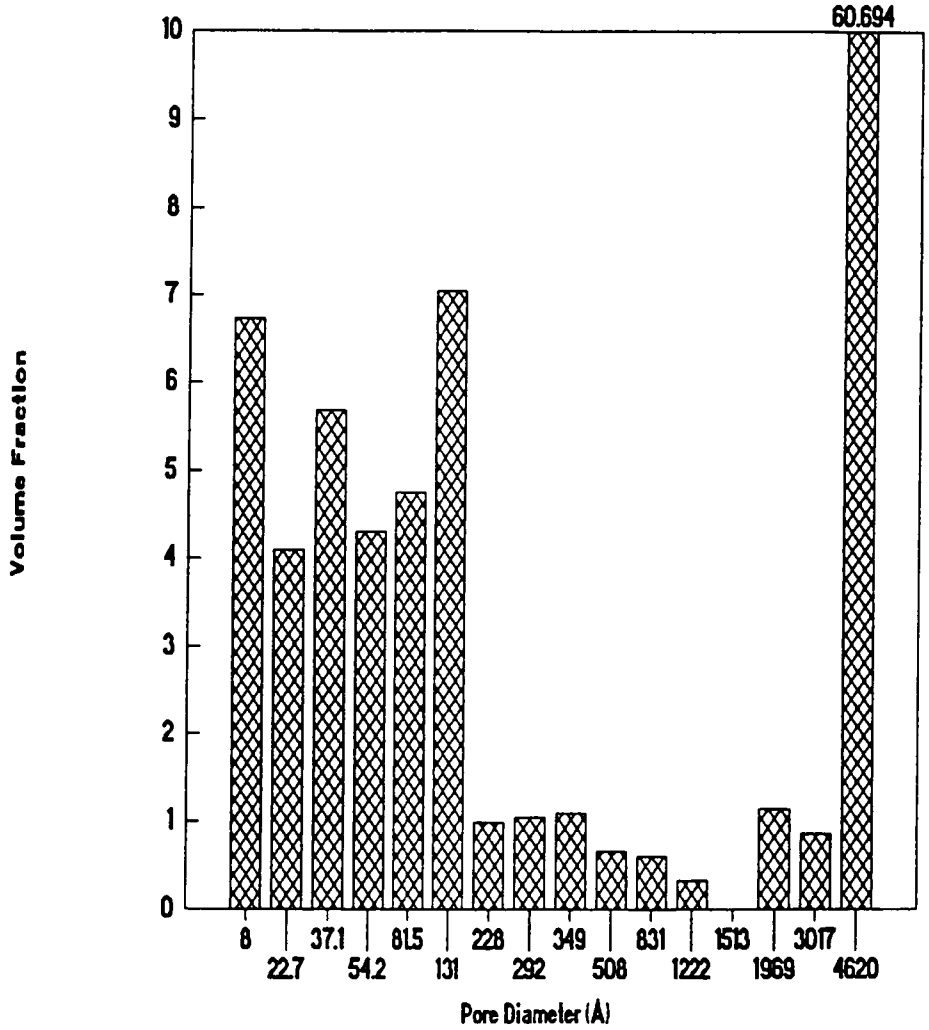
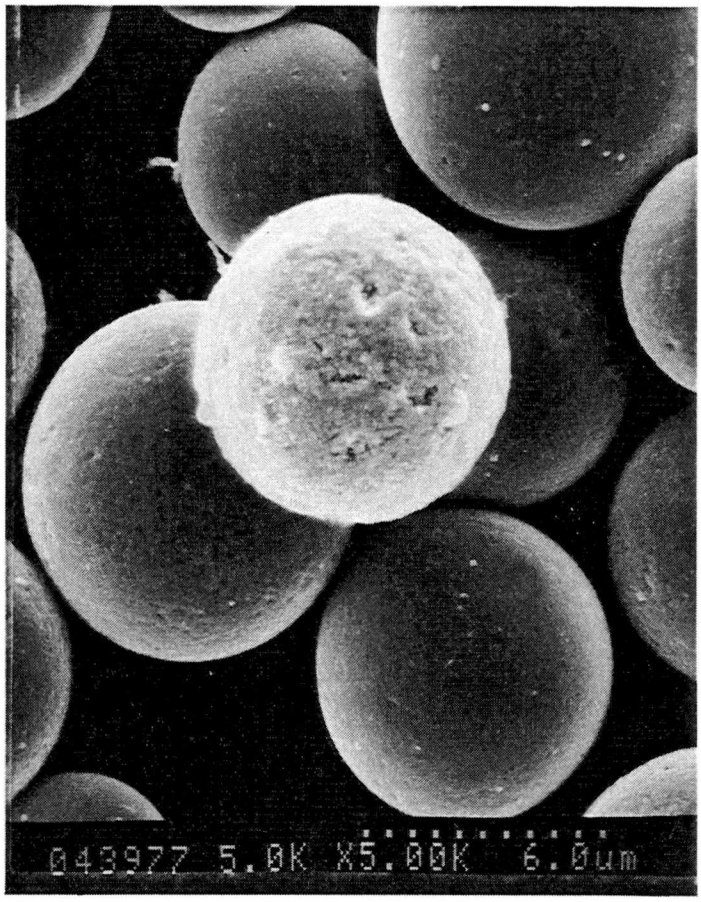
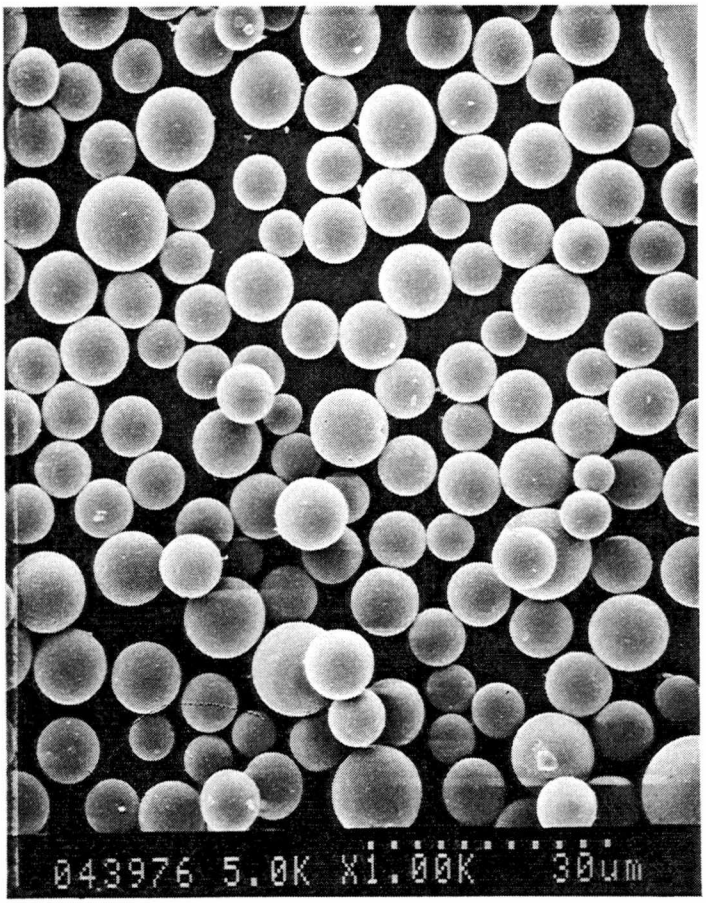


Figure 3.9 Average pore size distribution of ZORBAX columns.



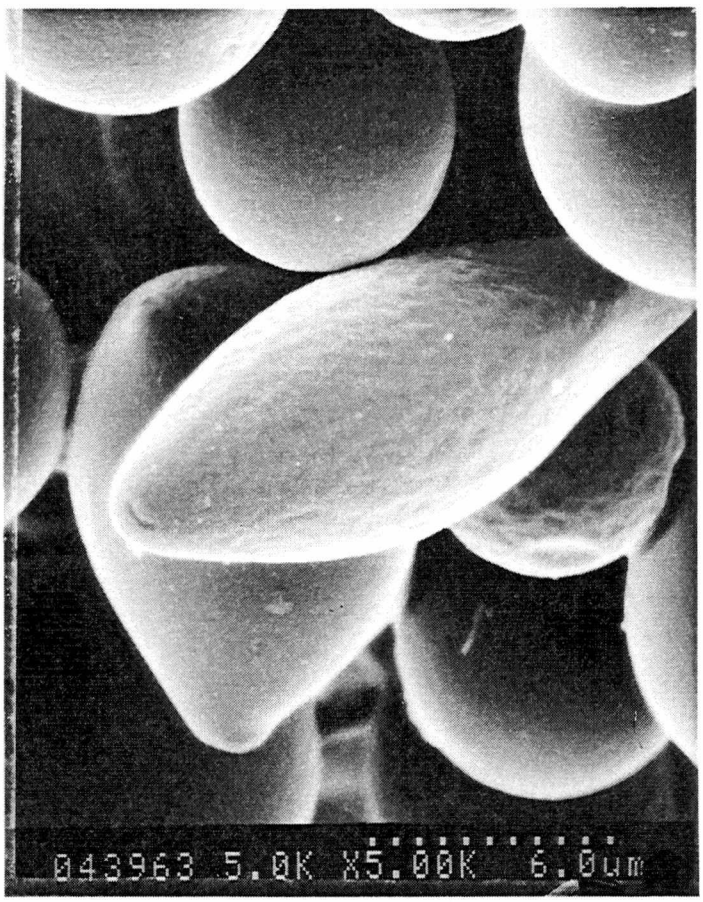
a. x5000

Figure 4.1 SEM microphotography of KROMASIL particles.



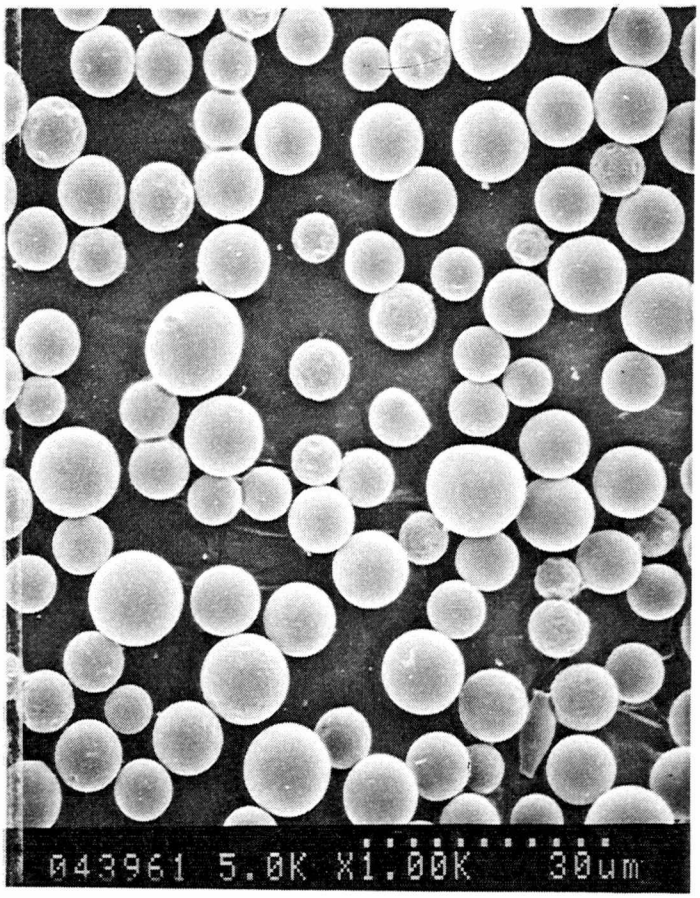
b. x1000

Figure 4.1 (continued)



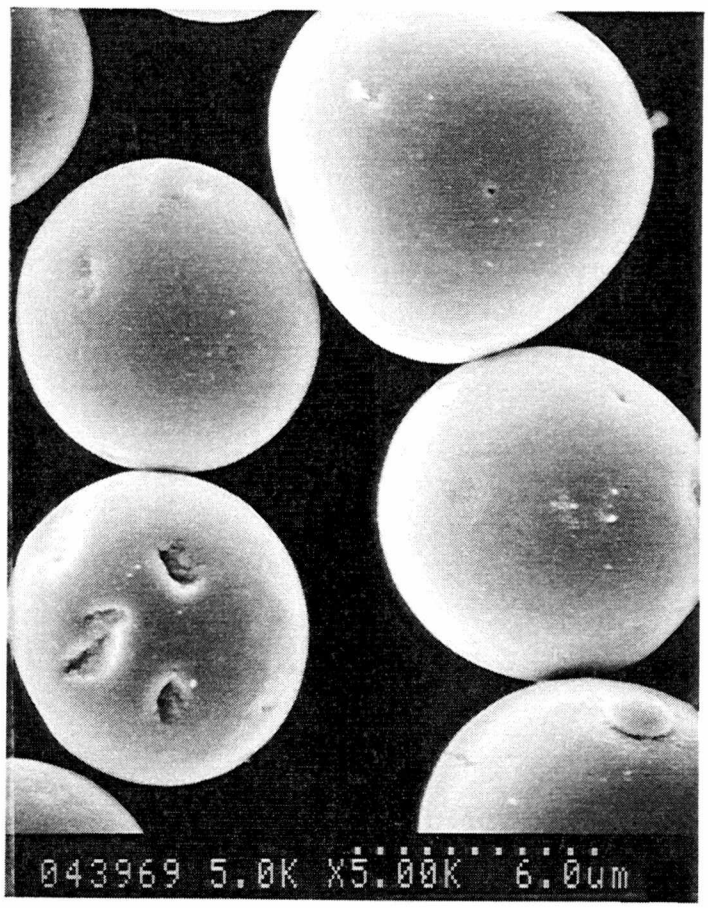
a. x5000

Figure 4.2 SEM microphotography of VYDAC particles.



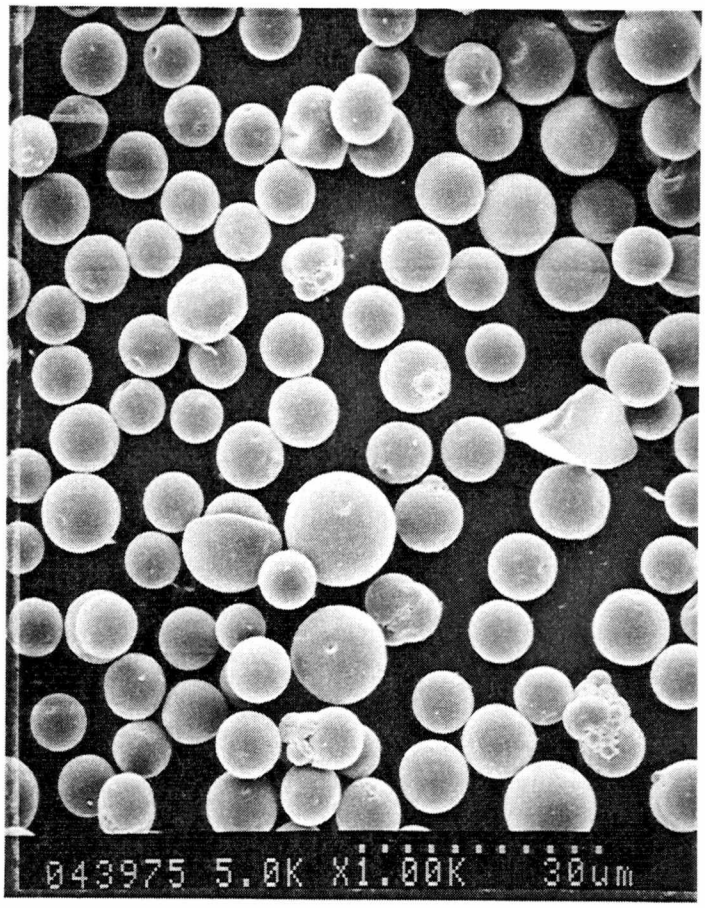
b. x1000

Figure 4.2 (continued)



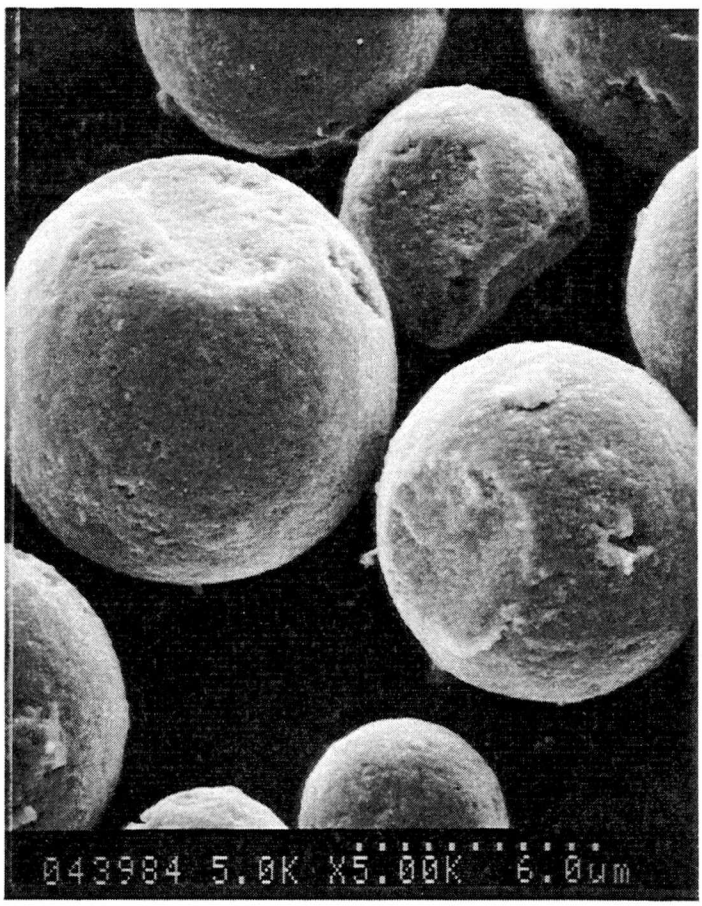
a. x5000

Figure 4.3 SEM microphotography of YMC particles.



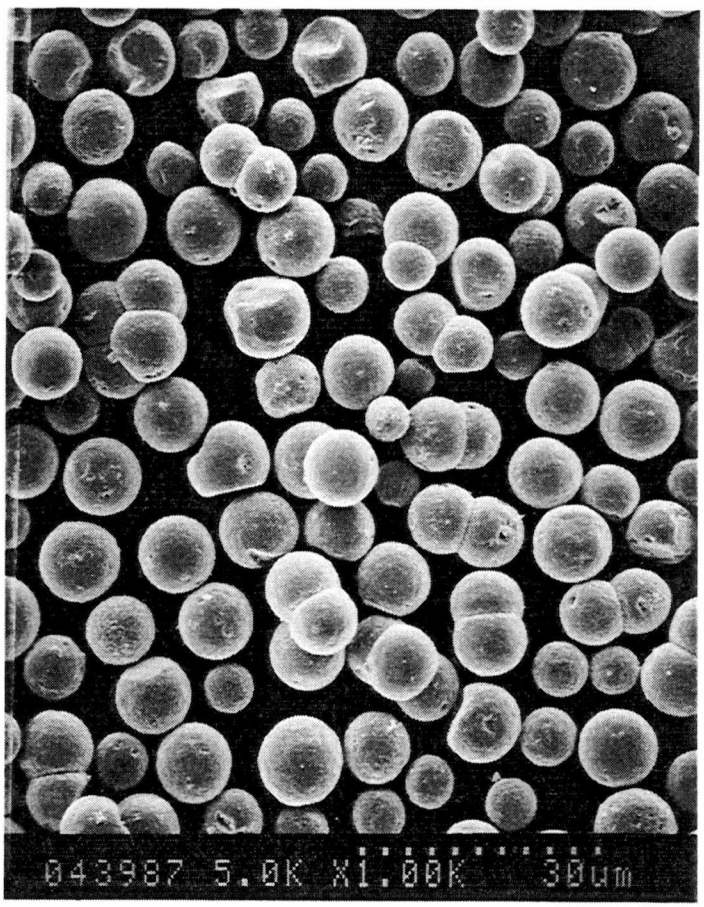
b. x1000

Figure 4.3 (continued)



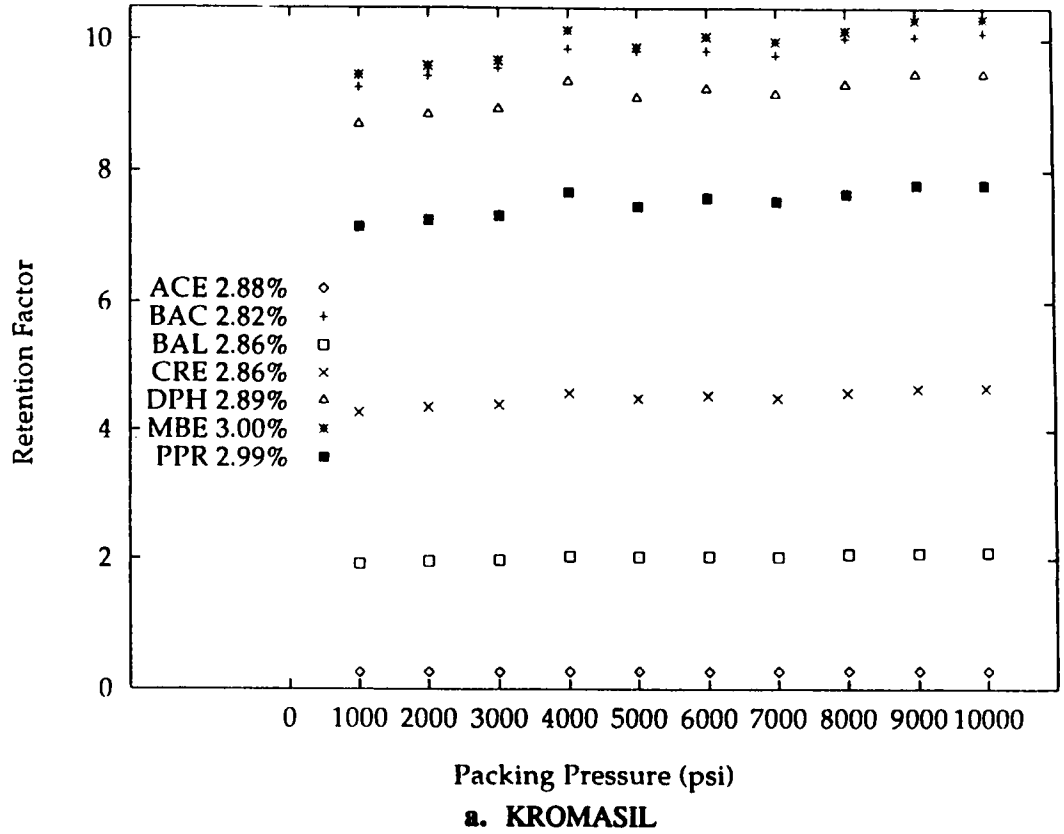
a. x5000

Figure 4.4 SEM microphotography of ZORBAX particles.



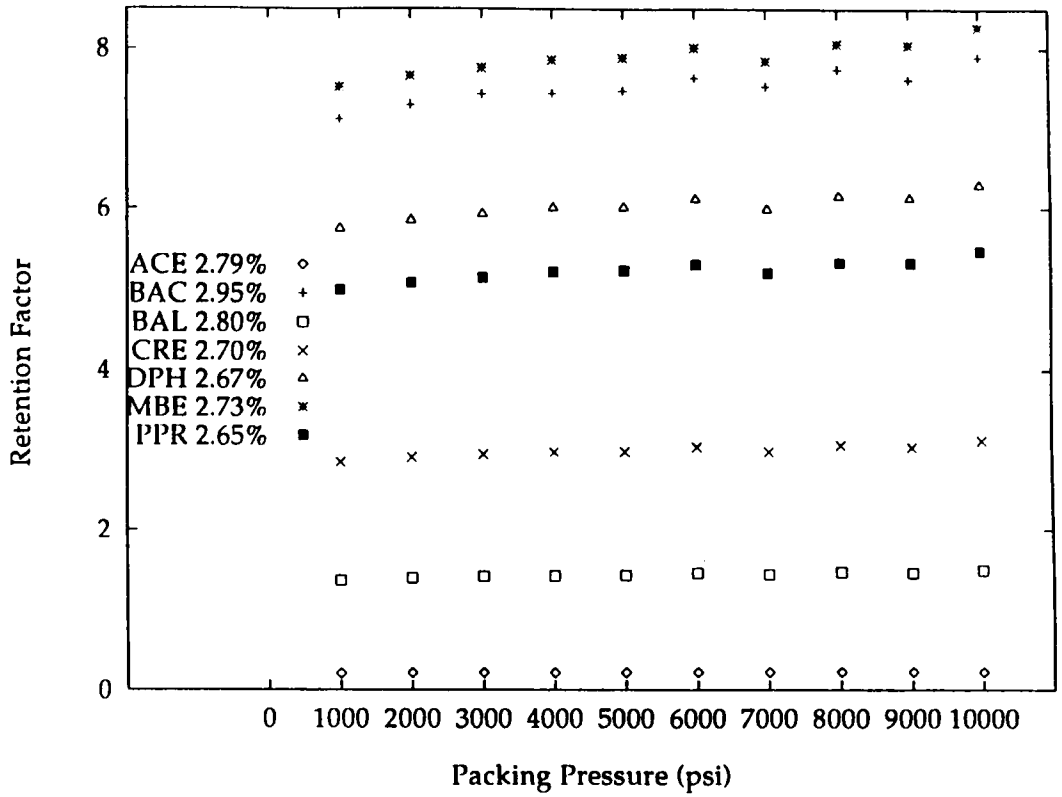
b. x1000

Figure 4.4 (continued)



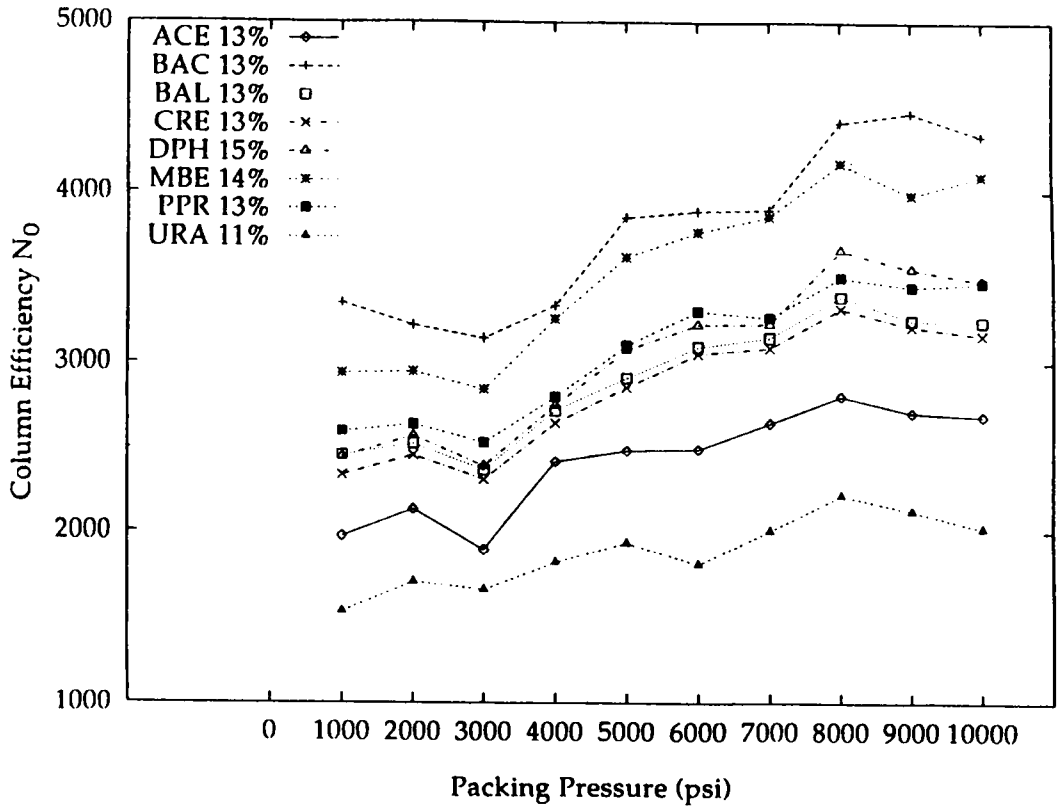
a. KROMASIL

Figure 5.1 Dependence of the retention factor on the packing pressure (psi). The percentage numbers in the figure legend represent the rsd of the results obtained on all ten columns. ACE: acetone; BAC: benzyl acetate; BAL: benzyl alcohol; CRE: m-cresol; DPH: 2,6-dimethyl phenol; MBE: methyl benzoate; PPR: 3-phenyl-1-propanol.



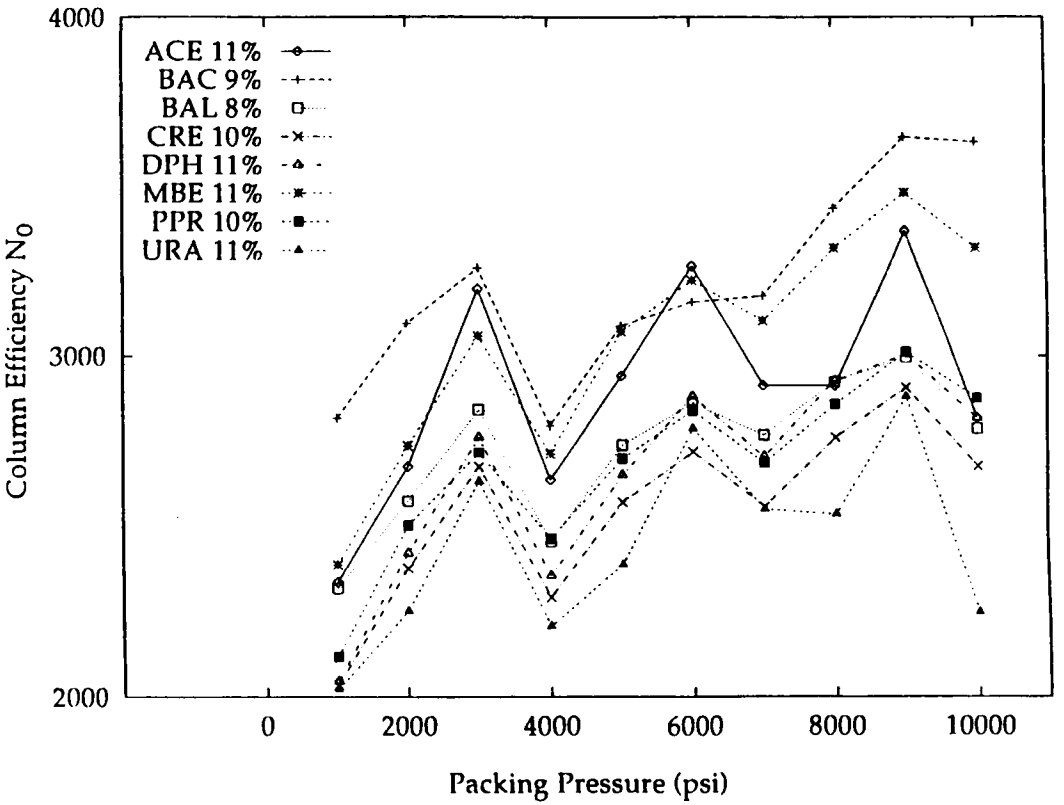
b. ZORBAX

Figure 5.1 (continued)



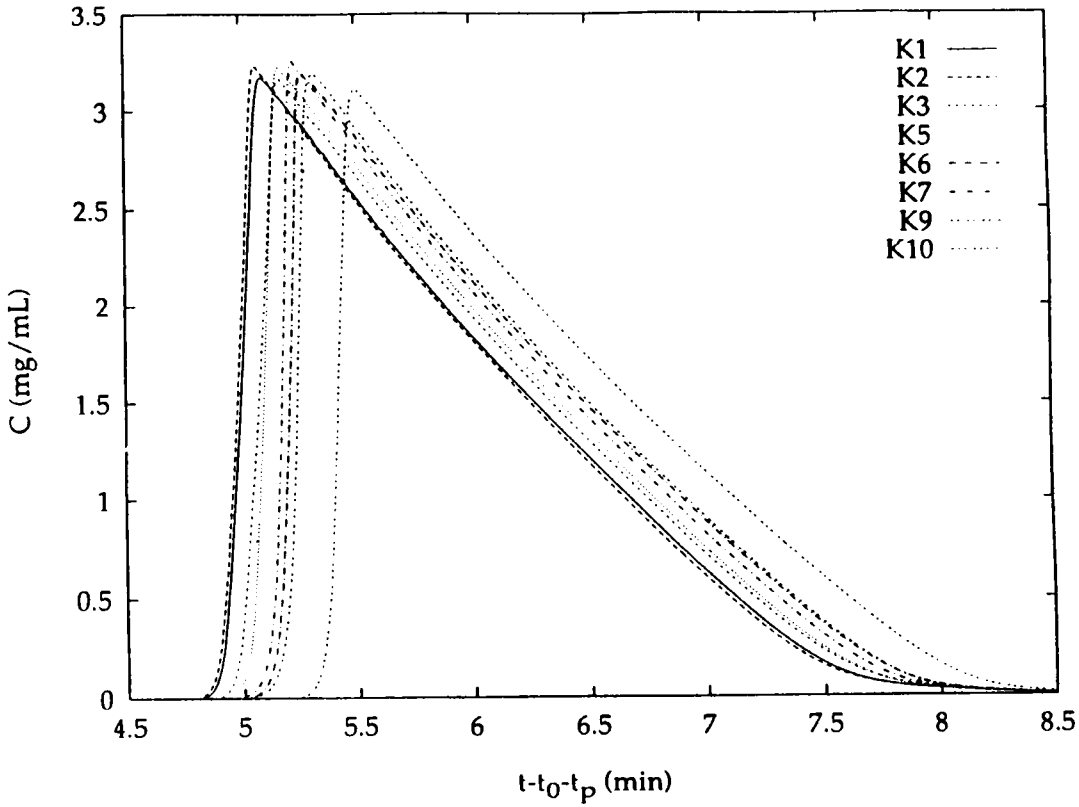
a. KROMASIL

Figure 5.2 Dependence of the column efficiency on the packing pressure (psi). The percentage numbers in the figure legend represent the rsd of the results obtained on all ten columns. ACE, BAC, BAL, CRE, DPH, MBE, PPR: same as in Figure 5.1.



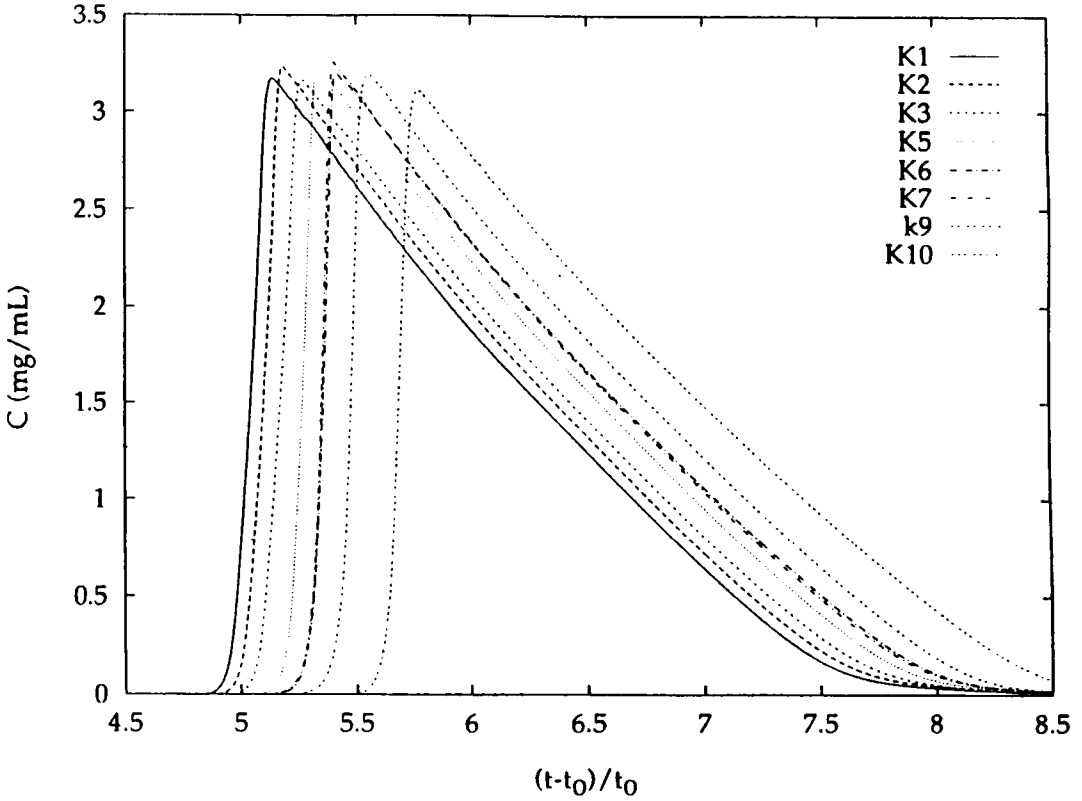
b. ZORBAX

Figure 5.2 (continued)



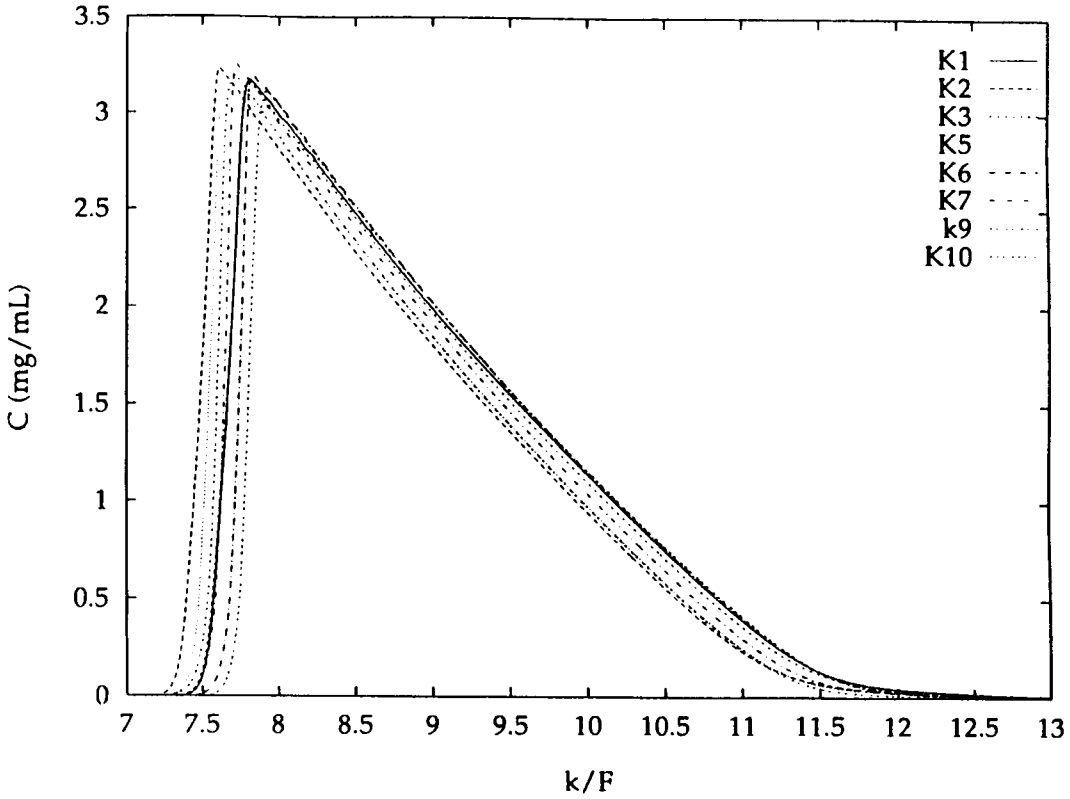
a. Plots of *C* (mg/mL) versus time (min)

Figure 5.3 Chromatograms obtained for 4.2 mg of 3-phenyl-1-propanol on eight of the ten columns. Mobile phase, 45/55 (v/v) methanol/water, 1 mL/min. KROMASIL.



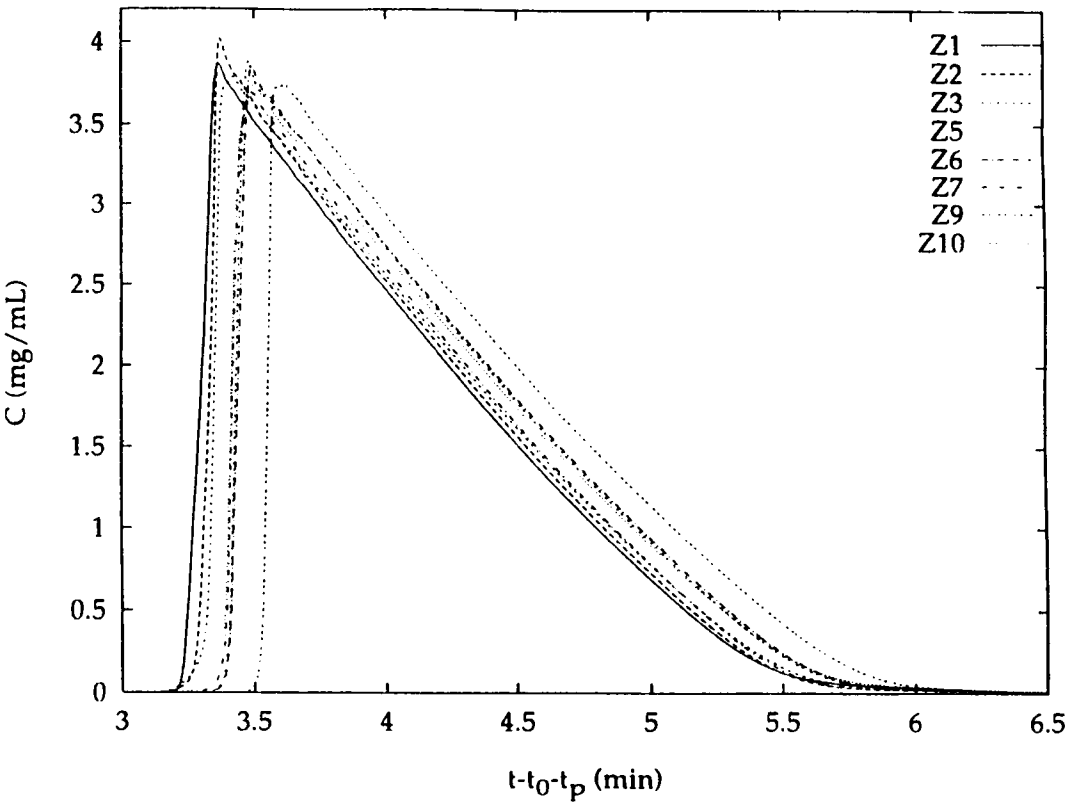
b. Plots of *C* (mg/mL) versus the retention factor

Figure 5.3 (continued)



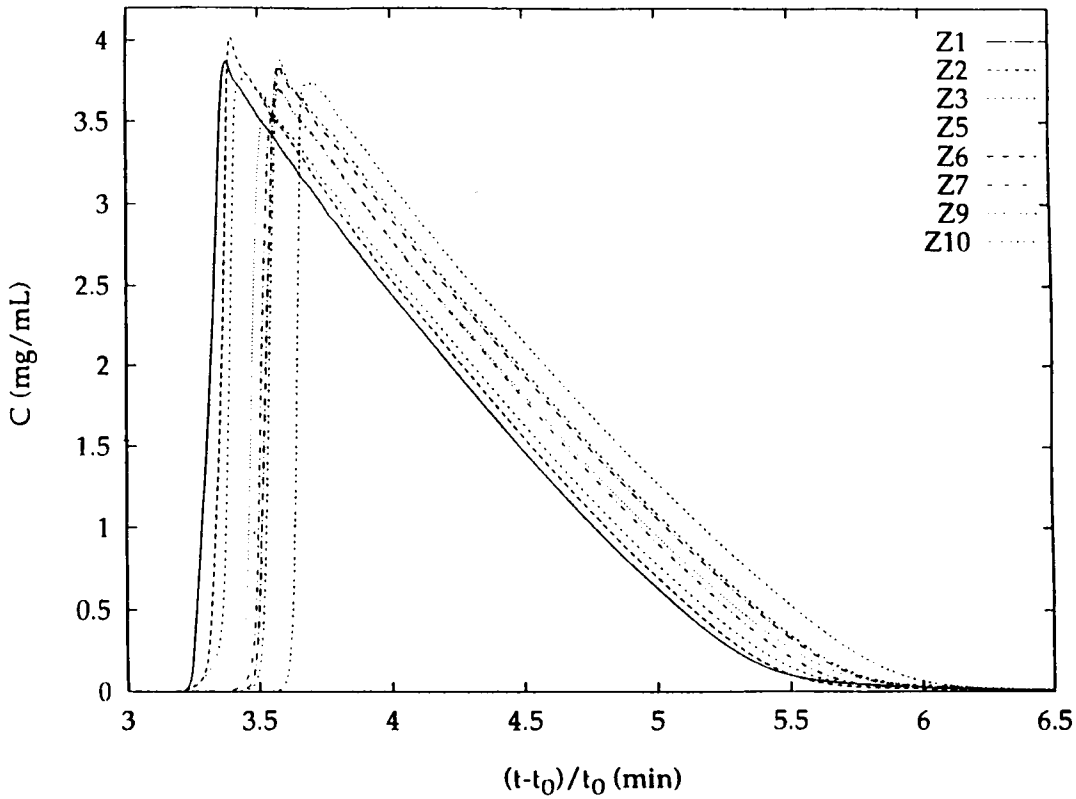
c. Plots of C (mg/mL) versus the ratio of the retention factor and the phase ratio

Figure 5.3 (continued)



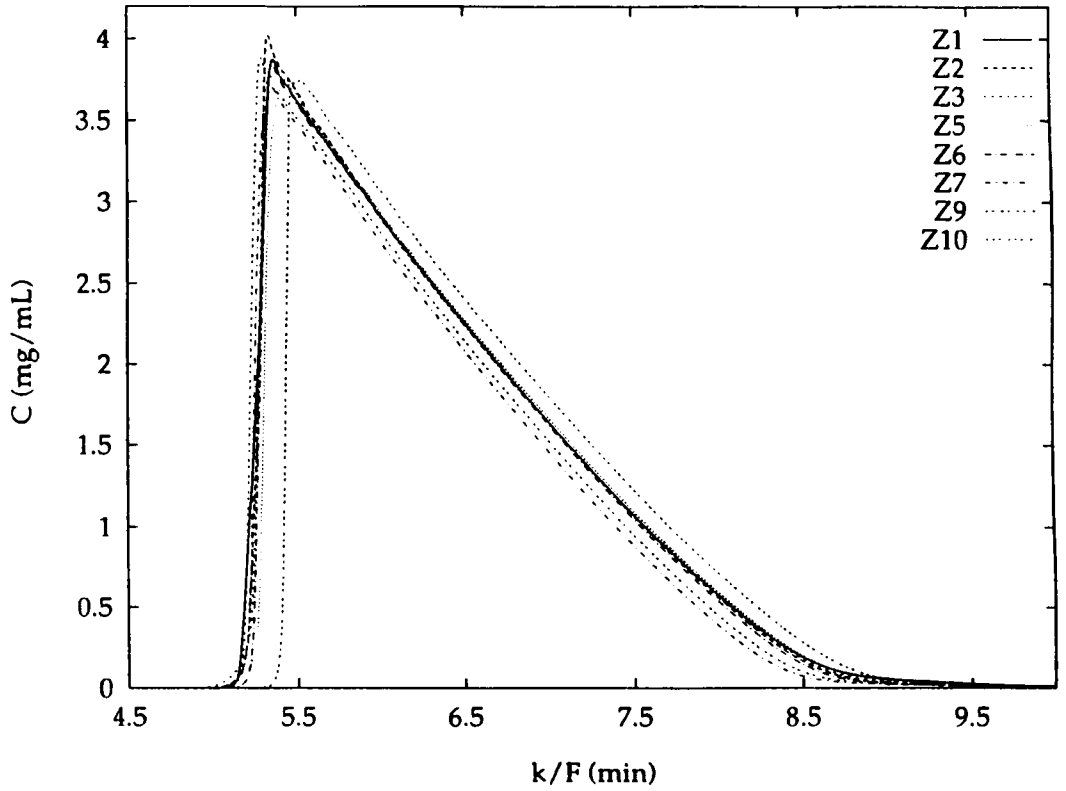
a. Plots of C (mg/mL) versus time (min)

Figure 5.4 Same as Figure 5.3, but stationary phase ZORBAX.



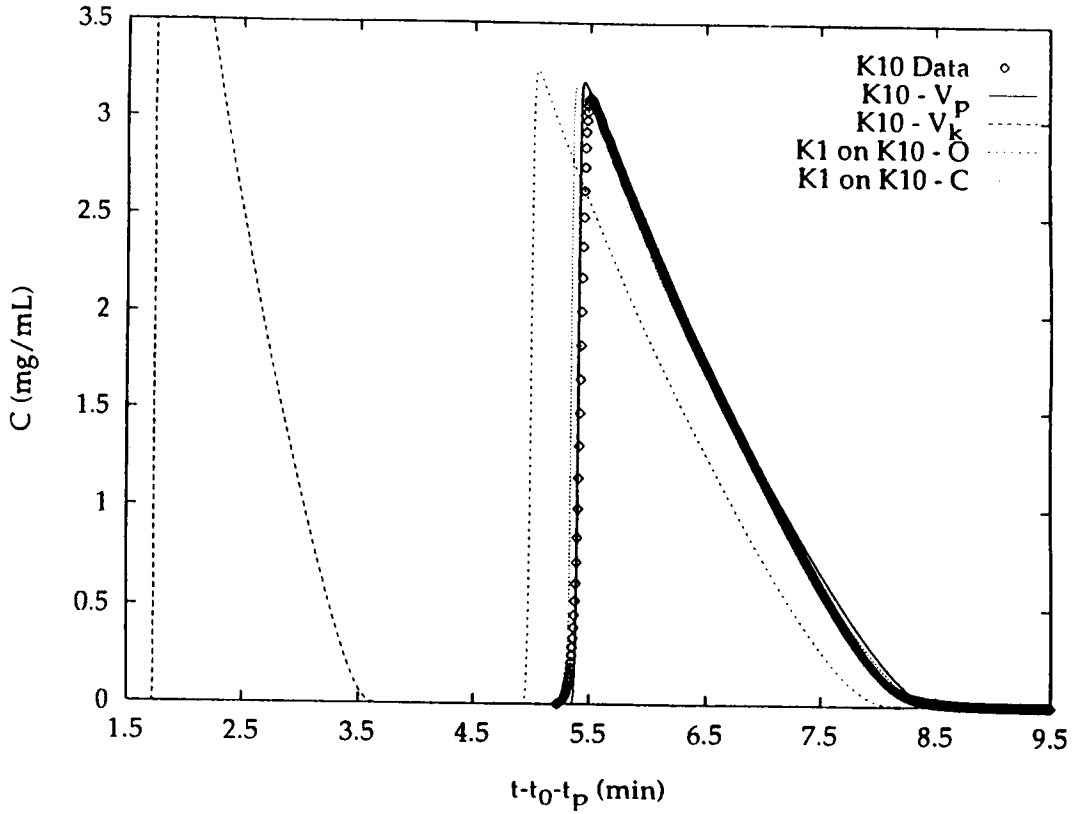
b. Plots of C (mg/mL) versus the retention factor

Figure 5.4 (continued)



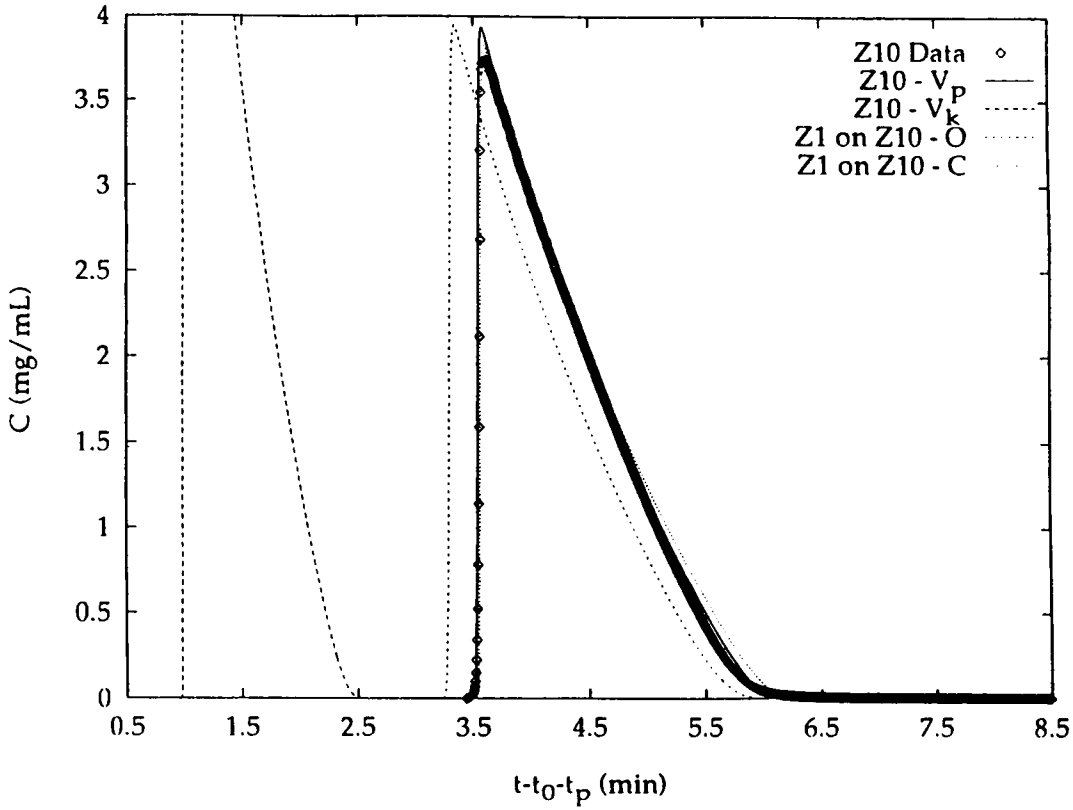
c. Plots of C (mg/mL) versus the ratio of the retention factor and the phase ratio

Figure 5.4 (continued)



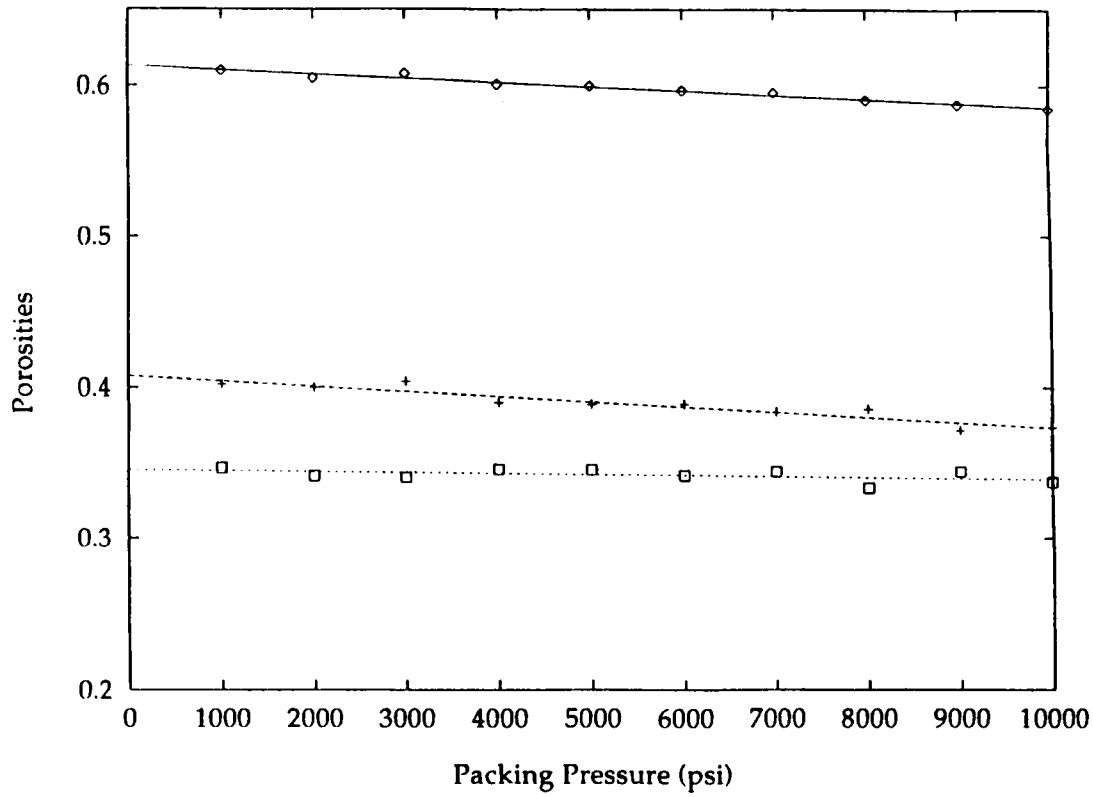
a. KROMASIL

Figure 5.5 Comparison between the experimental chromatogram (symbols) and the band profile calculated on column #10. Solid line: calculation made with the isotherm coefficients obtained on the same column and with its stationary phase volume V_p. Long chain line: calculation made with the isotherm coefficients obtained on the same column and with its geometrical volume V_t. Short chain line: calculation made with the isotherm coefficients obtained on the #1 column, without modification. Dotted line: calculation made with the isotherm coefficients obtained on the #1 column, modified by the weight ratio of packing material.



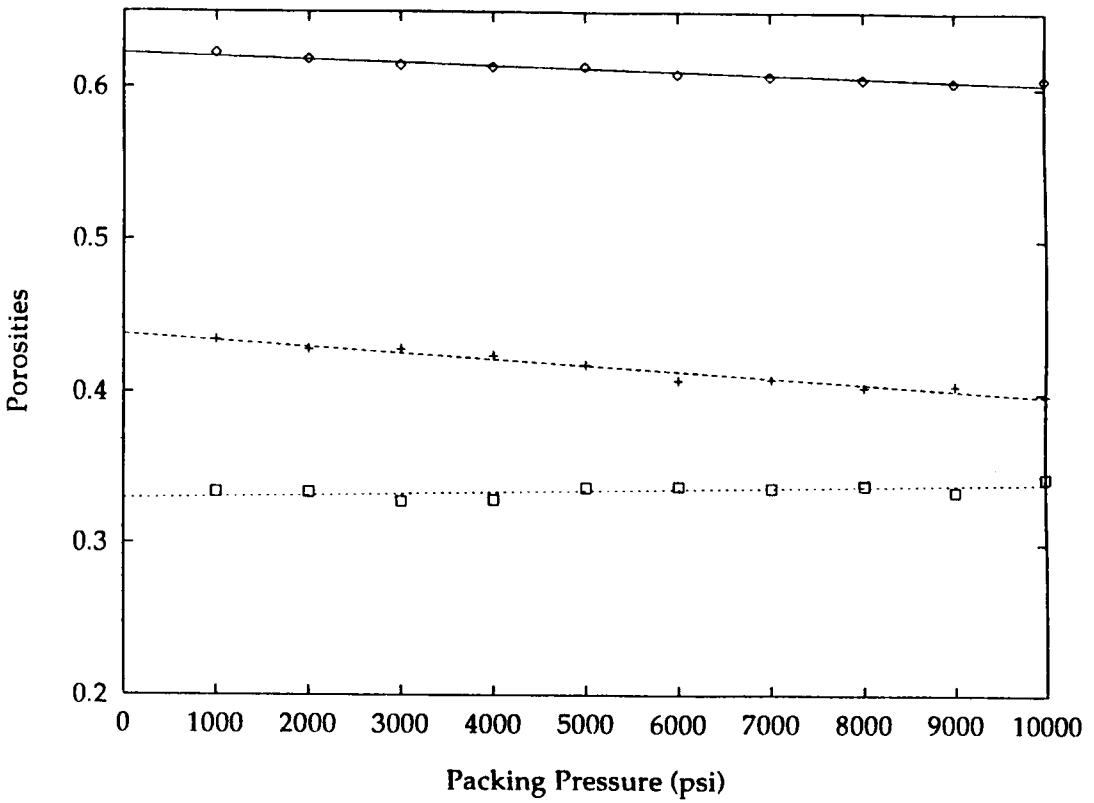
b. ZORBAX

Figure 5.5 (continued)



a. KROMASIL

Figure 5.6 Plot of the column total porosity ϵ_T (◇), external porosity ϵ_e (+), and internal porosity ϵ_i (□), versus the packing pressure P (psi). Solid line: $\epsilon_T = -2.7\text{x}10^{-6}*P + 0.6$; Long chain line: $\epsilon_e = -3.4\text{x}10^{-6}*P + 0.4$; Short chain line: $\epsilon_i = -6.2\text{x}10^{-7}*P + 0.3$.



b. ZORBAX

Figure 5.6 (continued) Solid line: ϵ_T = -2.0x10^{-6}*P + 0.6; Long chain line: ϵ_e = -3.9x10^{-6}*P + 0.4; Short chain line: ϵ_i = -1.1x 10^{-6}*P + 0.3.

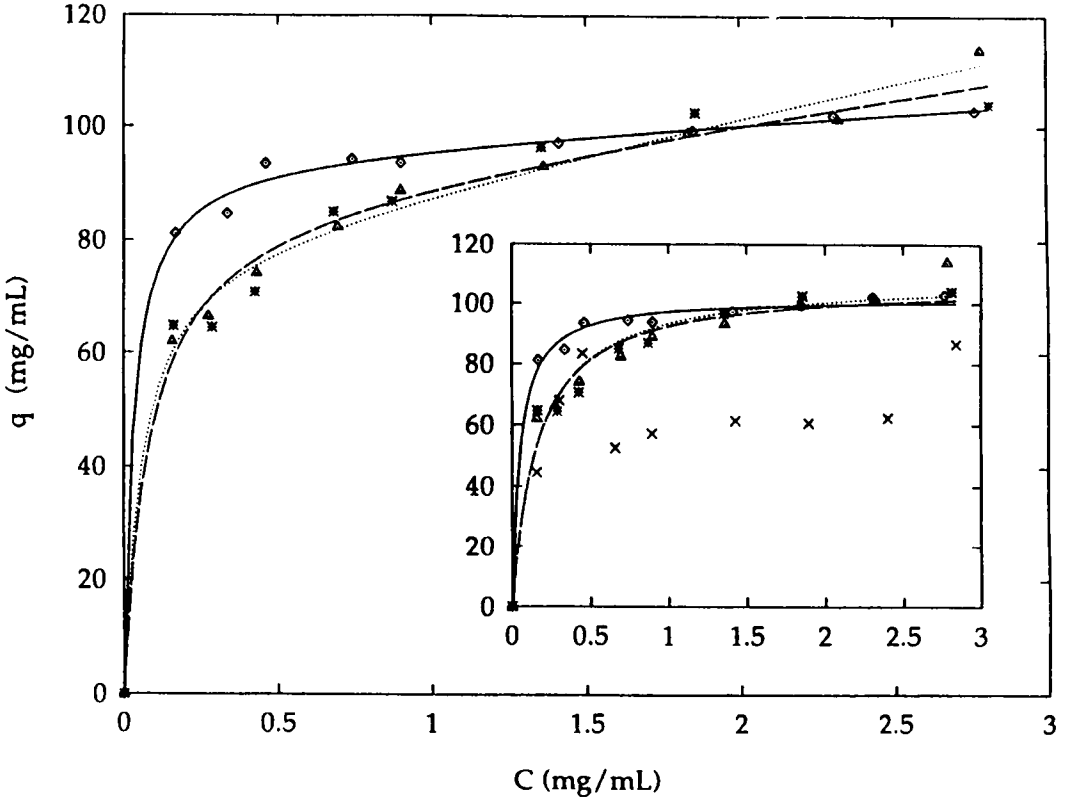


Figure 6.1 Calculated isotherm data points (symbols) and the bi-Langmuir model fitting (lines) plotted as q versus C. Inset shows the Langmuir model fitting (lines). Experimental conditions: pH=7.5 and 1 mL/min flow rate, diamonds and solid lines; pH=6.0 and 1 mL/min, triangles and dotted lines; 2 mL/min, stars and dashed lines; and 3 mL/min flow rate, crosses.

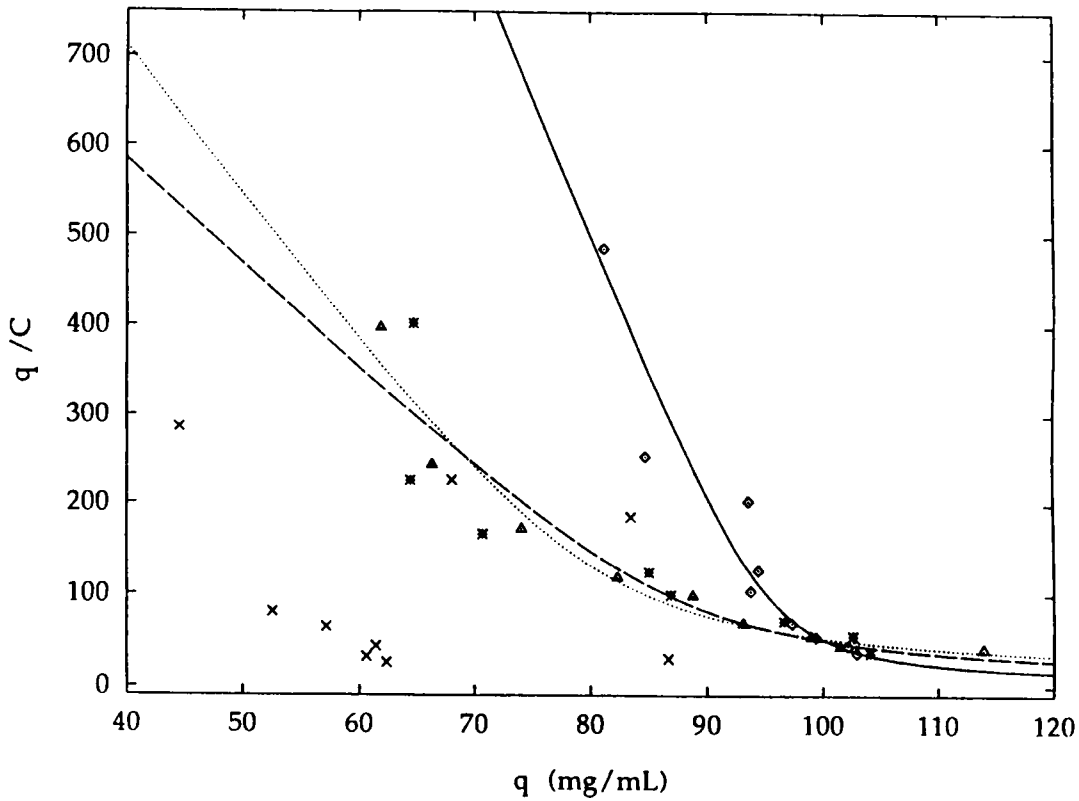


Figure 6.2 Scatchard plots of the isotherm data (symbols and lines correspond to conditions as described in Figure 6.1), q/C versus q.

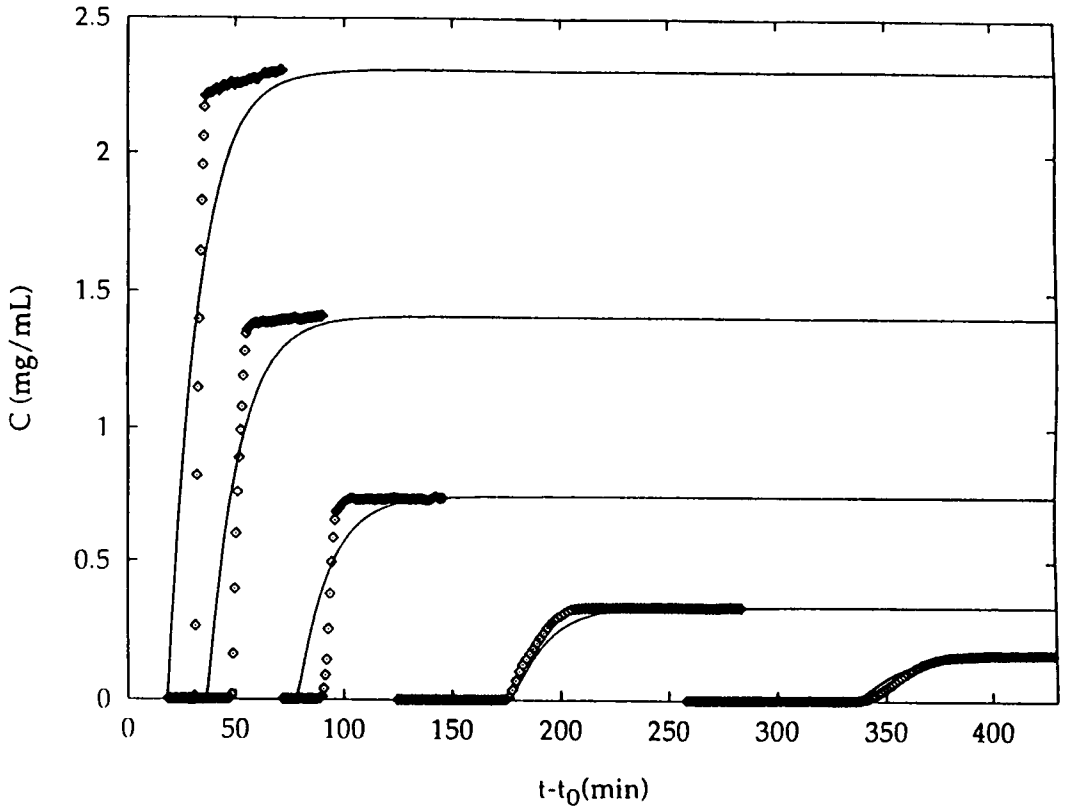


Figure 6.3 Comparison between the experimental breakthrough curves (symbols) and the simulated ones (lines) when the rate coefficient k_f is assumed to be independent of the sample concentration. Buffer pH = 7.5; Flow rate = 1.0 mL/min; k_f = 0.00133 s^{-1}.

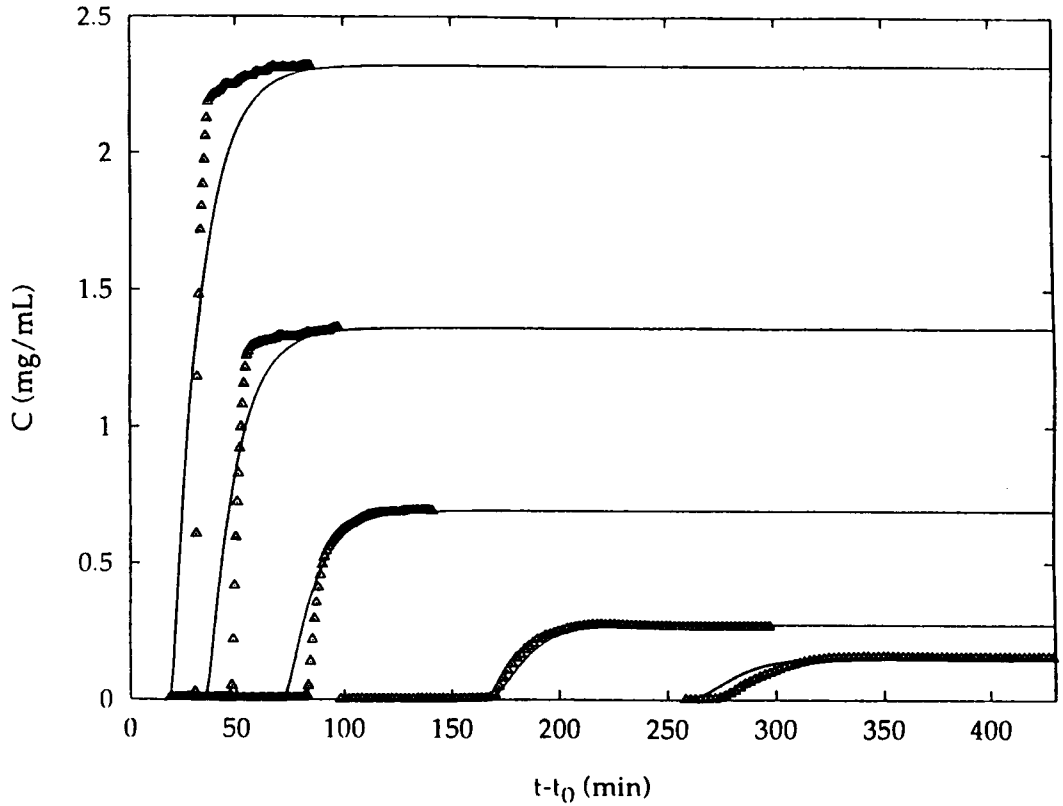


Figure 6.4 Same as Figure 6.3, but with Buffer pH = 6.0; Flow rate = 1.0 mL/min; $k_f = 0.00167\ s^{-1}$.

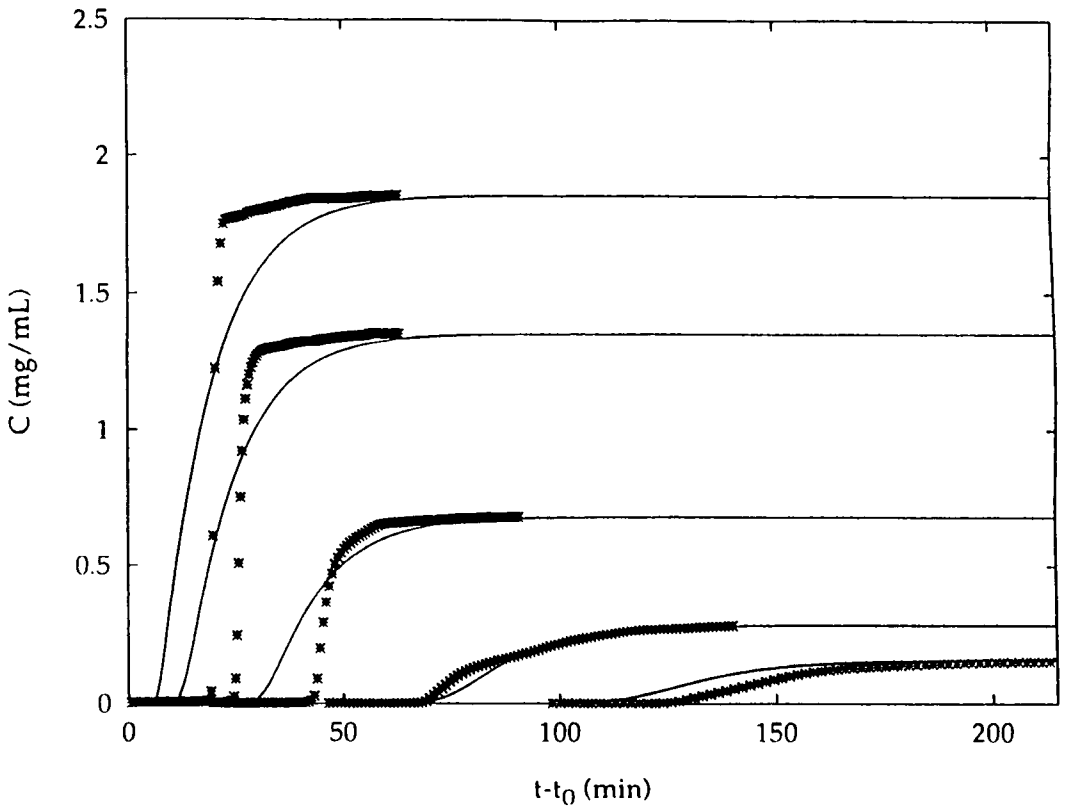


Figure 6.5 Same as Figure 6.3, but with Buffer pH = 6.0; Flow rate = 2.0 mL/min; $k_f = 0.00167\ s^{-1}$.

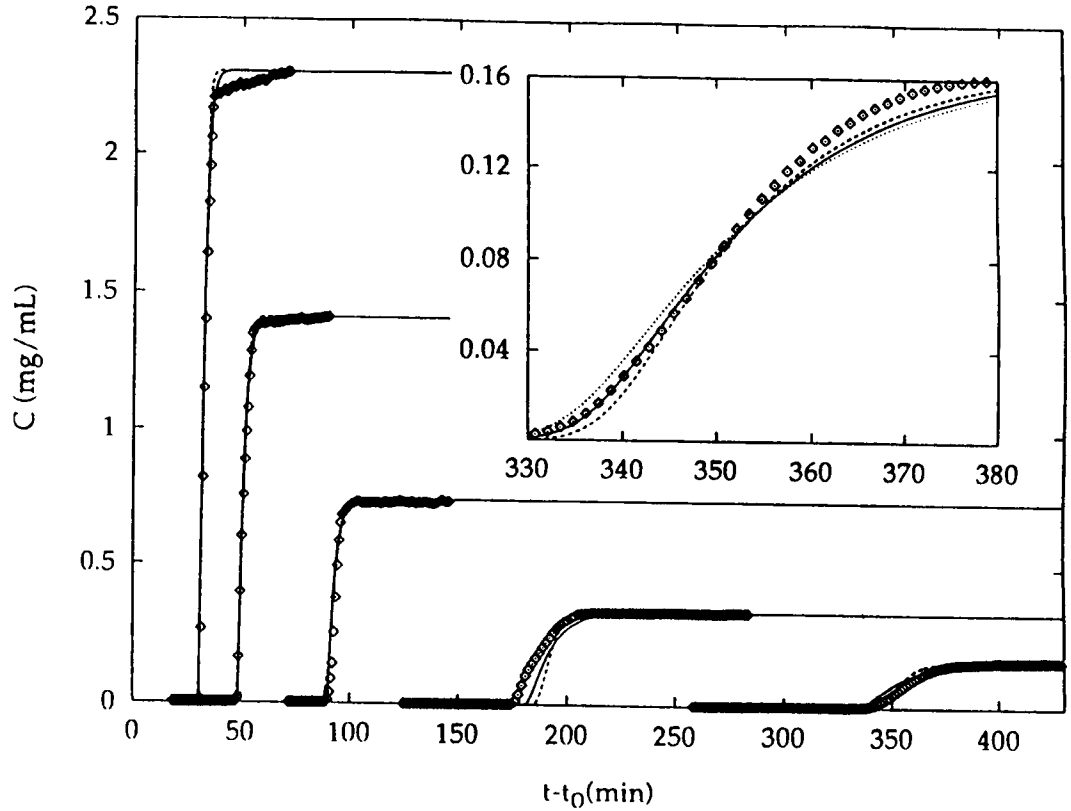


Figure 6.6 Comparison between the experimental breakthrough curves (symbols) and the simulated ones (lines) when the average rate coefficient k_f changes with the concentration. Simulated breakthrough curves are for the model with a constant best average rate coefficient which, however, depends on the height of the concentration step (solid lines) and for a model with a rate coefficient depending on the concentration (dashed lines). Buffer pH = 7.5; Flow rate = 1.0 mL/min. The inset illustrates the sensitivity of the curve fitting on the value of a constant rate coefficient for the lowest step concentration. Symbols - experimental results; solid line - calculation with the best rate coefficient; dashed line - calculation with a 10% larger rate coefficient; dotted line - calculation with a 10% lower rate coefficient. 6 minutes are subtracted from the time of the experimental data.

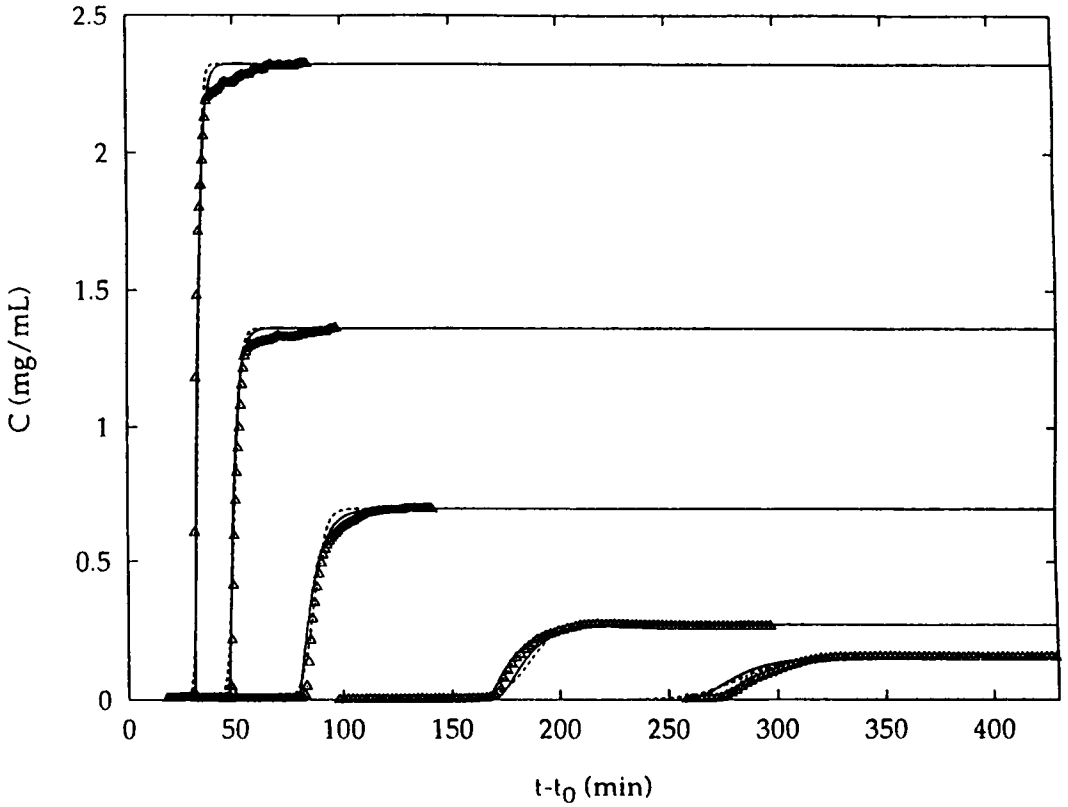


Figure 6.7 Same as Figure 6.6, but with Buffer pH = 6.0; Flow rate = 1.0 mL/min.

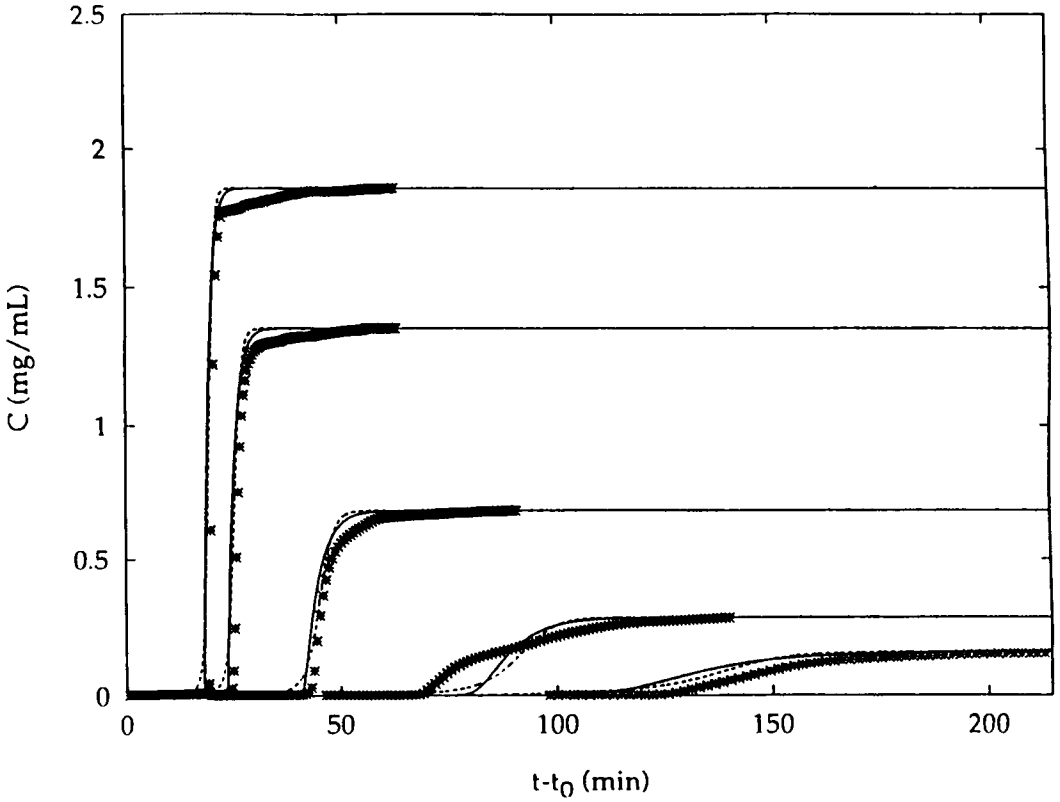


Figure 6.8 Same as Figure 6.6, but with Buffer pH = 6.0; Flow rate = 2.0 mL/min.

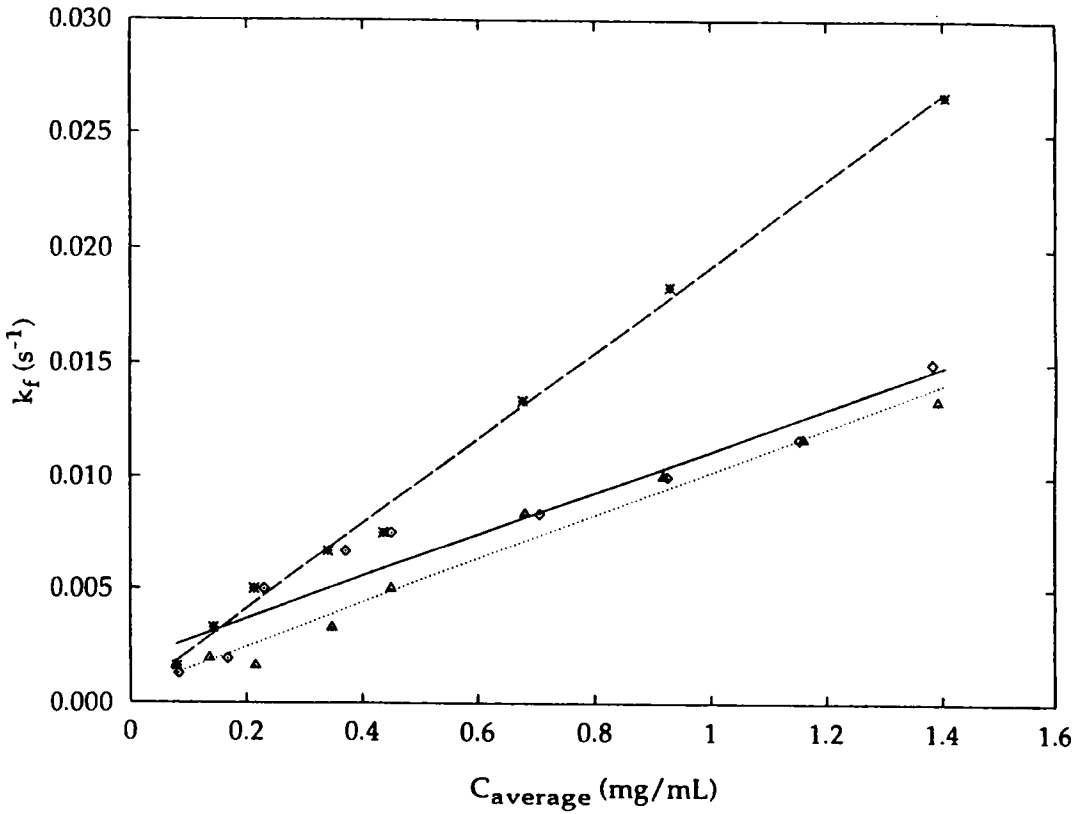


Figure 6.9 Rate coefficient concentration dependence. Plot of the average rate coefficient k_f versus the average sample concentration C_{ave} (symbols and lines as described in Figure 6.1). Correlation obtained:
At pH = 7.5, 1.0 mL/min, k_f = (9.3*C+1.9)/1000;
At pH = 6.0, 1.0 mL/min, k_f = (9.6*C+0.6)/1000;
At pH = 6.0, 2.0 mL/min, k_f = (18.8*C+0.4)/1000.

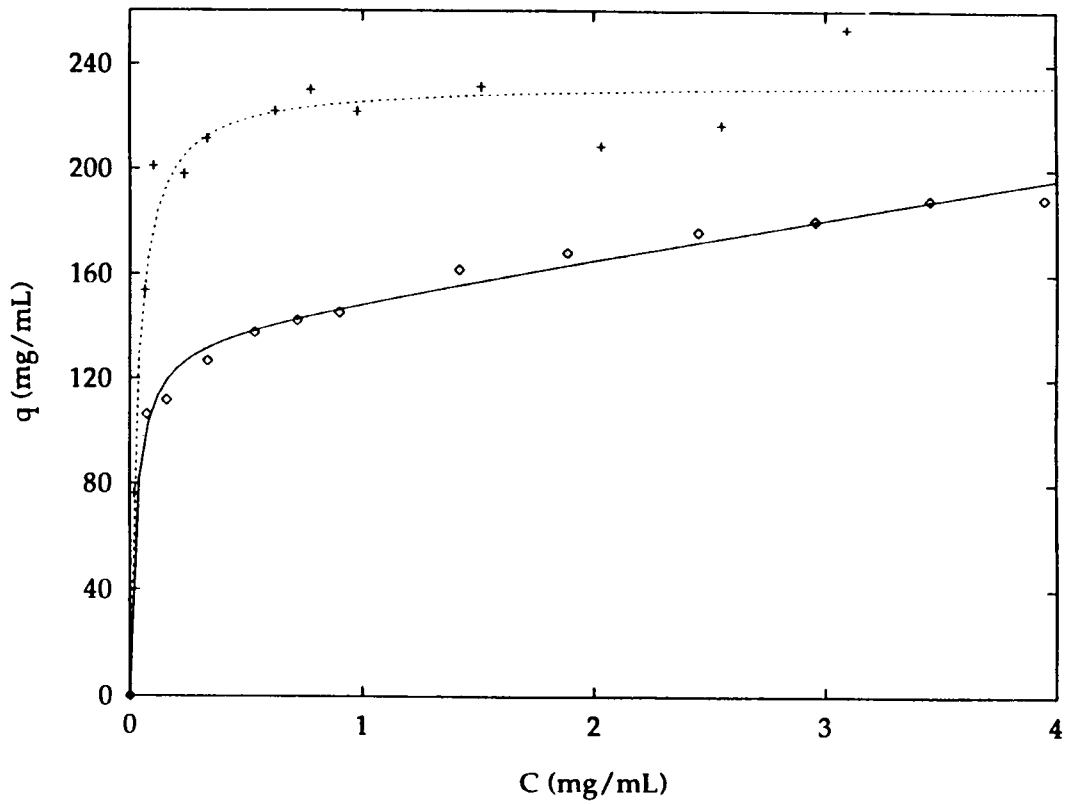
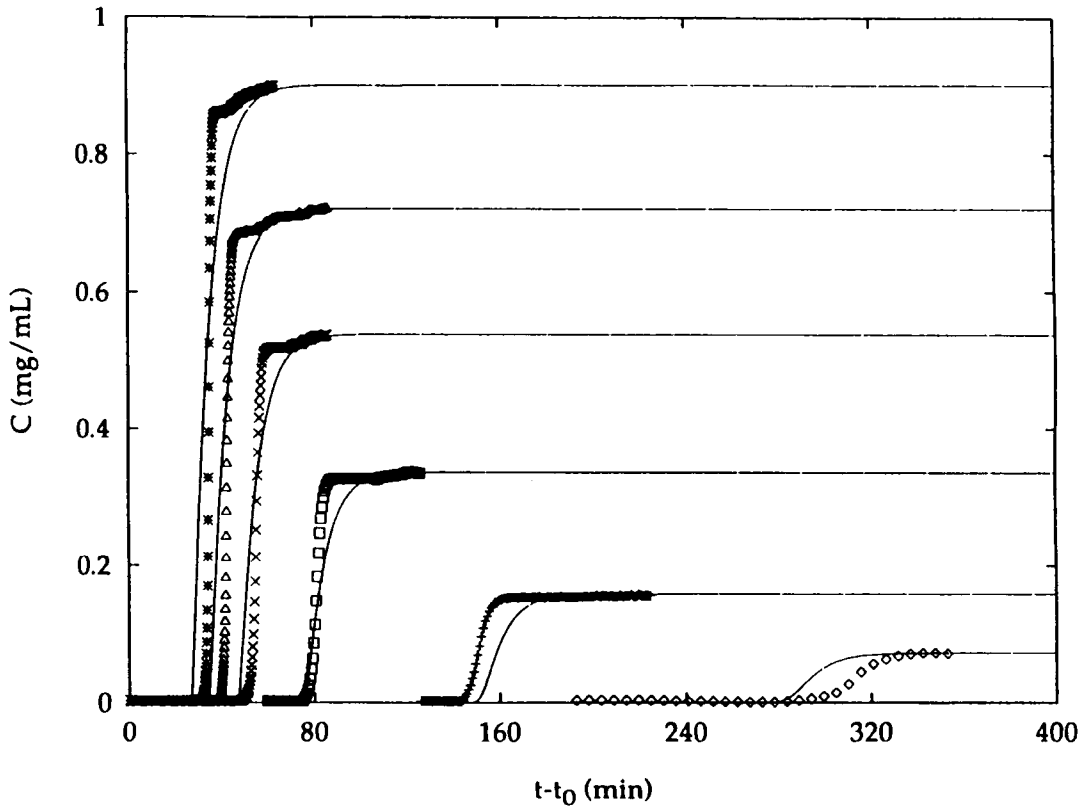
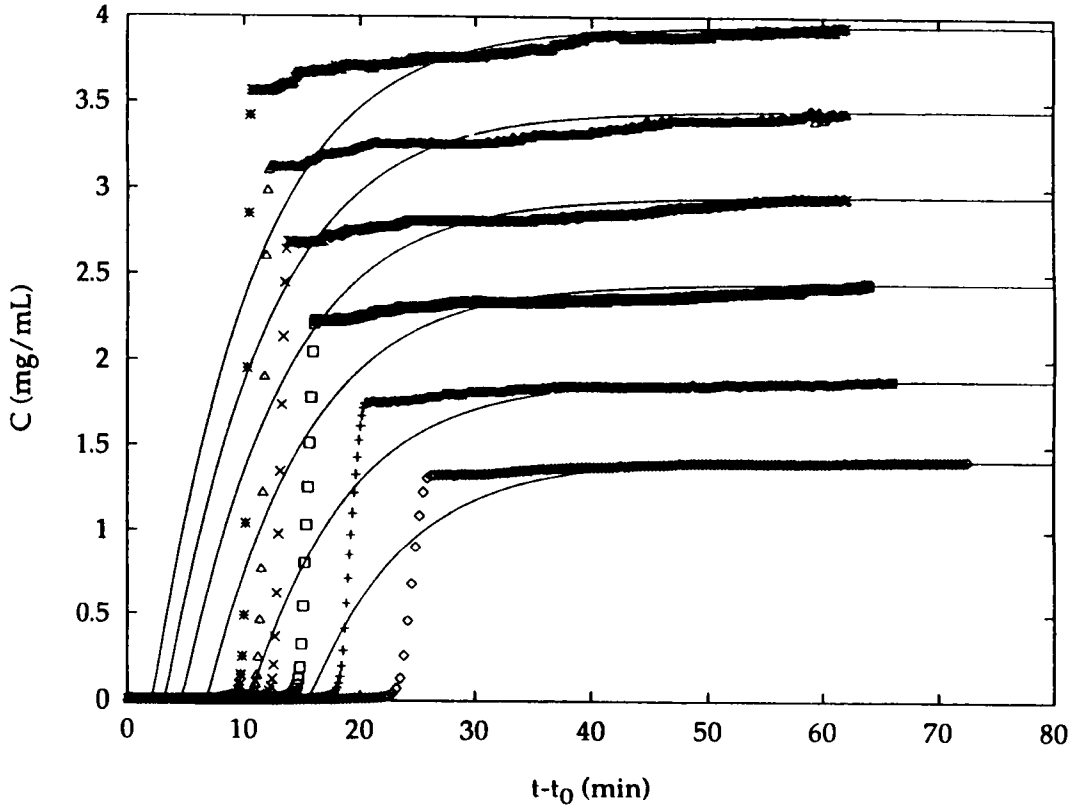


Figure 7.1 Calculated isotherm data points (symbols) and the bi-Langmuir model fitting (lines) plotted as q versus C. Resource-Q column No.1: ◇ and solid line; Resource-Q column No.2: + and dashed line.



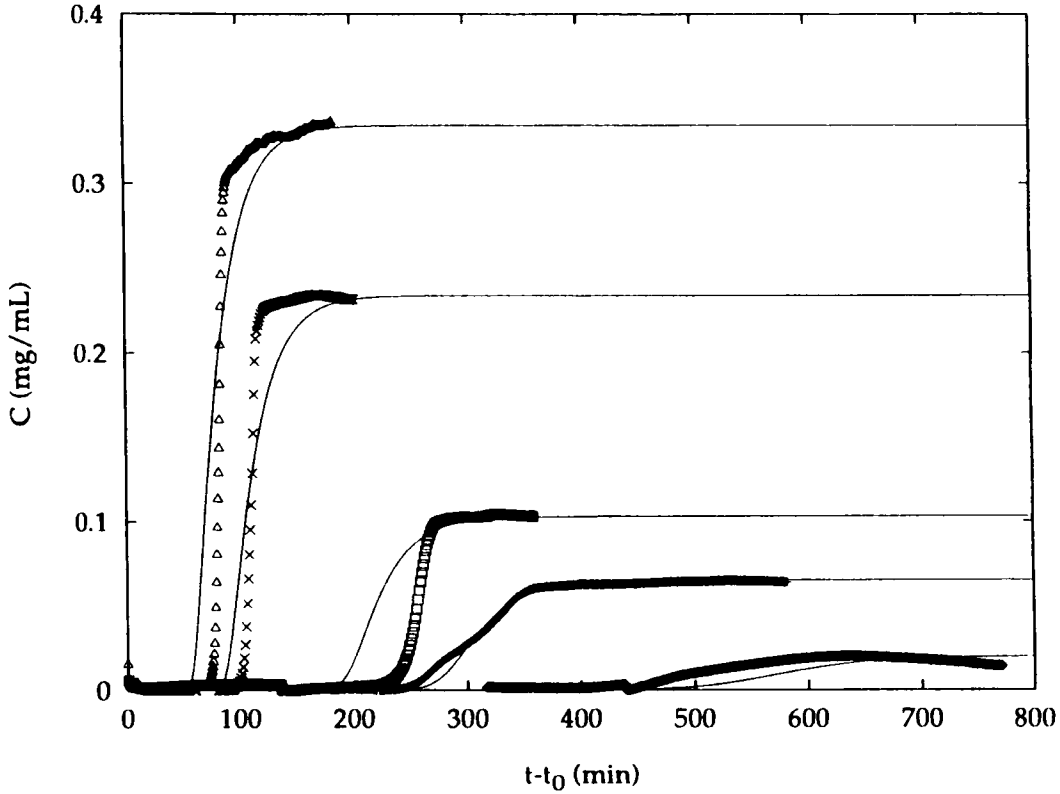
a. For low sample concentrations

Figure 7.2 Comparison between the experimental breakthrough curves (symbols) and the simulated ones (lines) when the rate coefficient k_f is assumed to be independent of the sample concentration. Resource-Q No.1.



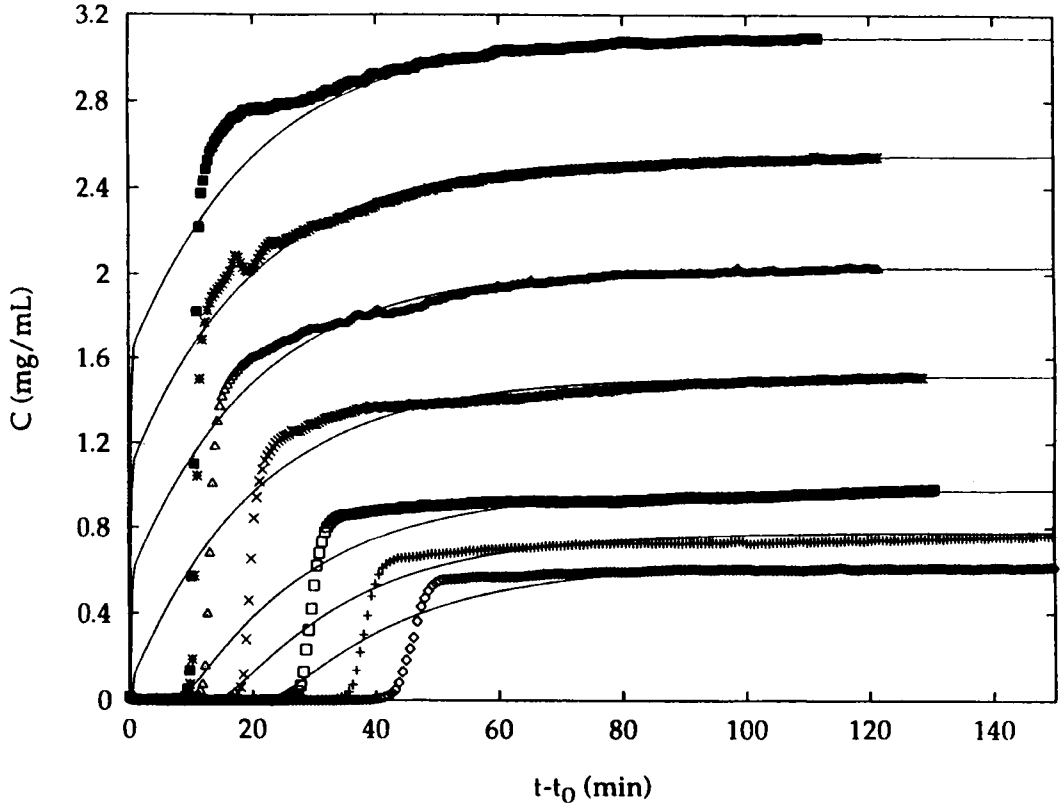
b. For high sample concentrations

Figure 7.2 (continued)



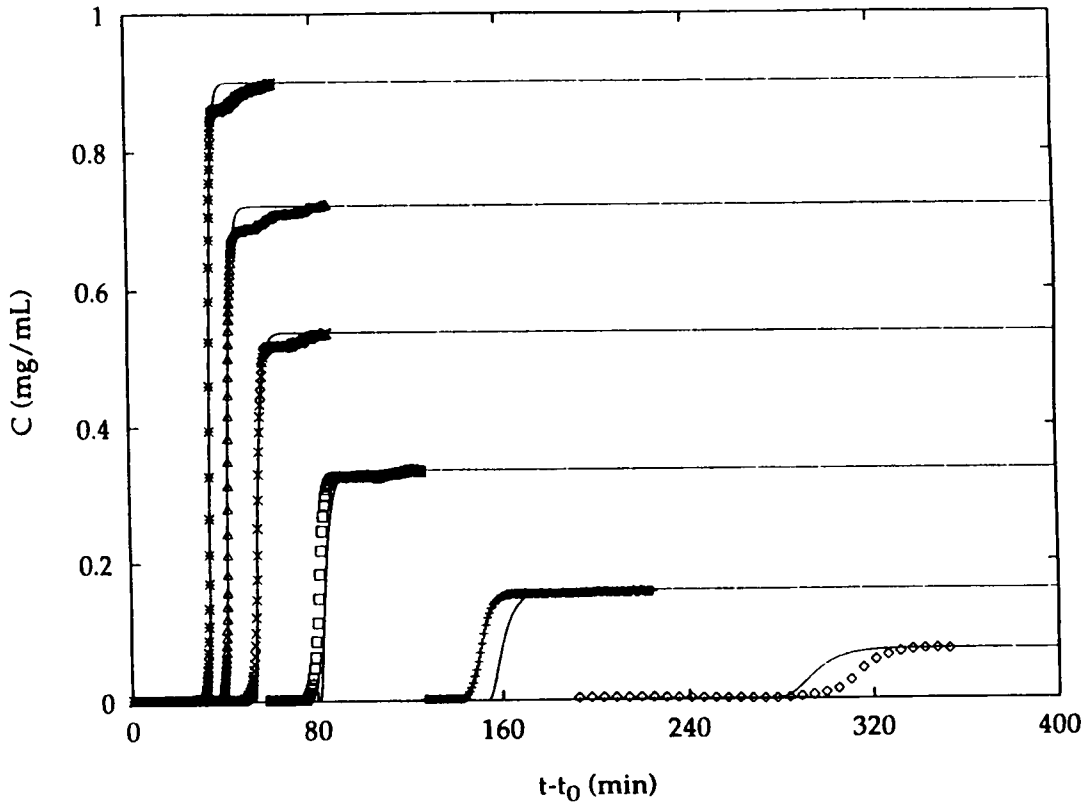
a. For low sample concentrations

Figure 7.3 Same as Figure 7.2, but for Resource-Q column No.2.



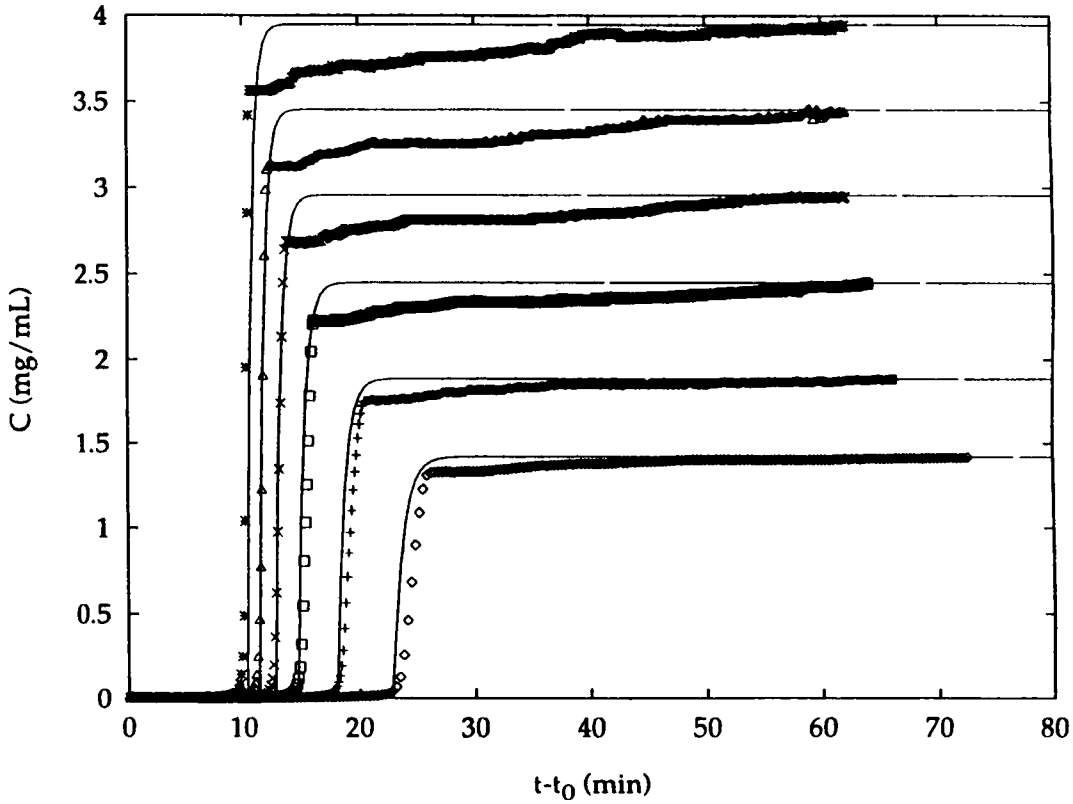
b. For high sample concentrations

Figure 7.3 (continued)



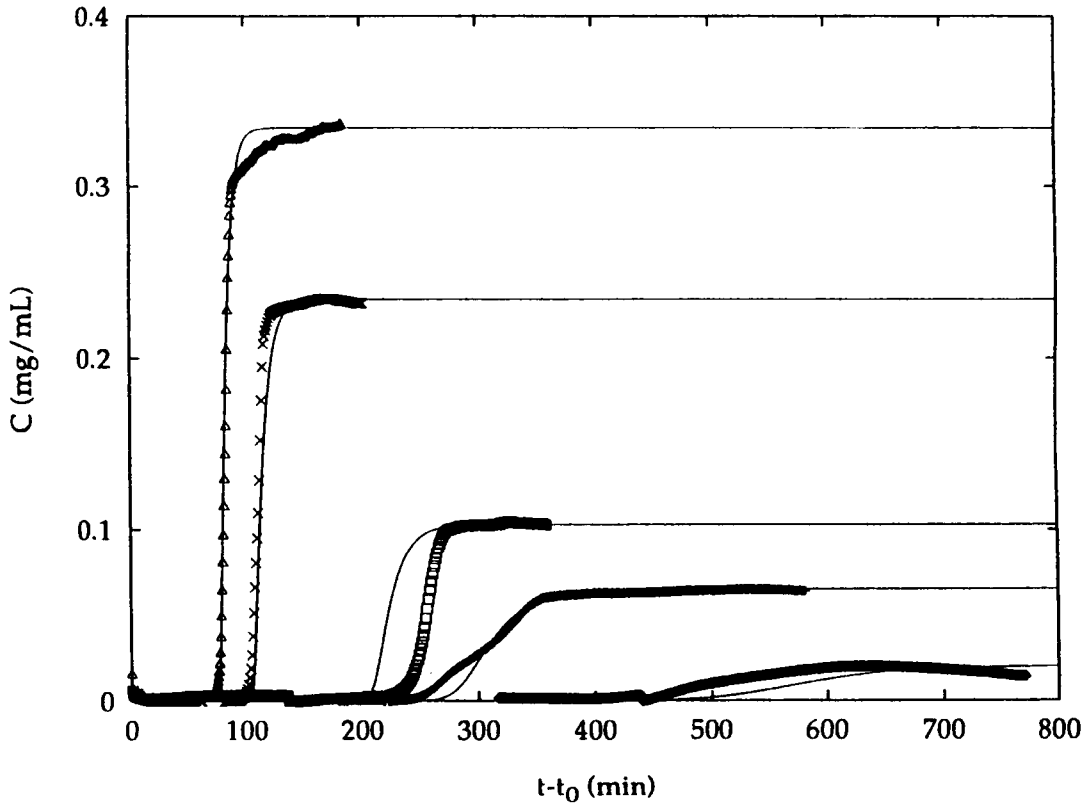
a. For low sample concentrations

Figure 7.4 Comparison between the experimental breakthrough curves (symbols) and the simulated ones (lines) when the rate coefficient k_f changes with the concentration. Resource-Q column No.1.



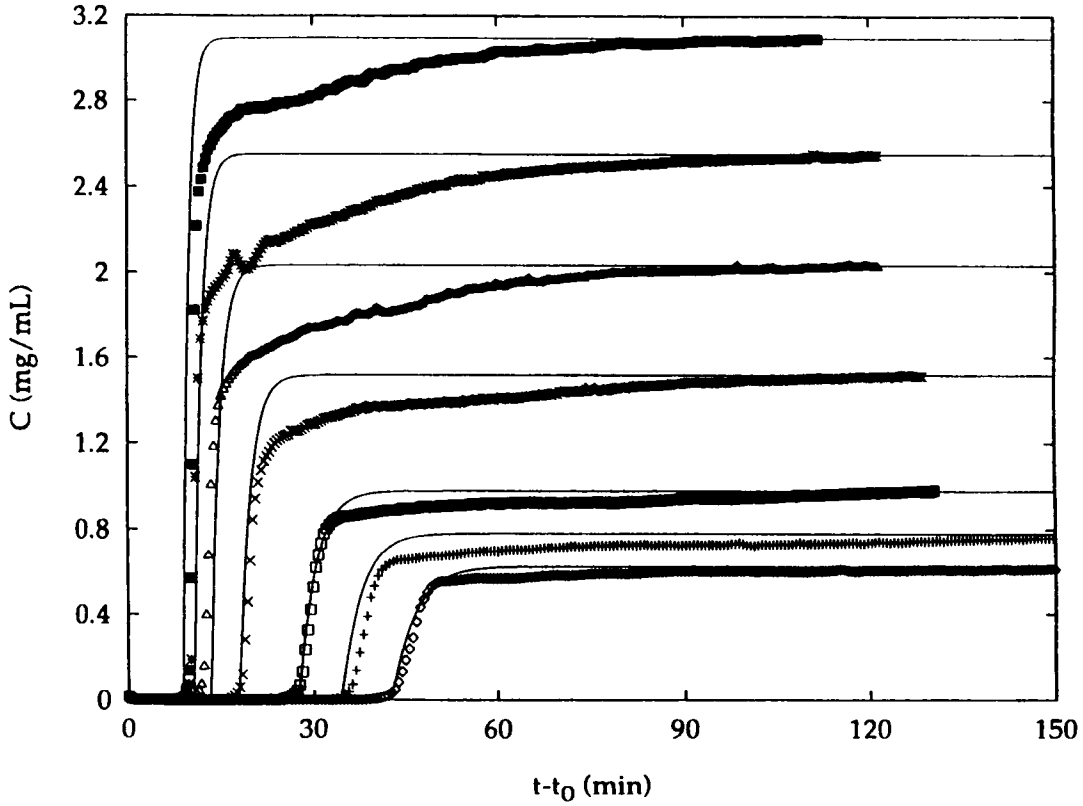
b. For high sample concentrations

Figure 7.4 (continued)



a. For low sample concentrations

Figure 7.5 Same as Figure 7.4, but for RESOURCE-Q column No.2.



b. For high sample concentrations

Figure 7.5 (continued)

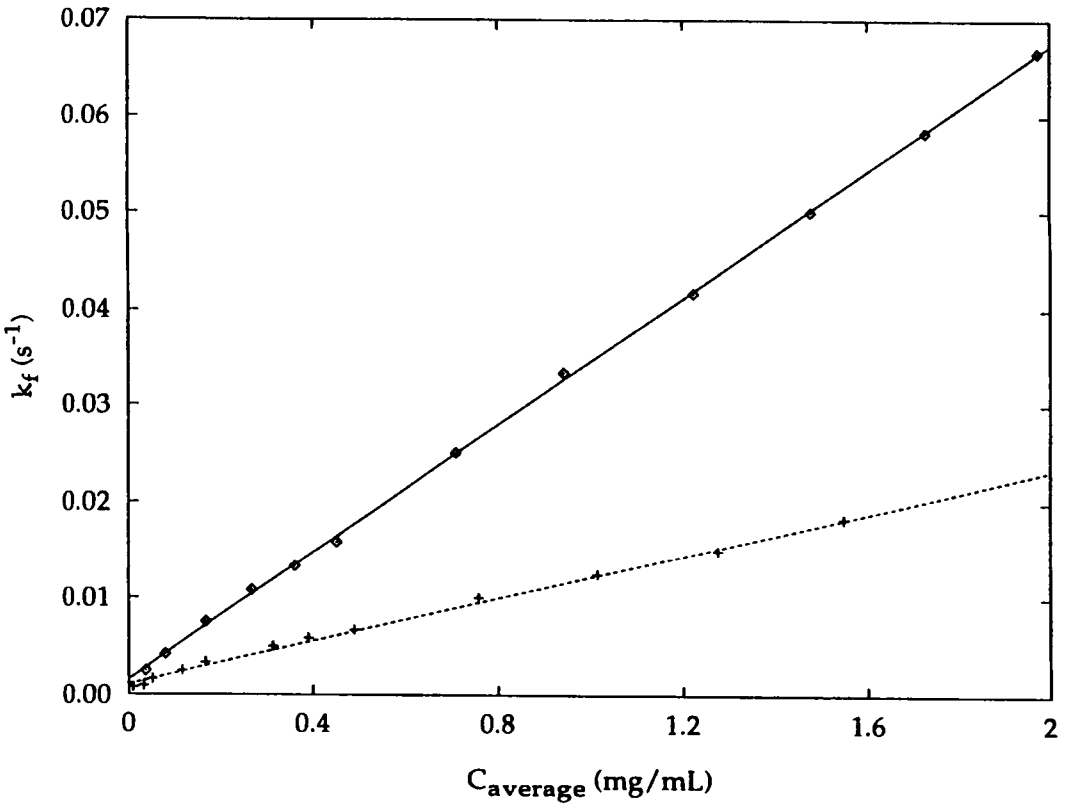


Figure 7.6 Rate constant concentration dependence for both Resource-Q columns No. 1 and 2. Plot of the average rate coefficient k_f versus the average sample concentration C_{ave}.

VITA

Hong GUAN was born in Beijing, People's Republic of China (PRC) on October 19, 1966. Six months later she was taken to Shanghai (PRC) by her grandparents while her parents, both graduated from the University of Moscow (Moscow, Russia) with a major in Chemistry, were sent to Fushun county in Sichuan province (PRC) to accept the re-education from poor peasants, as ordered by the Chinese Cultural Revolution. In August, 1973, she joined her parents in Fushun, where she then spent 8 years and finished her elementary and junior high school. In August, 1981, she returned to Shanghai (PRC) and finished her high school study in Shanghai No. 62 High School (Shanghai, PRC) in May, 1984. After passing the National College Entrance Examination, she was accepted by the East China University of Chemical Technology (ECUCT) (Shanghai, PRC) and received her Bachelor Degree of Science in Chemical Physics major in May, 1988. Upon graduation from ECUCT, she worked in the Acta Optica Sinica Editorial Board for 15 months. In January 12, 1990, she came to the United States of America and began her graduate study in the Physics department of the Wichita State University (Wichita, KS), where she received her Master Degree of Science in Physics major in May, 1991. In August, 1991, she began her Doctorate study in the Chemistry department of the University of Tennessee at Knoxville. On February 17, 1996, she married her German colleague, Mr. Peter Sajonz. Two weeks later, she defended her Ph.D. In May, 1996, she is to receive her Doctor of Philosophy with a major in Chemistry.